Università degli Studi di Napoli Federico II

Dottorato di Ricerca in
Ingegneria Strutturale, Geotecnica e Rischio Sismico
XXXVIII Cycle

THESIS FOR THE DEGREE OF DOCTOR OF PHILOSOPHY

Multi-Hazard Risk-Based Design and Analysis of Wind Turbines

by

STEFANIA ZIMBALATTI

Advisor: Prof. Fulvio Parisi

SCUOLA POLITECNICA E DELLE SCIENZE DI BASE
DIPARTIMENTO D STRUTTURE PER L'INGEGNERIA E L'ARCHITETTURA

You have to take care of yourself first

Multi-Hazard Risk-Based Design and Analysis of Wind Turbines

Ph.D. Thesis presented
for the fulfillment of the Degree of Doctor of Philosophy
in Ingegneria Strutturale, Geotecnica e Rischio Sismico
by

STEFANIA ZIMBALATTI

2025

Approved as to style and content by

Prof. Fulvio Parisi, Advisor

Università degli Studi di Napoli Federico II
Ph.D. Program in Ingegneria Strutturale, Geotecnica e Rischio Sismico
XXXVIII cycle - Chairman: Prof. Iunio Iervolino

www.dist.unina.it/dottorati-di-ricerca/dottorati

Candidate’s declaration

I hereby declare that this thesis submitted to obtain the academic degree of Philosophiæ Doctor (Ph.D.) in Ingegneria Strutturale, Geotecnica e Rischio Sismico is my own unaided work, that have not used other than the sources indicated, and that all direct and indirect sources are acknowledged as references.

Parts of this dissertation have been published in international journals and/or conference proceedings (see list of the author’s publications at the end of the thesis).

Napoli, December 31, 2025

Stefania Zimbalatti

Stefania Zimbalatti

Abstract

Over recent decades, the growing demand for wind energy has accelerated the deployment of onshore and offshore wind turbines, making increasingly evident the need for design and assessment methodologies capable of integrating multiple natural hazards in a coherent manner. In order to maximize the wind resource, onshore wind turbines are frequently installed on mountainous slopes, while offshore wind turbines are progressively located in deep waters.

In this context, this thesis develops and applies a multi-hazard risk-based analysis and design framework, in which environmental actions, structural response and the main sources of uncertainty are treated probabilistically and consistently with engineering-relevant performance levels.

For onshore wind turbines, the analysis considers the combined effects of wind, earthquakes and earthquake-induced landslides, explicitly including soil–structure interaction effects. For offshore wind turbines, with particular reference to floating systems installed in deep waters, the aero–hydro–structural interaction is modelled through time-domain simulations that include turbulent wind, wave action and marine currents. In both cases, advanced numerical models, validated against reference benchmarks, are adopted to derive fragility curves and surfaces and to estimate risk metrics.

A case study in Italy highlights how the combination of hazards can significantly influence wind turbine performance. In the onshore context, earthquake-induced landslides may become dominant in governing structural demand and loss of functionality, whereas in the offshore context the coupling between wind and wave loading leads to an amplification of structural response. Sensitivity analyses further quantify the impact of the main sources of uncertainty and provide useful insights for the definition of design margins and verification criteria consistent with predefined reliability targets.

Keywords: multi-hazard risk, wind turbines, fragility functions, risk-based design, OpenSees, OpenFAST.

Sintesi in lingua italiana

Negli ultimi decenni, la crescente domanda di energia eolica ha accelerato l'installazione di turbine eoliche onshore e offshore, rendendo sempre più evidente la necessità di metodologie di progettazione e valutazione in grado di considerare in modo integrato la presenza di pericoli naturali multipli. Al fine di massimizzare la risorsa eolica, le turbine onshore sono frequentemente installate su versanti montani, mentre le turbine offshore sono progressivamente collocate in acque profonde.

Alla luce di questo scenario, la tesi sviluppa e applica un framework di analisi e progettazione basato sul rischio multi-hazard, nel quale le azioni ambientali, la risposta strutturale e le principali fonti di incertezza sono trattate in modo probabilistico e coerente con livelli prestazionali ingegneristicamente significativi.

Per le turbine onshore, l'analisi considera l'effetto congiunto di vento, terremoti e frane sismo-indotte, includendo esplicitamente gli effetti dell'interazione suolo-struttura. Per le turbine offshore, con particolare riferimento a sistemi galleggianti in acque profonde, viene modellata l'interazione aero–idro–strutturale mediante simulazioni nel dominio del tempo che includono vento turbolento, moto ondoso e correnti marine. In entrambi i casi, si adottano modelli numerici avanzati, validati rispetto a benchmark di riferimento, per derivare curve e superfici di fragilità e per stimare metriche di rischio.

Un caso studio in Italia evidenzia come la combinazione dei pericoli possa influenzare in modo significativo le prestazioni delle turbine eoliche. In ambito onshore, le frane sismo-indotte possono risultare dominanti nel governare la domanda strutturale e la perdita di funzionalità delle turbine, mentre in ambito offshore l'accoppiamento tra vento e moto ondoso determina un'amplificazione della risposta strutturale. Le analisi di sensibilità consentono inoltre di quantificare l'impatto delle principali fonti di incertezza e di fornire indicazioni utili per la definizione di margini di progetto e criteri di verifica coerenti con prefissati obiettivi di affidabilità.

Parole chiave: rischio multi-hazard, turbine eoliche, funzioni di fragilità, progettazione basata sul rischio, OpenSees, OpenFAST.

Contents

Acknowledgements

I would like to express my sincere gratitude to my tutor, Prof. Fulvio Parisi, for his scientific guidance and support throughout the PhD programme.

I am also grateful to Prof. Alan O'Connor for supervising and supporting my research experience abroad, providing valuable insights and contributing to my academic growth.

I would like to thank the reviewers of this thesis, Prof. Nicola Caterino and Prof. Flavio Stochino, for their careful evaluation and constructive comments, which helped to improve the quality of this work.

The work was supported by the *Italian Ministry of University and Research* and *Ten Project s.r.l.*, within the framework of *the Next Generation EU programme and the Italian National Plan for Recovery and Resilience (PNRR).*

List of Acronyms

The following acronyms are used throughout the thesis.

HAWT	Horizontal Axis Wind Turbine
VAWT	Vertical Axis Wind Turbine
FEM	Finite Element Model
IDA	Incremental Dynamic Analysis
ABL	Atmospheric Boundary Layer
NWP	Normal Wind Profile
UHS	Uniform Hazard Spectra
PGA	Peak Ground Acceleration
PGV	Peak Ground Velocity
ULS	Ultimate Limit State
SLS	Serviceability Limit State
PL	Performance Level
IM	Intensity Measure
EDP	Engineering Demand Parameter
PSD	Power Spectral Density
SSI	Soil–Structure Interaction
RT	Reaction Time
TT	Travelling Time
TR	Time to Repair

OEMs	Original Equipment Manufacturers
BEM	Blade Element Momentum theory
FOWT	Floating Offshore Wind Turbine
MC	Monte Carlo
LHS	Latin Hypercube Sampling
SWL	Still Water Level

List of Figures

List of Tables

List of Symbols

The following symbols are used within the thesis

P Wind turbine output power

ρ_a Air density

v Wind speed

A Rotor swept area

z Tower elevation

z_g Gradient height

$v(z)$ Mean wind speed at height z

v_{hub} Mean wind speed at the hub height

h_{hub} Hub height above ground level

$F(z)$ Equivalent horizontal wind force associated with the wind speed at height z

$A(z)$ Tributary area of the tower elements at height z

F_{hub} Thrust force on the rotor

R_T Rotor radius

C_T Thrust coefficient

v_r Rated wind speed

$S_a(T)$ Spectral acceleration

D Permanent ground displacement

k_y Critical acceleration

r	Radius of the circular foundation
t	Thickness of the foundation
G	Shear modulus of the soil
ρ_S	Soil density
ν	Poisson's ratio of the soil
ξ	Equivalent damping ratio of the soil
ω_1	Fundamental frequency of the tower
K_S	Equivalent sway stiffness
K_R	Equivalent rocking stiffness
C_S	Equivalent sway damping coefficient
C_R	Equivalent rocking damping coefficient
σ	Meridional stress
τ	Shear stress
$\sigma_{x,Rd}$	Meridional design buckling stress
$\tau_{x\theta,Rd}$	Shear design buckling stress
k_x	Buckling reduction exponent for meridional stress
k_τ	Buckling reduction exponent for shear stress
Υ	Buckling interaction parameter
$\Delta\sigma_{Ed}$	Applied fatigue stress range
$\Delta\sigma_{Rd}$	Fatigue resistance (design stress range)
$\Delta\sigma_f$	Maximum applied stress range (fatigue demand)
$\Delta\sigma_c$	Detail category
γ_{FF}	Partial factor for fatigue loading
γ_{MF}	Partial factor for fatigue resistance
R	Seismic risk

H	Seismic hazard
V	Seismic vulnerability
E	Exposure
θ_{max}	Maximum chord rotation of the tower
Δ	Large displacement on top of the tower
$\mathcal{E}_m$	Average axial strain of electrical cable
$\mathcal{E}_y$	Yielding of electrical cable
$S_u(f)$	Power spectral density of the turbulent component of the wind
f	Wind fluctuation frequency
σ_u	Standard deviation of the turbulent component of the wind
I_u	Turbulence intensity
L_u	Integral length scale of the turbulence
μ	Median of the lognormal function
β	Logarithmic standard deviation of the lognormal function
R^2	Coefficient of determination of the regression model
D_v	Settlement at the center of gravity of the landslide-affected volume
α	Amplification coefficient
x_T	Turbine–slope distance
U_0	Free-stream wind velocity
U_1	Downstream wind velocity
u_{disc}	Wind velocity on the actuator disc
F_A	Axial thrust force acting on the rotor
A_{disc}	Actuator disc area

c	Local blade chord length
W	Relative wind velocity at the blade section
F_L	Lift force acting on the blade section
F_D	Drag force acting on the blade section
C_L	Lift coefficient of the airfoil
C_D	Drag coefficient of the airfoil
$\mathrm{S}(\omega)$	Wave energy spectral density
ω	Angular frequency
ω_p	Peak angular frequency of the wave spectrum
γ	Peak enhancement factor
g	Gravitational acceleration
H_s	Significant wave height
θ_{top}	Drift at the top of the tower
a	Nacelle acceleration
a_{max}	Threshold value of nacelle acceleration
M	Bending moment at the base of the tower
M_u	Ultimate bending moment capacity of the tower
T	Tension in the mooring line
T_{lim}	Limit tensile capacity of the mooring line
EDP	Engineering Demand Parameter
edp	Threshold value of the Engineering Demand Parameter
IM	Intensity measure

Chapter 1

Introduction

Experience is the hardest kind of teacher: it gives you the test first and the lesson afterward.

Oscar Wilde

1.1 Motivation

The need to reduce greenhouse gas emissions and to mitigate the effects of climate change has led, over recent decades, to a rapid expansion of renewable energy sources, among which wind energy plays a leading role. Owing to significant technological advancements and substantial investments, the wind energy sector has reached a high level of maturity, establishing itself as a reliable and competitive solution for electricity production.

In parallel with this growth, a marked dimensional evolution of wind turbines has been observed. Modern utility-scale machines exhibit hub heights exceeding 100 m and increasingly larger rotor diameters, both in onshore and offshore applications (see Figure 1.1.1). This development has made it possible to improve energy efficiency and to address the inherent challenge posed by the low energy density of wind, but it has also introduced new challenges from a structural perspective [1]. The increased slenderness of the towers, the concentration of masses at the top and the overall flexibility of the system make wind turbines particularly sensitive to environmental actions and dynamic phenomena.

A further important aspect concerns the installation context of wind energy systems. Onshore wind turbines are frequently located on ridges or mountainous slopes in order to maximize wind resources, often in areas characterized by high seismic hazards and complex geotechnical conditions. Offshore wind turbines, by contrast, are progressively installed in deep waters, where floating solutions become necessary and where the interaction between turbulent wind, wave motion and marine currents governs the structural behaviour. In both cases, wind turbines operate in environments where multiple natural hazards may act simultaneously or sequentially, leading to complex and potentially cumulative damage mechanisms.

Despite this, current design and verification practices are still predominantly based on single-hazard approaches, in which environmental actions are considered separately or combined through simplified schemes. Such approaches often prove inadequate to represent the actual level of structural demand and risk, particularly when secondary hazards come into play, such as earthquake-induced landslides in the onshore case or coupled wind–wave effects in the offshore context.

In light of these considerations, there is a clear need to adopt advanced methodologies based on probabilistic, performance-based and risk-oriented approaches, capable of accounting for uncertainties, interactions among natural hazards and the actual modes of collapse or loss of functionality of wind turbines. In this context, fragility analysis and multi-hazard risk quantification represent fundamental tools to support more informed design choices and effective risk mitigation strategies.

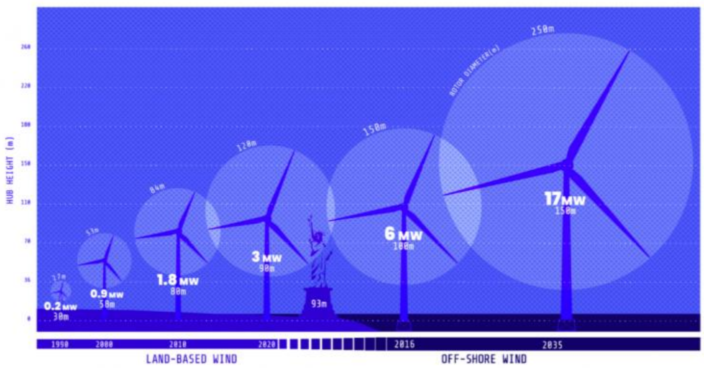

Figure 1.1.1 Trends in the size and power of wind turbines [2].

1.2 Objectives

The main objective of this thesis is the development and application of a multi-hazard risk-based analysis and design framework for wind turbines, capable of consistently integrating natural hazard characterization, structural vulnerability and risk quantification.

In particular, the thesis pursues the following objectives:

• Develop an integrated probabilistic approach for the assessment of the structural performance of wind turbines subjected to multiple natural hazards, overcoming the limitations of traditional deterministic and single-hazard approaches.

• Contribute to the state-of-the-art in the analysis of onshore wind turbines, explicitly addressing an aspect that is still scarcely explored in the literature and in professional practice, namely the combined effects of wind, earthquakes and earthquake-induced landslides for turbines installed on slopes or near unstable slopes. In this context, the role of soil–structure interaction and permanent ground displacements as potentially dominant factors in the structural response is analyzed.

• Develop fragility models based on nonlinear numerical analyses, capable of describing the probability of exceeding different performance levels as a function of the intensity of environmental actions.

• Extend the multi-hazard framework to the offshore context, with particular reference to floating wind turbines installed in deep waters, in which aero–hydro–structural interaction plays a central role. In this framework, the combined effects of wind, waves and marine currents are investigated through time-domain simulations.

• Provide engineering-relevant indicators, such as fragility curves and surfaces, annual performance exceedance rates, and economic loss metrics, aimed at supporting design decisions, safety assessments and risk mitigation strategies.

Overall, the thesis proposes and applies a performance-based and risk-oriented methodology, providing tools that are applicable both to the assessment of existing wind energy installations and to the design of future wind farms.

1.3 Organization of the thesis

The thesis is organized into seven chapters. Following this introductory chapter, Chapter 2 provides a critical review of the state of the art on wind turbine technology, structural modelling strategies, recurring failure modes and multi-hazard risk assessment methodologies. Chapter 3 focuses on onshore wind turbines, describing the characterization of environmental actions, the development of structural and soil–structure interaction models and their numerical implementation and validation. Chapter 4 introduces the proposed multi-hazard risk assessment framework for onshore turbines and applies it to a representative case study in a seismically active and landslide-prone area, with results expressed in terms of fragility, annual failure rates and economic losses.

In the following chapters, the focus shifts to offshore wind power. Chapter 5 provides an overview of offshore wind turbine technology and modelling approaches, while Chapter 6 presents detailed numerical analyses of a floating offshore wind turbine subjected to combined wind, wave and current loading, including sensitivity analyses and multi-variable fragility assessment. Finally, Chapter 7 summarizes the main findings of the thesis and outlines future research perspectives.

Chapter 2

State of the art

Progress in science depends on new techniques, new discoveries and new ideas.

Sydney Brenner

Wind energy is regarded as one of the most feasible renewable energy sources in light of global environmental challenges such as climate change.

In recent decades, the wind power sector has experienced rapid growth and significant dimensional evolution, characterized by a steady increase in hub height and rotor diameter, as discussed in Chapter 1. This trend, driven by the need to enhance energy capture under low wind speed conditions, has profoundly influenced both technological choices and the criteria adopted for structural design and verification, as will be discussed in more detail later.

From a technological perspective, the increase in blade lengths has been made possible by the use of advanced composite materials (glass and carbon fibers), optimized structural configurations and advanced active control strategies (pitch and yaw systems). Tower technology has evolved from tubular steel solutions to hybrid steel-concrete configurations and, more recently, to prestressed concrete towers for tall onshore applications [3]. In the offshore sector, the increase in turbine capacity has promoted the adoption of large diameter monopiles and jacket structures for intermediate water depths, while in deep waters, floating platforms (spar, semisubmersible types) have become more widespread, enabling larger rotors and higher hub heights [4].

The dimensional evolution of wind turbines has direct implications for modelling and verification. Consequently, there is growing attention to aeroelastic phenomena and soil-structure interactions in onshore applications, as well as to fluid–structure interactions in offshore environments. For onshore installations located in seismic areas, the increase in mass and slenderness requires careful consideration of the combined effects of wind and earthquake loading, as well as the potential impact of earthquake-induced slope instabilities. In the offshore field, the coupled wind-wave-current interaction, and for floating structures the dynamics of the mooring-platform system, introduce advanced modelling requirements and the need for integrated probabilistic analyses.

There is also a growing availability of operational data from SCADA (Supervisory Control and Data Acquisition) systems and digital twins, which enable the calibration of numerical and dynamic models and the implementation of predictive maintenance strategies [5], [6]. These tools, together with the continuous evolution of technical standards and design guidelines, are fostering the adoption of performance-based approaches and reliability-based design and risk assessment methodologies.

Given this scenario, it is evident that the scientific literature has also evolved to keep pace with the rapid technological and dimensional transformation of the sector. In the onshore field, many aspects are now well established thanks to a broad base of studies and experimental validations, whereas in the offshore context, particularly for floating systems, several issues remain under investigation, requiring innovative modeling approaches. In this context, the present chapter aims to provide a clear overview of the current state of the art, focusing on the main topics addressed in the following sections: turbine typologies and construction technologies, recurring failure modes, structural modelling strategies and multi-risk analysis.

2.1 Wind Turbine Types and Technologies

The design of wind turbines is governed by various standards and supporting documents that specify a comprehensive set of design requirements. The most widely recognized standards are provided by the *International Electrotechnical Commission* (IEC) 61400 series, which are complemented by other standards, such as *Det Norske Veritas - Germanischer Lloyd* (DNV GL) standards and recommendations and those issued by the *International Organization for Standardization* (ISO).

The IEC 61400-1:2005 standard [7] and DNV's Guidelines for Design of Wind Turbines [8] establish the fundamental requirements for the design of onshore wind turbines. Wind turbines can be classified according to their axis configuration, mainly into horizontal axis wind turbines (HAWTs) and vertical axis wind turbines (VAWTs), as illustrated in Figure 2.1.1. Commonly used HAWTs feature blades that rotate around a horizontal axis and are typically installed on tall towers to maximize exposure to the wind. In contrast, VAWTs are generally shorter and designed to capture wind from any direction, making them more suitable for use in urban environments or areas characterized by low wind speeds.

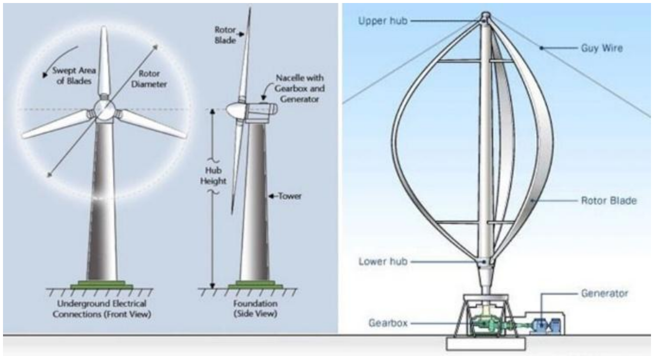

Figure 2.1.1 Horizontal VS Vertical Axis Wind Turbines [9].

In addition to design aspects, construction technologies are continuously evolving, introducing innovations aimed at enhancing the efficiency and durability of wind turbines. Advanced materials, such as carbon fiber reinforced composites, are now frequently used to optimize the aerodynamic and structural performance of turbine blades [10], [11]. Furthermore, recent advances in control and monitoring systems enable more accurate management of power generation, allowing real-time response to changing wind and weather conditions.

In 2019, General Electric developed the first prototype of the Haliade-X wind turbine, which was subsequently commercialized in 2021. This model has a rated capacity of 12 MW and a total height of approximately 260 m, about five times the height of the Arc de Triomphe in Paris, as shown in Figure 2.1.2. Over the course of a year, this turbine can generate around 67 GWh of electricity, sufficient to meet the annual energy demand of approximately 16000 households.

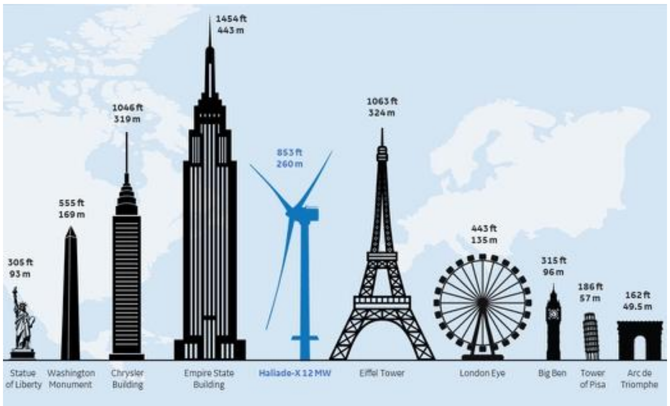

Figure 2.1.2 The Haliade-X wind turbine with a capacity of 12 MW [12].

Subsequently, the Vestas V236 15 MW became widely recognized as the first 15 MW model to be introduced to the market in February 2021. The installation of the first prototype was completed in December 2022 at the National Test Centre in Osterild, Denmark. With a swept area exceeding 43000 m², the V236-15 MW shifts the boundaries of wind energy production, reaching an annual output of approximately 80 GWh. The turbine was designed to deliver exceptional performance while reducing the number of units required per wind farm.

Consequently, turbine technology has advanced considerably, leading to a substantial increase in structural and energy performance. Turbines with capacities of up to 18 MW have now been achieved, such as the model developed by MingYang Smart Energy Group [13], which reaches a total height of approximately 305 m. As turbine size continues to increase, growing attention is being devoted to structural analysis, since these systems now exhibit configurations of increasing complexity and demand more sophisticated modeling and design approaches.

2.2 Operational range of the wind turbine

Each wind turbine is characterized by a specific power curve, which describes the relationship between wind speed and the instantaneous electrical power output delivered by the generator. The operational range of a wind turbine is defined by two characteristic wind speeds. The cut-in wind speed, which is the minimum wind speed at which the turbine starts generating electricity, and the cut-off wind speed, which is the maximum wind speed at which the turbine can safely operate. Another characteristic wind speed is the rated wind speed. It is the wind speed at which the rated (nominal) power of a wind turbine is reached. The rated power represents the maximum continuous electrical output that the generator is designed to deliver under standard operating conditions. Beyond this point, control systems (such as pitch and yaw regulation) limit the aerodynamic efficiency to maintain the power output constant and prevent mechanical overload. These three wind speeds are shown in the power curve of wind turbines (see Figure 2.2.1).

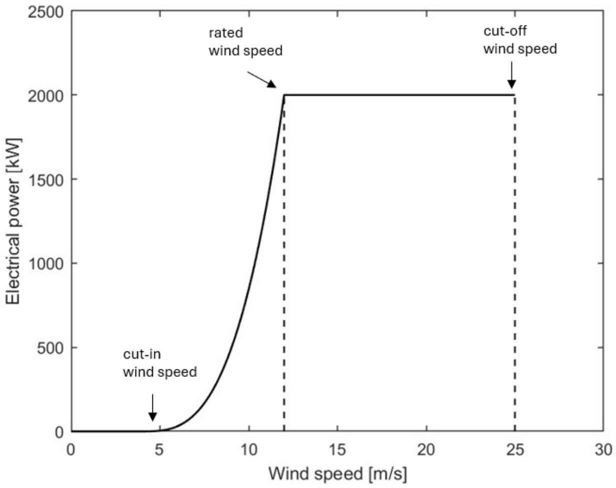

Figure 2.2.1 Power curve of a wind turbine.

When the wind speed reaches the cut-in threshold, the turbine begins to operate, and the power output increases approximately with the cube of the wind speed until the rated value is attained. Once the maximum tolerated threshold is exceeded, the turbine automatically shuts down to prevent structural damage.

2.3 Recurring failure modes

A preliminary study was carried out to identify the main causes that can lead to the failure of one or more wind turbine components. Studies in the scientific literature by Chou et al. (2011 [14], 2019 [15]) present a collection of cases of damaged wind turbines from various countries, providing an in-depth understanding of the main causes of failure of these structures. Observations indicate that 52.2% of large-scale wind tower collapses were caused by high winds and storms. Descriptive statistical analysis of 44 failure cases identified between 1997 and 2009 shows that storms (34.1%) and high winds (18.1%) were the primary external forces responsible for turbine collapses worldwide. Therefore, storms and high winds should be regarded as the main factors when assessing risks throughout the life cycle of a wind turbine, from planning and design to construction and operation.

Other identified causes included fire (five cases), ice storms (four cases), material fatigue (three cases), impact of the blade on the tower (three cases), lightning (two cases), faulty welds (two cases) and braking system failure (two cases), as illustrated in Figure 2.3.1.

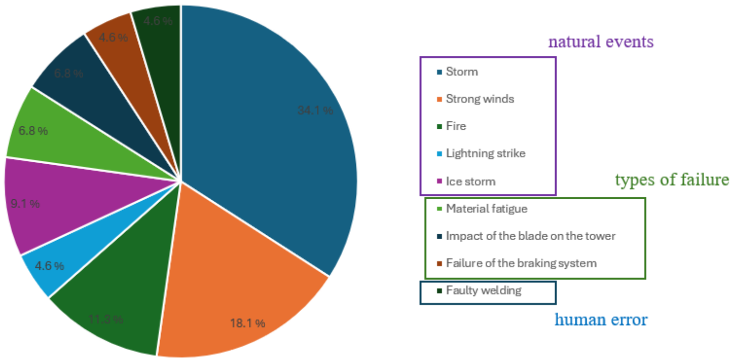

Figure 2.3.1 Main causes of tower collapse in the period 1997-2009: 44 collapses.

The integration of data from the literature and industrial evidence made it possible to outline a mapping of the most recurrent failure modes for each component of the wind turbine. To provide an overview of the main elements and their interconnections, Figure 2.3.2 illustrates the principal components of a horizontal-axis wind turbine. This diagram shows the main mechanical, electrical and control systems that contribute to converting the wind’s kinetic energy into electrical energy.

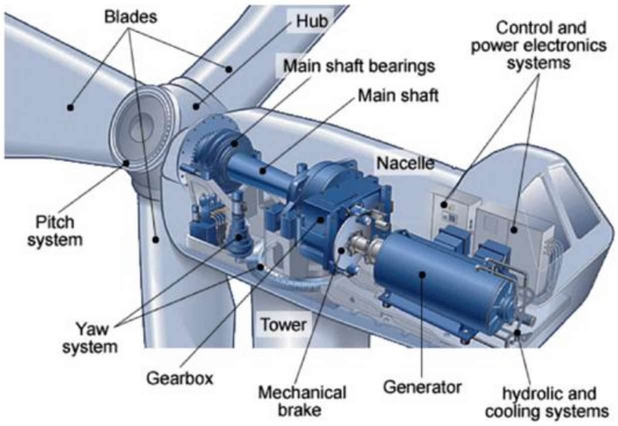

Figure 2.3.2 Typical main components of a horizontal-axis wind turbine [16].

After identifying the main subsystems of a wind turbine, it is possible to analyze in detail the potential failure modes associated with each component. Table 2.3.1 summarises the main subsystems, their corresponding components, and the most frequent related failure modes, as also discussed in several studies from the literature [16], [17], [18].

Table 2.3.1 Overview of the main wind turbine subsystems with typical components and associated failure mechanisms.

WT subsystems	Components	Possible failures
Rotor	Blades	Deterioration, cracking and adjustment error
	Bearings	Spalling, wear, defect of bearing shells and rolling element
	Shaft	Fatigue and crack formation
Drive train	Main shaft bearing	Wear and high vibration
	Mechanical brake	Locking position
	Gearbox	Wear, fatigue, oil leakage, insufficient lubrification, breaking in teeth, displacement and eccentricity of toothed wheels
Generator		Wear, electrical problems, winding damage, rotor asymmetries, bar break, overheating and over speed
Auxiliary systems	Yaw system	Yaw motor problem, brake locked and gear problem
	Pitch system	Pitch motor problem
	Hydraulic system	Pump motor problems and oil leakage
	Sensors	Broken and wrong indication
Electrical system	Control system	Short circuit, component fault and bad connection
	Power electronics	Short circuit, component fault and bad connection
Tower	Nacelle	Fire and yaw error
	Tower	Crack formation, fatigue, excessive deformation, foundation weakness
System transformer		Problem with contamination, breakers, disconnectors and isolators

It is observed that the most common failures concern the mechanical subsystems, in particular the rotor and the drive train, where wear, fatigue, loss of lubrication, and cracking represent the predominant causes.
The auxiliary and control subsystems (yaw, pitch and hydraulic systems) are instead more prone to electrical and hydraulic issues, often related to motor malfunctions or oil leaks.
As for the tower and the system transformer, the main failures originate from vibrations, contamination, or structural failures, which can compromise the overall stability of the system.

The analysis of the main failure modes of wind turbine components represents a fundamental preliminary step for the subsequent vulnerability assessment and risk analysis of the structure. Understanding the damage mechanisms and their underlying causes makes it possible to identify the system's critical points and to more consciously define the performance levels to be adopted during the structural behaviour assessment phases.

From this perspective, the results obtained provide the conceptual basis for the analyses presented in the following sections.

2.4 Structural modelling and analysis

Accurate structural modelling of wind turbines represents a fundamental step for the reliable prediction of their response under the combined action of environmental loads. Wind turbines are tall, slender and dynamically sensitive systems, subjected to time-varying loads of aerodynamic, gravitational, and in many cases, seismic origin. The complex interaction between rotor, nacelle, tower and foundation requires the use of models capable of realistically representing both the global behaviour of the structure and the local stresses in critical areas.

Finite element models (FEM) are used in the design phases, which allow a detailed representation of the wind turbine, including any geometric nonlinearities and local instabilities. These models also allow to analyze the mechanisms of local collapse and to accurately evaluate the distribution of stresses and deformations.

The dynamic behaviour of wind turbine towers plays a crucial role, as resonance phenomena can cause significant amplification of displacements and stresses. In this context, Bernuzzi et al. (2015) [19] analyzed the dynamic performance of steel wind turbine towers, highlighting the high sensitivity of slender structures to resonance effects. The authors demonstrated that an inaccurate estimation of modal properties can lead to severe fatigue damage or even tower collapse. Their work proposed several mitigation strategies, including stiffness optimization through geometric modification, the use of additional damping devices and the definition of structural configurations capable of shifting the fundamental frequency outside the critical excitation range. This study emphasizes the importance of accurate dynamic modelling and the direct link between design choices and the operational safety of the system.

A fundamental contribution to the modelling of steel wind turbine towers was provided by Lavassas et al. (2003) [20], who presented one of the first comprehensive numerical analyses of a full-scale 1 MW wind turbine tower. The authors developed and validated a detailed finite element model, taking into account the effects of geometric imperfections and the construction details of the joints. The study highlighted the need to adopt advanced nonlinear analyses and to calibrate numerical models through experimental data in order to ensure the reliability of predictions. The work of Lavassas et al. laid the foundation for modern design procedures that integrate numerical modelling, experimental validation, and probabilistic approaches.

In recent years, the evolution of computational tools and the availability of field monitoring data have enabled the development of increasingly realistic models. In addition to these advances, a transition has occurred from traditional deterministic approaches towards risk-based and performance-based analysis and design methodologies. In this context, structural modelling is no longer seen merely as a tool for strength verification, but as the basis for the probabilistic assessment of reliability under multiple hazards. The integration of uncertainties related to materials, loads and model parameters now allows for the quantification of structural fragility and risk, supporting the development of multi-hazard design procedures that account for the combined effects of wind, earthquakes and other environmental events.

2.5 Multi-Hazard Risk Analysis

Multi-hazard analysis considers systems that may be threatened by more than one natural hazard, such as energy infrastructures located in seismically active regions, which may be subject to both earthquakes and secondary, potentially damaging seismic events, such as landslides and land liquefaction. Several previous studies have examined multi-hazard modelling with respect to the combined effects of wind and seismic actions. Among these, Asareh et al. (2016) [21] developed a finite element model of a 5 MW wind turbine (National Renewable Energy Laboratory) to evaluate the nonlinear structural response of the system under the combined action of wind and earthquake loading. The authors integrated aerodynamic and seismic analyses through incremental dynamic simulations (IDA) and computed fragility curves, highlighting how the interaction between aeroelastic loads and seismic excitations can significantly influence the probability of structural damage. The results showed that, although seismic loads are predominant, wind intensity can accelerate the attainment of damage limit states, especially when the turbine operates near its rated wind speed. A similar approach, but extended to the offshore context, thus including the combined effect of wave motion in addition to wind and seismic actions, was recently proposed by Zhang et al. (2023) [22]. The authors developed a multi-hazard fragility model for offshore wind turbines with monopile foundations, showing that seismic and environmental loads can generate comparable structural effects under realistic operating conditions. They integrated nonlinear dynamic simulations under simultaneous wind, wave, and earthquake loading to construct the multi-hazard fragility framework. The proposed framework allows the evaluation of the probability of exceeding damage limit states as a function of multiple hazard intensities, demonstrating that the interaction between environmental and seismic loads can significantly amplify the structural demand compared to single-hazard analyses. The results highlighted that, under realistic operating conditions, the combined effects of wave motion and wind can contribute to an increase in the global response of the tower and foundation, making an integrated assessment of multi-hazard risk essential.

In this thesis, attention is devoted to the cumulative damage to wind turbines caused by seismic shaking and landslides, as this topic has yet to be fully explored despite its critical importance in hilly and mountainous regions. Therefore, part of this research, as will be discussed in the following chapters (Chapter 3 and Chapter 4), aims to fill this research gap by developing a methodology for the seismic fragility assessment of onshore wind turbines located upstream of slopes in seismically active areas. The proposed fragility models incorporate both primary and secondary seismic effects, providing a more comprehensive evaluation of the seismic risk of wind turbines.

Most often, in multi-hazard analyses, individual hazards are considered separately, even though natural processes may be interconnected rather than independent, and interactions among hazards can produce effects that are not captured by single-hazard analyses. Multi-hazard analysis is employed for risk assessment by considering the simultaneous or sequential occurrence of multiple hazards at the site of interest. Instead of analyzing each hazard independently, multi-hazard analysis should ideally account for the interactions and combined effects of various natural events.

Hazard analysis quantifies the degree of threat to which a site of interest is exposed to a natural phenomenon by evaluating, through probabilistic approaches, the frequency of events whose intensity exceeds a given threshold. The intensity measures of a natural event are physical quantities that characterize its magnitude and severity. A natural event has an intrinsically random nature, as its time of occurrence, location, intensity, and triggering cause cannot be predicted with certainty.

In this thesis, the concept of multi-hazard risk is analyzed as a cascading risk, since the case under study concerns landslides that can be triggered by the same seismic events. According to the *Catalogue of Earthquake-Induced Ground Failures in Italy* (CEDIT, 2017) [23], more than half of the ground effects recorded after earthquakes in Italy consist of landslides (55%), followed by ground cracking (23%), liquefaction phenomena (13%), morphological changes of the ground surface (5%), and surface faulting (4%), as illustrated in Figure 2.5.1.
These data confirm that landslides represent the most frequent type of secondary earthquake-induced effect, highlighting the strong interconnection between seismic hazard and slope instability in the Italian context.

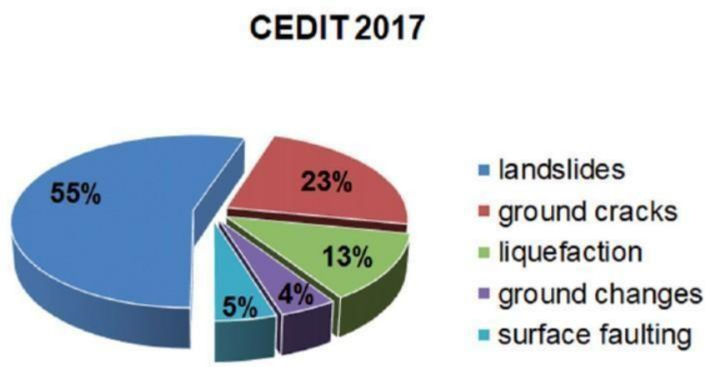

Figure 2.5.1 CEDIT statistics on the effects of earthquakes on the ground in Italy [23].

High-magnitude earthquakes can produce significant co-seismic deformations that, in morphologically complex settings, promote the triggering of landslides and mass movements. In areas characterised by steep slopes and fractured or weathered lithologies, even moderate seismic accelerations can compromise slope stability, generating rockfalls, slides or flows. Historical events such as those in Friuli (1976), Irpinia (1980) and Central Italy (2016) have shown that the interaction between seismic hazard and mountainous morphology increases the probability of earthquake-induced landslides and, consequently, the associated risk for existing infrastructures [24]. Furthermore, identifying a well-defined area for risk assessment is challenging, as seismic sources capable of triggering significant landslides may be located at considerable distances from the site of interest. Therefore, this thesis will examine in detail how to address this scenario, still scarcely explored in scientific literature and will apply the developed methodology to a case study.

Chapter 3

Onshore Wind Turbines

The science of today is the technology of tomorrow.

Edward Teller

The analysis of onshore wind turbines represents the first step in applying the multi-hazard risk assessment framework developed in this thesis. After analyzing the main structural characteristics of wind turbines and existing approaches to risk assessment in Chapter 2, attention now turns to defining a numerical model capable of coherently describing the structural response of a turbine subjected to different natural hazards.

Onshore wind turbines are widespread energy infrastructures. Their exposure to potentially concurrent natural phenomena, such as wind, earthquakes and secondary seismic events, requires an integrated approach that allows for a quantitative assessment of the combined effects of these actions on structural safety. Therefore, we initially analyze the actions acting on the structure, discussing their physical characterization and modelling criteria. Next, we proceed with the analysis of the structural model and its numerical implementation in OpenSees, where the model is validated by comparison with experimental data and simulations found in the literature. Finally, a safety assessment is carried out in accordance with the main design codes, as a reference for performance analysis. The results obtained form the basis for subsequent extensions of the proposed framework, aimed at including additional and more complex multi-hazard scenarios.

3.1 Identification of actions

The structural behaviour of onshore wind turbines is governed by a combination of various mechanical and environmental actions. Proper identification and characterization of these actions is a fundamental step in the modelling and safety assessment process, as they directly affect the design loads and dynamic response of the structure.

In general, the actions acting on wind turbines can be classified as persistent, transient and accidental, according to structural design standards such as IEC 61400-1 [7] and EN 1990:2002 [25]. Persistent actions include the self-weight of the tower, nacelle and rotor. Transient and accidental actions are mainly associated with wind, seismic action and geotechnical phenomena that may be triggered by seismic events.

Among these, wind represents the primary operating force governing energy production. Seismic action, on the other hand, is considered an accidental action, relevant for installations located in seismically active areas. In such areas, the dynamic interaction between the tower, foundation and soil can significantly influence not only the global response of the turbine, but also the interruption of electricity production caused by the failure of the associated electrical systems. Finally, phenomena triggered by seismic events, such as earthquake-induced landslides, constitute a secondary but potentially critical hazard for turbines installed on slopes or unstable ground, as they may cause foundation displacements and loss of bearing capacity.

3.1.1 Wind

Wind is one of the main environmental agents acting on structures and, in particular, on wind turbines. When wind blows over the Earth's surface, it generates a frictional force that opposes the motion of the air, reducing its speed in the layers closest to the ground. The effect of this force extends vertically up to a certain altitude, called the gradient height z_g, which delimits the Atmospheric Boundary Layer (ABL). Above z_g, where the influence of friction becomes negligible, the wind is defined as friction-free wind (FFW). Within the ABL, the friction force increases progressively from zero to $z = z_g$, resulting in an increasing vertical profile of wind speed, as shown in Figure 3.1.1. In wind engineering, in accordance with CNR-DT 207 R1/2018 guidelines [26], it is established practice to represent the instantaneous wind speed $V(t)$ in the atmospheric boundary layer as the sum of a mean component and a fluctuating component, according to the relationship:

$$V\ (t) = \bar{V} +\ v\ (t) \tag{1}$$

where $\bar{V}$ is the mean wind speed in stationary conditions, depending on the exposure category and terrain roughness. This component is typically described by a power law or logarithmic law, which expresses the increase in wind speed with height (Figure 3.1.1). On the other hand, $v(t)$ represents turbulence, that is the turbulent fluctuations of speed around the mean value. The turbulent component is generally treated as a stationary Gaussian stochastic process, described by statistical parameters such as turbulence intensity, gust factor and power spectra. In general, turbulence intensity decreases with altitude due to the reduced influence of surface roughness on atmospheric flow (CNR-DT 207 R1/2018, §2.3–2.6).

According to the World Meteorological Organization (WMO), the mean wind speed is calculated over a reference period of $T = 10$ minutes, which is considered long enough to ensure the stationarity of the process and short enough to capture the main short-term fluctuations.

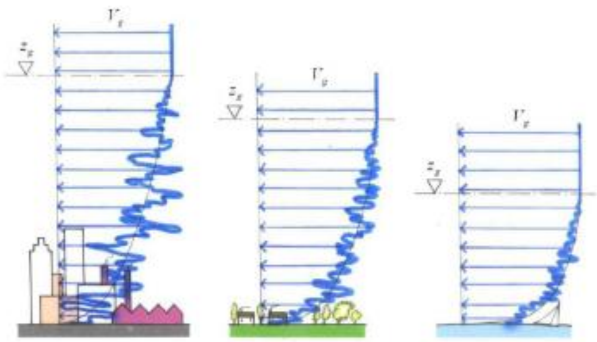

Figure 3.1.1 Representation of wind speed characteristics for different site conditions (adapted from [26]).

As illustrated in Figure 3.1.1, the mean wind profile increases with height, while the fluctuating components gradually become more attenuated. This representation provides a rigorous physical basis for modelling wind actions on structures, distinguishing between the statistically persistent effect and the dynamic fluctuating effect.

For the purposes of modelling wind actions on the turbine under study, a simplified approach in line with the requirements of ASCE/SEI 7-10 (2010) [27] and IEC 61400-3 (2009) [28] is adopted. Although this approach neglects the fluctuating wind component, it is adequate for evaluating equivalent static loads along the height of the tower and allows the mean wind profile to be represented through the Normal Wind Profile (NWP) model.

For a standard class wind turbine, the mean wind speed along the tower height is described through the power-law profile reported in Eq. (2), from which equivalent horizontal forces are derived through Eq. (3):

$$v\,(z) = v_{hub} \cdot \left(\frac{z}{h_{hub}}\right)^{\alpha} \tag{2}$$

$$F\,(z) = 0.5 \cdot \rho_a \cdot v(z)^2 \cdot A(z) \tag{3}$$

In these equations, $v\ (z)$ indicates the mean wind speed at the height z, while v_{hub} represents the mean wind speed at the hub height. For normal wind conditions, v_{hub} is commonly assumed equal to the rated wind velocity v_r, both taken as 15 m/s, which is a typical value at which most wind turbines operate at constant power. The parameter α is assumed equal to 0.2 in accordance with ASCE/SEI 7-10, h_{hub} is the vertical distance between the hub centre and the ground level, ρ_{a} is the air density (assumed equal to 1.25 kg/m³), and $A(z)$ is the tributary area of the tower elements. The term $F(z)$ represents the nodal wind forces associated with the wind velocity at height z.

In addition to the distributed forces acting on the tower, the thrust force on the rotor is also considered. This force is evaluated using a simplified model that expresses the horizontal force acting on the hub as follows [29]:

$$F_{hub} = 0.5 \cdot \rho_a \cdot {v_{hub}}^2 \cdot \pi \cdot R_T \cdot C_T \tag{4}$$

where R_T is the rotor radius and C_T represents the thrust coefficient, calculated as follows:

$$C_T = 3.5 \cdot v_r \cdot \frac{2\ \cdot v_r + 3.5}{v_{hub}^3} \tag{5}$$

The latter coefficient describes the efficiency with which a wind turbine converts the kinetic energy of the wind into thrust force on the rotor [30].

The approach adopted allows the general theoretical and regulatory framework proposed by CNR-DT 207 R1/2018, which describes wind as a three-dimensional turbulent phenomenon, to be linked to a simplified engineering model based on the mean wind profile. This choice is consistent with international standards for wind turbines and allows for an effective representation of the equivalent static wind actions required for the structural analysis of the wind turbine.

3.1.2 Earthquake

Earthquakes represent one of the most significant environmental actions in the design and verification of structures, particularly for wind towers which, being slender structures, can be sensitive to dynamic excitations. However, when considering seismic actions, this sensitivity is not always straightforward, since the first natural frequencies of such slender systems are often lower than the predominant frequencies of typical earthquakes. Nevertheless, higher vibration modes and second order (P–Δ) effects may contribute significantly to the overall seismic response and should therefore be properly taken into account in the dynamic analysis.

In structural analysis, seismic action may be represented in the form of an equivalent static load or through dynamic analysis (linear or non-linear), depending on the complexity of the problem and the objectives of the study.

The main reference standards, Eurocode 8 (EN 1998-1) [31] and the Norme tecniche per le costruzioni (NTC 2018) [32], define seismic action through the elastic response spectrum in acceleration, constructed as a function of the structure's natural period, the subsoil category and the expected seismic intensity at the site.

In particular, NTC 2018 adopts a fully site-dependent approach, deriving seismic actions directly from the Uniform Hazard Spectra (UHS) studies of the Istituto Nazionale di Geofisica e Vulcanologia (INGV). These studies provide, for each node of 5-km grid, the spectral acceleration values $S_a(T)$ corresponding to different return periods. In this way, the design spectrum is consistent with the local seismic hazard and depends on the parameters: nominal life, use class and the considered limit state.

The seismic input used in dynamic analyses must therefore represent the design seismic scenarios, ensuring spectral compatibility with the reference site. For this purpose, the UHS associated with the study area, representative of potential onshore wind farm locations, typically characterised by wide open areas, has been adopted.

The selection of real ground motions was carried out using REXEL software (Iervolino et al., 2009) [33], which allows the identification of sets of accelerometric recordings from the European Strong-Motion Database that are compatible, on average, with the target UHS. A detailed selection of accelerograms compatible with the design spectrum for the L’Aquila site, adopted as the case study in this work, is presented in Section 4.1.

3.1.3 Earthquake-induced landslides

Earthquakes are one of the main triggering mechanisms of landslides in hilly and mountainous areas, where pre-existing geomorphological and geotechnical conditions make slopes particularly vulnerable. Seismic activity can alter the static equilibrium of slopes through the application of inertial forces that reduce the slope's safety factor, promoting shallow or deep-seated sliding, rockfalls and debris flows [34]. The response of the ground to an earthquake depends on multiple factors, including local morphology, the mechanical properties of the materials, soil saturation and the intensity of ground motion.

Numerous studies ([35], [36]) have shown that the spatial extent and density of earthquake-induced landslides are strongly correlated with seismic parameters such as Peak Ground Acceleration (*PGA*) and Peak Ground Velocity (*PGV*), as well as slope stiffness and inclination. Past events, such as the 2009 L'Aquila earthquake or the 2016 Amatrice-Norcia earthquake, have highlighted the combined hazard posed by seismic shaking and slope instability, with amplified destructive effects on infrastructure, buildings and energy facilities located near slopes.

In the context of the design and structural analysis of onshore wind turbines, consideration of earthquake-induced landslides is particularly important, as these installations are often located in hilly or mountainous areas, where topographic conditions ensure favourable wind exposure but simultaneously increase landslide susceptibility. The loss of slope stability may compromise not only the turbine foundation, but also the integrity of auxiliary infrastructure, such as underground or surface electrical cables, which extend for several kilometres to convey the energy produced to substations or collection centres.

For the purposes of quantitatively assessing the permanent ground displacement (D) induced by seismic action, the empirical model proposed by Fotopoulou and Pitilakis (2015, 2017) [37], [38] was adopted. This model, derived from an extensive database of numerical simulations and experimental observations, expresses the logarithm of the slope displacement as a function of the main seismic and geotechnical parameters, according to the following relationship:

$$\ln(D) = -8.360 + 1.873\ln(PGV) - 0.347\ln\left(k_y/PGA\right) - 5.964k_y \pm 0.64\varepsilon \qquad (6)$$

In Eq. (6), ε is the normally distributed standard variable with zero mean and unit standard deviation, while the value 0.64 represents the logarithmic standard deviation. In order to apply the formulation proposed by Fotopoulou and Pitilakis to a quantitative assessment of earthquake-induced permanent ground displacements, the model was implemented by considering different slope stability conditions, represented through discrete values of the critical acceleration k_y, which depends on the geometric and mechanical properties of the slope. Five values of k_y were therefore assumed: 0.05 g, 0.10 g, 0.15 g, 0.20 g and 0.25 g. For each k_y value, 100 PGA levels were considered, ranging from 0 to 1 g. For each combination of k_y and PGA, 10^4 random displacement realizations were generated using the Monte Carlo method, in order to obtain a statistically representative sample of co-seismic displacement.

The displacements obtained represent a fundamental input parameter for the subsequent assessment of the soil-structure interaction for the wind turbine, as they allow the quantification of the differential effects of movement that may affect the dynamic response of the tower and the overall stability of the installation. In particular, these D values are used to define equivalent static load scenarios, which simulate the permanent effects of soil deformation due to earthquake-induced landslides.

3.2 Structural modelling

Structural modelling of wind turbines is an essential step for understanding and interpreting the dynamic behaviour of the system in the presence of different environmental actions. In this work, a numerical model of the 5 MW wind turbine defined by the National Renewable Energy Laboratory (NREL) was developed. This turbine, widely documented in scientific literature, is commonly adopted as a reference model for both onshore and offshore configurations [39] and is frequently used as a benchmark for numerical analyses and code-to-code comparisons.

The use of this reference configuration made it possible to represent the dynamic response of the wind tower in a simplified but physically consistent manner, including its interaction with the foundation soil. To this end, the structural system was modelled according to two different configurations: the first, with a fixed base, which is the reference condition commonly assumed in analytical studies; the second, with an elastic and damped base, which allows the effects of soil deformability on the overall response of the structure to be evaluated.

The comparison between the two models enables the quantification of the influence of boundary conditions and, in particular, the analysis of the additional effects induced by a potential earthquake-induced landslide, which would otherwise not be captured in a rigid-base model. This comparison is therefore fundamental for understanding the global dynamic behaviour of the system and for providing a more realistic evaluation of the turbine’s response to the combined actions of seismic loading and ground deformation.

3.2.1 Reference turbine: NREL 5 MW modelling framework

This section describes the reference wind turbine selected for the case study, namely the NREL 5 MW turbine, which is adopted as a benchmark for the subsequent numerical analyses.

The NREL 5 MW wind turbine is a three-bladed, horizontal-axis machine featuring a rotor with a diameter of 126 m and a tapered steel tower 87.6 m above ground level. It represents a typical configuration of large-scale turbines currently installed in onshore sites and provides a well-established reference for numerical modelling and validation.

From a mechanical point of view, the turbine was represented following the approach proposed by Lavassas et al. (2003) [40], using a finite element model (FEM) in which the tower is discretized into a set of lumped masses m_i distributed along its height, while the combined mass of the nacelle and rotor is represented by a concentrated mass m_0 located at the tower top (Figure 3.2.1). This schematisation captures the main aspects of the structural behaviour of the wind turbine, enabling effective analysis of modal and dynamic responses.

The modelling choice of representing the nacelle–rotor assembly through an equivalent concentrated mass is motivated by the primary focus of the present study on the global dynamic response and stability of the supporting tower–foundation system. Since the detailed aeroelastic behaviour of the blades is not explicitly investigated, their contribution is accounted for in an equivalent manner, allowing a significant reduction in computational complexity while preserving the essential dynamic characteristics of the system.

The tower is made of S355 steel, characterised by an elastic modulus of 210 GPa, a density of 7850 kg/m³ and a Poisson's ratio of 0.3. The cross-section varies linearly along the height, in accordance with the data provided in the NREL model, as illustrated by sections A-A and B-B in Figure 3.2.1. The main geometric and mass properties of the reference turbine are reported in Table 3.2.1.

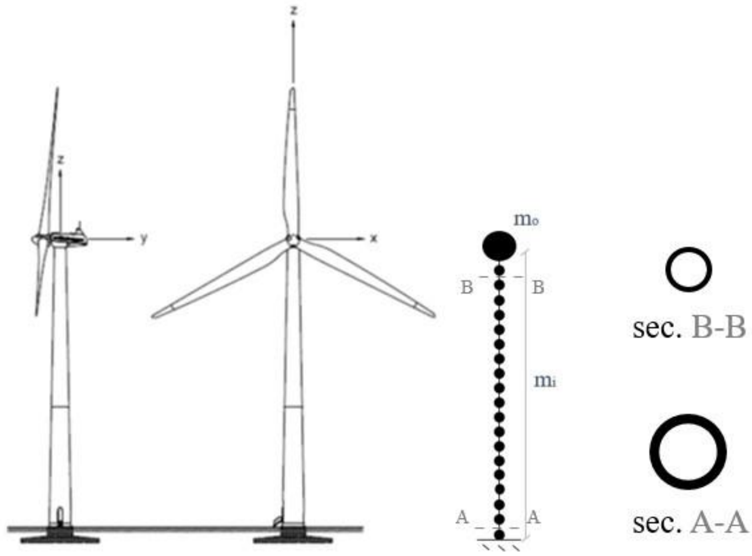

Figure 3.2.1 Schematic representation of the NREL 5 MW wind turbine model, including cross-sections A-A and B-B.

Table 3.2.1 Main geometric and mechanical characteristics of the NREL 5 MW wind turbine.

Rated Power	5 MW
Rotor Orientation, Configuration	Upwind, 3 Blades
Rotor, Hub Diameter	126 m, 3 m
Tower-Top Height Above Ground Level	87.6 m
Cut-in, Rated, Cut-out Wind Speed	3 m/s, 11.4 m/s, 25 m/s
Cut-in, Rated Rotor Speed	6.9 rpm, 12.1 rpm
Tower Base Diameter (section A-A)	6 m
Tower Base thickness	0.027 m
Tower Top Diameter (section B-B)	3.87 m
Tower Top thickness	0.019 m
Rotor Mass	110000 kg
Nacelle Mass	240000 kg
Tower Mass	347460 kg

With regard to the foundation, two configurations were considered, as shown in Figure 3.2.2. In the fixed-base model, the tower is rigidly constrained to the ground, assuming that the deformability of the soil is negligible (Figure 3.2.2 a). In the elastic and damped base model, the foundation is represented by the so-called ‘sway-rocking model’, introduced by Kitahara and Ishihara (2022) [41], in which the soil-structure interaction (SSI) is idealised by a pair of equivalent springs and dashpots arranged in the sway and rocking directions (Figure 3.2.2 b). The mechanical parameters of the springs and dashpots were determined on the basis of the formulations proposed by Gazetas ([42], [43], [44]) as a function of the mechanical properties of the soil and the geometry of the foundation.

Considering a shallow foundation with a circular plan with radius r and thickness t, resting on homogeneous soil with shear modulus G, density ρ_S and Poisson's ratio ν, the equivalent sway (K_S) and rocking (K_R) stiffnesses are expressed as:

$$K_S = \frac{8 \cdot G \cdot r}{2 - \mathrm{v}} \tag{7}$$

$$K_R = \frac{8 \cdot G \cdot r^3}{3 \cdot (1 - \mathrm{v})} \tag{8}$$

The equivalent damping coefficients are given by:

$$C_S = \frac{2 \cdot \xi \cdot K_S}{w_1} \tag{9}$$

$$C_R = \frac{2 \cdot \xi \cdot K_R}{w_1} \tag{10}$$

where ξ is the equivalent damping coefficient of the ground and ω_1 is the fundamental frequency of the tower.

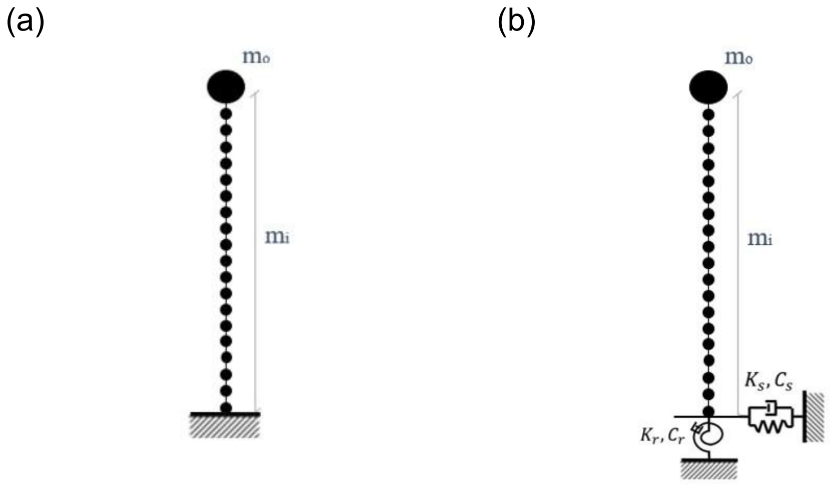

Figure 3.2.2 Wind turbine structural model: (a) fixed-base configuration and (b) soil–structure interaction (SSI) model.

The second foundation configuration, which is more physically realistic, allows assessment of the impact of soil deformability on the dynamic characteristics of the tower. In particular, the introduction of the elastic base leads to an increase in tower-top displacement, which has significant effects in terms of seismic analysis and control of vibrations induced by secondary seismic events, such as earthquake-induced landslides.

3.2.2 Implementation in OpenSees

The numerical model of the wind turbine was implemented in OpenSees [45], a software that enables advanced structural modelling under both static and dynamic conditions. This computational environment allows the definition of structural geometry, material properties, boundary and load conditions, enabling accurate simulation of the overall response of the system.

The tower was discretised along the vertical axis using 180 *elasticBeamColumn* elements, with an average length of approximately 0.5 m and a hollow circular cross-section with variable geometric properties along its height. The properties of the section (area, moment of inertia and elastic modulus) were defined according to the geometric data of the NREL 5 MW reference model. The mass of the tower was uniformly distributed among the elements, while the mass of the rotor-nacelle assembly was applied at the top node. This approach allows for an accurate representation of the inertial effects of the top assembly on the overall dynamic response [46].

The boundary conditions were implemented according to the two configurations described previously. In the fixed-base model, the bottom node is completely constrained. When soil–structure interaction is considered, the base of the tower is connected to a rigidly fixed “soil” node through a *zeroLength* element that explicitly activates horizontal translation (sway) and rotation around the horizontal axis (rocking). The equivalent viscoelastic behaviour of the soil was modelled with elastic-viscous materials in the two directions considered; the impedances (stiffnesses and damping coefficients) were obtained from Gazetas' expressions based on the geotechnical parameters of the site profile.

The analysis sequence first involves the application of a horizontal static load distributed along the tower to represent the mean effects of wind action on the structural profile. Subsequently, in cases where the potential influence of slope-instability phenomena is considered, a horizontal displacement and a rigid rotation are imposed at the base, calculated from the expected landslide displacement obtained from Pitilakis's relationship (Eq. (6)). Seismic shaking is applied using ground-motion records that are spectrum-compatible with the reference site, selected and scaled according to the local soil characteristics.

The results of the simulations, following the model validation phase, are presented and discussed in the following sections.

3.3 Model validation

The validation of the numerical model is a fundamental step in verifying the ability of the proposed model to realistically reproduce the dynamic behaviour of the wind turbine. In this section, the results obtained from the developed model are compared with the data and information available in the literature in order to assess its reliability and suitability for the objectives of the study.

The main reference adopted is the work of Lavassas et al. (2003) [40], which presents the dynamic analysis of a steel tower for a 1 MW wind turbine, modelled as a continuous element with distributed mass and lumped mass at the top. Although the machine size is smaller than the 5 MW turbine analysed in this work, the structural configuration is fully comparable, making this study a useful benchmark for methodological validation. Furthermore, the results were compared with the data reported in the NREL report (Jonkman et al., 2009 [39]), which provides the modal properties of the NREL 5 MW reference turbine.

The modal analysis performed on the fixed-base model returned a fundamental flexural frequency of 0.30 Hz, in close agreement with the reference value of 0.31 Hz reported for the NREL 5 MW turbine model. This correspondence confirms the correct representation of the overall stiffness and mass distribution along the tower. The modal shapes obtained are perfectly in line with the modal profiles reported in scientific literature, confirming the correctness of the adopted discretisation and the modelling assumptions introduced. Therefore, the results of the modal validation demonstrate that the developed model is able to represent the dynamic behaviour of the reference wind turbine tower with good accuracy. This outcome provides a solid basis for subsequent time-domain dynamic analyses aimed at evaluating the structural response to seismic actions and soil deformability.

3.4 Code-based safety assessment

The safety assessment of the wind turbine tower was performed in accordance with the criteria prescribed by the relevant technical standards, with the aim of verifying the consistency of the structural behavior obtained from the numerical analyses with respect to safety requirements. The reference regulatory framework includes Eurocode 1 (EN 1991-1-4) for the definition of wind actions [47], Eurocode 8 (EN 1998-6) for structures subjected to seismic actions [48] and Eurocode

3 (EN 1993-1-6 and 1993-1-9) for strength and stability checks and for fatigue checks of steel structures [49], [50]. These standards are accompanied by the specific recommendations for wind turbines provided in the IEC 61400-1 standard [7], which defines the design classes, reference loads and structural safety criteria.

The verifications were performed considering both Ultimate Limit States (ULS) and Serviceability Limit States (SLS), evaluated based on the load combinations prescribed by the normative references. Wind action was defined according to the formulation illustrated in section 3.1.1, while seismic action was represented by sets of real accelerograms selected and scaled to be, on average, compatible with the elastic design spectrum defined by Eurocode 8. The latter spectrum was calibrated according to the soil category and the nominal life of the turbine (see Section 3.1.2 for accelerogram selection criteria).

The internal stresses obtained from the numerical analyses (σ, τ), reported in Figure 3.4.1, were compared with the strength and stability limits for shell structures prescribed in Part 1-6 of the Eurocode 3. In detail, Annex D of this standard was used to calculate the design buckling stress for unstiffened cylindrical and truncated conical shells. To account for the buckling strength limitations, the following relationship is adopted:

$$Y = (\frac{\sigma}{\sigma_{x,Rd}})^{k_x} + (\frac{\tau}{\tau_{x\theta,Rd}})^{k_\tau} \leq 1 \tag{11}$$

where $\sigma_{x,Rd}$ denotes meridional design buckling stress, $\tau_{x\theta,Rd}$ the shear design buckling stress and k_x, k_τ are the corresponding buckling reduction factors. This verification was carried out for the base section of the structure, where the highest stress levels were observed.

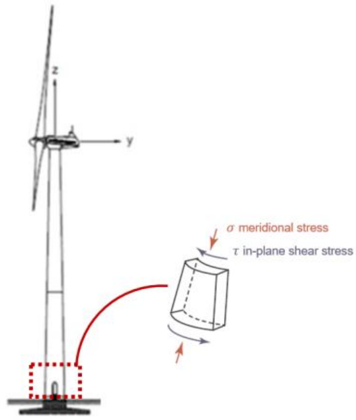

Figure 3.4.1 Wind turbine schematic showing membrane stresses at the tower base.

From an operational standpoint, maximum tower-top displacements were verified and compared with the limits imposed by international standards (IEC 61400-1) to ensure rotor alignment and correct turbine operation.

Fatigue assessment of the wind turbine tower was conducted in accordance with Part 1-9 of Eurocode 3, which defines the fatigue strength criteria through S–N curves and detail categories. The design stresses were derived from the numerical analysis results for the most structurally stressed points, with particular attention to the tower base, for which the appropriate detail category was identified according to Table 8.5 - EN 1993-1-9. Fatigue assessment was expressed in the simplified form:

$$\Delta\sigma_{Ed} \leq \Delta\sigma_{Rd} \quad (12)$$

$$\gamma_{FF} \cdot \Delta\sigma_f \leq \frac{\Delta\sigma_c}{\gamma_{MF}} \quad (13)$$

where $\Delta\sigma_c$ is the detail category, $\Delta\sigma_f$ is the maximum stress demand. Demand is amplified for γ_{FF} (which is generally taken as 1), while capacity is reduced for γ_{MF}, a coefficient dependent on the consequences of failure (Low or High consequences, Table 3.1 - EN1993-1-9) and on the adopted assessment method.

In conclusion, the checks carried out in accordance with the Eurocodes and the IEC 61400-1 standard confirmed the compliance of the wind turbine tower with structural safety requirements, both in terms of strength and stability and in terms of fatigue performance. These results validate the numerical model adopted and form the basis for subsequent multi-hazard risk analyses.

Chapter 4

Multi-Hazard Risk Quantification of Onshore Wind Turbines

Uncertainty is not a weakness of science, but its driving force.

Freeman Dyson

Onshore wind farms are increasingly being deployed in geographically complex environments, often characterized by severe environmental conditions and the potential interaction of various natural hazards. In such contexts, the assessment of structural safety cannot be limited to the analysis of a single hazard, but must instead adopt a multi-hazard approach that considers the potential concurrence or sequential occurrence of natural events and their impact on structural vulnerability.

Within the broader field of risk engineering, the literature extensively documents how natural phenomena such as earthquakes, landslides, tsunamis and extreme weather events can generate significant impacts on critical infrastructure, with potential economic and environmental consequences ([22], [51]).

In this framework, seismic engineering plays a central role, as one of its fundamental objectives is risk mitigation, understood as reducing human, social, and economic losses and ensuring an adequate level of operation for critical and strategic infrastructure even following extreme events. Direct losses include structural damage or collapse, while indirect losses include service disruptions, loss of functionality, plant downtime and restoration costs. These concepts, well-established in earthquake engineering, are also applicable to multi-hazard risk assessment for renewable energy infrastructure, such as onshore wind turbines.

Given the high seismic risk in Italy, a clear understanding of the fundamental components into which risk can be decomposed is essential. In a probabilistic sense, seismic risk (R) is defined as the probability that a given loss level (L) will be exceeded within a specified time interval. Classically, it is expressed by the functional product:

$$R = H \cdot V \cdot E \tag{14}$$

where H represents seismic hazard, V represents seismic vulnerability, and E represents exposure. This paradigm finds general application in all modern risk quantification approaches, both single-hazard and multi-hazard.

In the analysis presented in this thesis, multi-hazard risk arises from the interaction of three hazards relevant to wind turbines located upstream of slopes: wind, earthquake and earthquake-induced landslides. These phenomena may occur simultaneously or sequentially, with interaction mechanisms that significantly influence the structural response of the turbine.

The risk analysis framework adopted in this thesis is consistent with modern probabilistic approaches, systematically integrating the hazard of natural phenomena, the structural vulnerability of the turbine and the final risk quantification. The process begins with hazard assessment, that is the estimation of seismic hazard. We proceed with the evaluation of the vulnerability of the wind turbine for each of these phenomena. This evaluation is conducted using a set of nonlinear dynamic numerical analyses, which allow us to characterize the structural response of the system under various levels of environmental load intensity. The results are summarized in the form of fragility curves, categorized by whether they represent only an earthquake or an earthquake accompanied by a landslide. Fragility curves express the probability that the structure will reach or exceed specific performance levels as a function of the intensity of the applied loads and form the central core of any risk assessment procedure.

In the context of this thesis, the concept of “failure” is not limited to structural damage to the tower or foundation alone, but also includes the failure of electrical cables, which leads to the interruption of energy production and therefore represents a fundamental criterion for evaluating the functionality of the system. The final stage of the process concerns the quantification of risk. By combining information from hazard curves and fragility curves, we obtain the annual turbine failure rate, defined as the average annual number of events that could result in loss of function or significant structural damage. This quantity represents the final measure of the structural risk of the wind turbine. This approach therefore provides a comprehensive and quantitative view of turbine behavior in a multi-hazard context, allowing for the evaluation of system robustness and the support of potential risk mitigation strategies.

4.1 Selection of the case study

A multi-hazard risk analysis is carried out for an onshore wind turbine located in the L’Aquila area, in the Abruzzo region of central Italy (Figure 4.1.1 a). The site lies within a mountainous environment characterized by extensive high-altitude terrains and highly favourable wind exposure conditions. These conditions, typical of the central Apennines, result in strong wind resources and make the area particularly suitable for the installation of wind farms.

In addition to favorable anemometric conditions, the region exhibits considerable seismic hazard due to its location within a highly active seismic zone. Moreover, the widespread presence of steep slopes leads to significant susceptibility to instability phenomena, including earthquake-induced landslides, which can be activated or accelerated by moderate or strong seismic events. The combination of these factors makes the L'Aquila site particularly representative for the development of a multi-hazard risk analysis methodology, in which wind, earthquake and slope instability can be considered sequentially. Accordingly, a wind turbine located upstream of a slope affected by the landslide was considered, following the configuration illustrated in Figure 4.1.1 b.

For the seismic hazard characterization of the selected site, a set of real ground motions was selected using REXEL software (Iervolino et al., 2009) [33]. The program allows the identification of sets of accelerometric recordings from the European Strong-Motion Database that are compatible, on average, with the target Uniform Hazard Spectrum (UHS) for the L’Aquila area. The selected combination (“Combination no. 1”) corresponds to the best-fitting set of records within the defined period range (indicated by red dashed lines), as shown in Figure 4.1.2.

From a structural perspective, the selected turbine is supported by a surface circular reinforced-concrete foundation (plinth), a widely adopted solution for onshore wind farms constructed on granular soils or rock. This foundation type is designed to effectively transfer vertical loads and counteract the significant overturning moments generated mainly by wind actions and the dynamic effects of the earthquake. The diameter of the foundation typically varies between 15 m and 30 m, depending on the turbine class and its truncated-conical geometry allows the pressures to be distributed homogeneously on the ground, maintaining wide safety margins with respect to the bearing capacity [52].

Overall, the selected case study represents a typical configuration of wind turbines installed in the mountainous areas of central Italy and is well suited for the application of a probabilistic multi-hazard approach. This scenario enables a comprehensive analysis of the interactions among different environmental actions, providing a robust basis for estimating the annual failure rate of the turbine and assessing the associated risk.

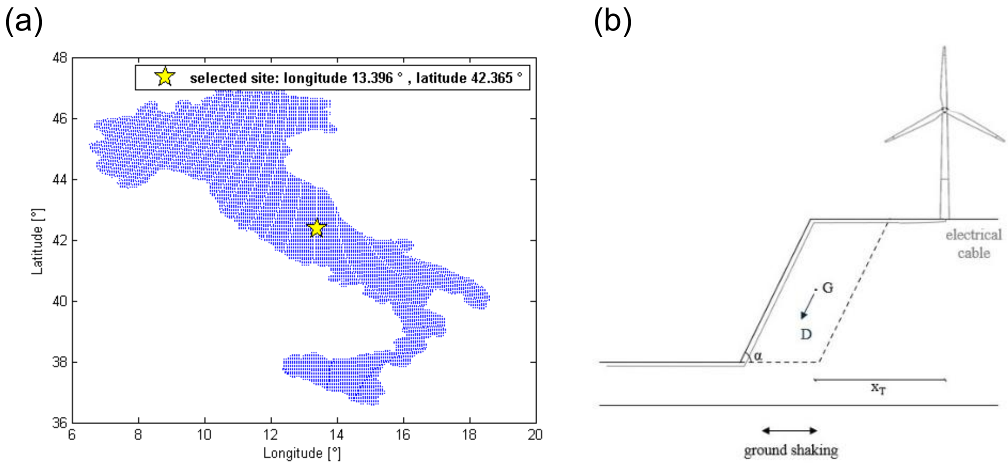

Figure 4.1.1 (a) Location of the case-study wind turbine in the L'Aquila area (Italy). (b) Schematic representation of the turbine–slope model adopted for the multi-hazard analysis.

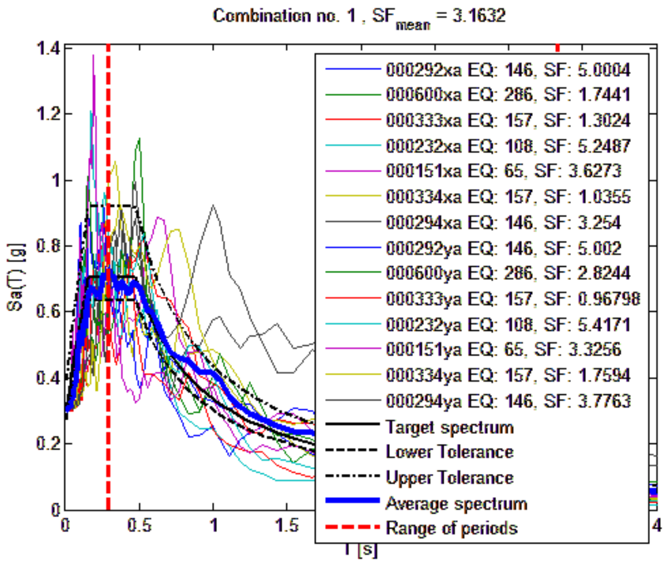

Figure 4.1.2 Combination of accelerograms selected for the L'Aquila case study using *REXEL*.

4.2 Definition of performance levels

A performance level represents a condition beyond which the structural system can no longer satisfy the specified functional or safety requirements. To develop fragility curves for wind turbines, performance levels should be defined based on different turbine demand parameters, relevant to different hazard intensities ranging from emergency shutdown to structure failure and total collapse.

Because a wind turbine is a system composed of multiple subsystems, the performance levels adopted in this study are divided into two categories:

(i) structural performance levels, related to the deformation response and stability of the tower;

(ii) a non-structural performance level, relating to the functionality of the buried electrical cable.

This distinction ensures consistency with the multi-hazard fragility analyses presented in the following sections. Wind and earthquake fragility assessment consider only structural performance levels. In contrast, in the case of earthquake-induced landslides, the performance level of the electrical cable is also considered, as underground cables connecting turbines to substations over distances of several kilometres may experience significant deformation due to ground displacement, potentially compromising system operation. The performance levels adopted are summarised in Table 4.2.1.

Table 4.2.1 Performance levels considered for fragility analysis of onshore wind turbines.

Category	PL	Failure mode	Performance measure	Threshold
Structural PLs	S-PL1	Large chord rotation on tower top	θ_{max}	0.5°
	S-PL2	Large top displacement	Δ	$1.25\% \cdot h_{hub}$
	S-PL3	Instability of shell structure	Y	1
Cable PLs	C-PL1	Yielding of electrical cable	ε_m	ε_y

The selected performance thresholds are based on established industry standards and previous studies. The first structural performance level (S-PL1) is related to maximum chord rotation of the tower (θ_{max}). The capacity value of 0.5 degrees corresponds to the maximum rotation for which the turbine is switched off ([8], [53]). The non-structural performance level (C-PL1) relates to the loss of electrical cables' functionality, evaluated by comparing the average axial strain of cable due to slope movement (ε_m) to the yield axial strain of the cable material (ε_y). The second structural performance level (S-PL2) is related to excessive displacements on top of the tower. The threshold, equal to 1.25% of the tower height h_{hub}, reflects conditions that may cause a loss of energy efficiency, similarly to S-PL1 ([54], [55]). In modern utility scale wind turbines this case is also known as earthquake-induced emergency shutdown. Finally, the third structural performance level (S-PL3) is assessed in accordance with the requirements of Eurocode 3 – Part 1-6, concerning the strength and stability of shell structures and Part 1-9, concerning fatigue verification. A representative case of local buckling observed in a wind turbine following the 2016 Kumamoto earthquake (Japan) is shown in Figure 4.2.1 [56]. These verifications correspond to the assessments based on the regulations presented in Section 3.4.

Figure 4.2.1 Example of local buckling observed in a wind turbine tower [56].

4.3 Fragility analysis

The structural vulnerability of a wind turbine represents the measure of its propensity to reach or exceed specific performance levels when subjected to varying intensities of environmental actions. Vulnerability quantifies the sensitivity of the system to increases in the intensity of the natural phenomenon under consideration and constitutes a key component in multi-hazard risk assessment. Similar to seismic engineering for building performance evaluation, vulnerability of wind turbines is defined through the relationship between the structural demand induced by external actions and the capacity of the structure or its components.

Within a probabilistic framework, this relationship is formalized by means of fragility curves, which express the probability that a given performance level will be reached or exceeded for a specified value of the intensity measure (IM).

For onshore wind turbines, fragility analysis is particularly relevant, as these structures are simultaneously exposed to multiple natural hazards. Moreover, their structural configuration, characterized by slender elements, extensive shallow foundations and critical components (e.g., electrical cables extending for many kilometers underground), introduces additional vulnerability mechanisms compared with more conventional civil engineering structures.

In this thesis, the fragility analysis is developed by progressively considering the three main hazards to which the turbine is exposed: wind, earthquake and earthquake-induced landslides. The analysis begins with the assessment of wind fragility, which represents the primary action to which the turbine is subjected during its operational life. Subsequently, attention is turned to seismic vulnerability, using two different structural models: a fixed-base model and a model with springs and dashpots that represents the soil-structure interaction (as described in Section 3.2.1). The comparison between these two configurations enables the evaluation of the influence of boundary conditions on seismic demand and on the probability of exceeding the defined performance levels.

Finally, the analysis is extended to earthquake-induced landslides, a particularly significant phenomenon in mountainous regions where wind farms are frequently located. In this context, the vulnerability of the turbine depends not only on the structural response of the tower, but also by the functionality of its electrical cables, which may be compromised by slope instability. The loss of cable integrity, in fact, leads to an interruption of energy production and thus represents an additional criterion for functional failure. For this analysis, the soil–structure interaction model with springs and dashpots at the base is adopted, which allows for a more accurate representation of the effects of permanent ground displacement on the tower-foundation system.

The fragility curves of the wind turbine, located in an area potentially affected by earthquake-induced landslides, constitute the essential probabilistic basis for the subsequent quantification of multi-hazard risk, as they allow the rigorous combination of hazard and vulnerability information and the estimation of the system's annual failure rate.

4.3.1 Wind fragility analysis

In Chapter 3, wind action was modeled using an equivalent static approach, based exclusively on the mean component of the velocity profile, defined according to the NWP model. While this modeling strategy is adequate for describing turbine behavior under ordinary operating conditions, it does not capture the dynamic effects associated with atmospheric turbulence. Therefore, the fluctuating wind component is introduced, with the aim of evaluating the dynamic response of the wind tower under turbulent wind action and deriving the corresponding wind fragility curves.

The spectral properties of the turbulent component, modeled as a zero-mean stationary Gaussian process, are defined using the Kaimal spectrum (Eq. (15)), in accordance with the prescriptions of IEC 61400-1 (2005) [7]. The spatial coherence along the tower height is represented by an exponential coherence function, ensuring realistically correlated fluctuations between different elevations.

$$S_u(f) = \frac{4 \cdot {\sigma_u}^2 \cdot L_u / V}{[1 + 6 \cdot f \cdot L_u / V]^{5/3}} \tag{15}$$

In the adopted equation, $S_u(f)$ represents the power spectral density of the turbulent component of the wind, while f is the fluctuation frequency. The quantity σ_u, defined as $\sigma_u = I_u \cdot V(z)$, represents the turbulence standard deviation and depends on the turbulence intensity I_u and the mean wind speed at height z, $V(z)$. The scale length L_u is assumed to be $8.1 \cdot z$, i.e. proportional to the height above the ground, in accordance with the parameterization provided by IEC 61400-1. Finally, $V = \bar{V}(z)$ indicates the mean wind speed at altitude z, obtained from the static wind profile.

Based on these assumptions, synthetic wind time histories were generated at each tower elevation and used as input for the dynamic analysis. The vulnerability assessment of the tower was carried out through Incremental Dynamic Analysis [57]. In this context, the adopted intensity measure is the mean hub-height wind speed, V_{hub}, which was incrementally varied between 5 m/s and 25 m/s, in accordance with the operating range of the NREL 5 MW wind turbine, as inferred from its power curve and discussed in Section 2.2.

For each wind intensity level, the corresponding Engineering Demand Parameters (EDPs) were computed, coinciding with the performance measures defined in Table 4.2.1 and representative of the structural and functional demands on the turbine. The EDPs were derived from the dynamic response of the tower subjected to turbulent wind. These demand values were then compared with the capacities associated with each performance level, allowing us to determine, for each considered intensity, whether the PL was exceeded. This comparison produced a set of discrete points expressing the probability of exceeding each performance level as a function of the mean wind speed at the hub (v_{hub}).

The resulting points were interpolated using a lognormal distribution [58]. The resulting statistical model defines fragility for each PL, describing the probability that the wind turbine will exceed a given performance level as the wind intensity increases. The fragility curves for the different performance levels are presented in Figure 4.3.1, and the corresponding lognormal distribution parameters (median μ and logarithmic standard deviation β) are reported in Table 4.3.1.

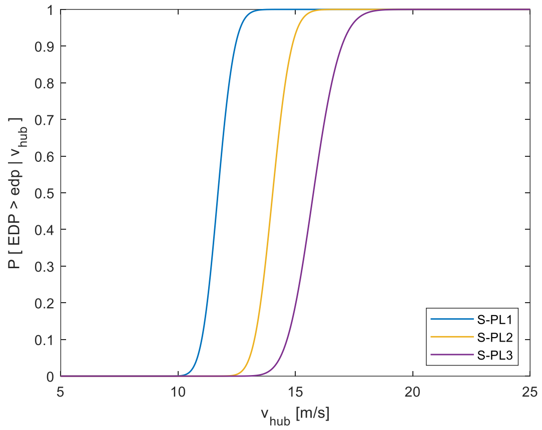

Figure 4.3.1 Wind fragility curves of the turbine.

Table 4.3.1 Parameters of wind fragility curves.

Fragility curve	μ [m/s]	β
S-PL1	11.70	0.048
S-PL2	14.03	0.045
S-PL3	15.76	0.058

4.3.2 Seismic fragility analysis

To assess the seismic fragility of the wind turbine, the first phase consisted of applying wind loads through a static, force-controlled analysis. The second phase involved the application of seismic input, followed by a nonlinear Incremental Dynamic Analysis (IDA) to evaluate the structural performance under earthquake excitation. For each PGA level, the seismic demand was computed and compared with the capacity associated with each PL, as defined in Section 4.2, allowing the exceedance of each PL to be evaluated.

The accelerograms used for the analyses were selected to be spectrum compatible with the L'Aquila site, based on the Uniform Hazard Spectrum (UHS), using REXEL software, as described in detail in Section 3.1.2.

The analysis was performed considering the two structural models presented in Section 3.2.1: a configuration with a rigid, fixed-base constraint at the tower base and a configuration in which the foundation is represented by an equivalent spring and dashpot. The corresponding seismic fragility curves, obtained through lognormal regression of the IDA results, are shown in Figure 4.3.2 a (fixed foundation) and Figure 4.3.2 b (flexible foundation). Table 4.3.2 reports the fragility parameters for different PLs for both structural models.

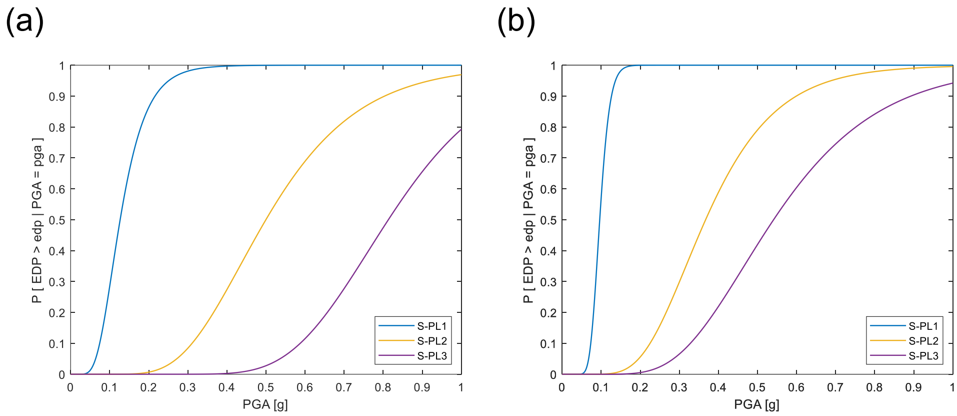

Figure 4.3.2 Seismic fragility curves of the wind turbine. (a) Model with fixed-base boundary condition. (b) Model with flexible foundation including soil–structure interaction.

Table 4.3.2 Parameters of seismic fragility curves.

Boundary conditions	Parameter	S-PL1	S-PL2	S-PL3
Fixed-base model	μ [g]	0.13	0.50	0.81
	β	0.42	0.37	0.25
SSI model	μ [g]	0.09	0.37	0.54
	β	0.21	0.38	0.39

The comparison of the seismic fragility curves reveals significant differences between the fixed-base configuration and the model that incorporates soil–structure interaction (SSI). In the rigid-base model, the structure exhibits greater overall stiffness and, therefore, reduced deformability under seismic loading. Conversely, in the SSI model, the presence of the equivalent spring and dashpot reduces the overall stiffness of the tower–foundation system. This effect leads a shift of the fragility curves to the left, with lower median values for all performance levels. Such behavior indicates an increase in the seismic vulnerability of the turbine when SSI is considered, particularly for performance levels associated with top displacement (S-PL2) and turbine collapse (S-PL3).

Overall, these findings highlight the importance of adopting realistic foundation models in vulnerability assessments of onshore wind systems, especially in areas characterized by moderate or high seismic hazard.

4.3.3 Earthquake-induced landslide fragility analysis

Interruption of wind turbine operation can be caused both by excessive displacement and rotation on top of the tower, but also by breakage of underground electrical cables used to transport energy. Therefore, earthquake-induced landslide fragility analysis is performed on both the electrical cables embedded in the subsoil and the superstructure, considering both earthquake ground shaking and slope movements. Such analysis is discussed in the following sections.

Fragility analysis of the wind turbine superstructure

In the earthquake-induced landslide fragility analysis, the foundation model incorporating soil–structure interaction (SSI) was adopted exclusively, as this is necessary to properly capture the kinematic effects generated by slope movement. Unlike seismic analysis, in which a fixed joint at the turbine base may be considered, the presence of a landslide instead requires the possibility of imposing both co-seismic displacement and rotation on the foundation, induced by ground shaking.

Co-seismic displacements were evaluated using the empirical relationship proposed by Fotopoulou & Pitilakis (2017), discussed in Section 3.1.3, which provides the expected co-seismic motion as a function of seismic shaking intensity and local geotechnical conditions. The resulting displacement was applied at the tower base as an imposed motion and scaled consistently with each level of the IDA. Additionally, a rotation was imposed at the base of the structure, formulated to reproduce the deformation kinematics of the soil volume and thus capture the additional effects of the landslide beyond those associated with seismic shaking alone.

The rotation was defined assuming that the settlement at the center of gravity of the volume affected by the landslide (point *G* in Figure 4.1.1 b) is related to the co-seismic horizontal displacement derived from the Fotopoulou & Pitilakis relationship and that the subsidence profile at the turbine base follows a linear trend, with a maximum value at point *G* and zero at the opposite edge of the landslide slope. This assumption allows the rotation to be computed as a function of the landslide extent. In the first stage, the settlement at *G* was assumed to be equal to the calculated co-seismic displacement; subsequently, this ratio was varied to assess the sensitivity of the structural response to different hypotheses regarding the deformation field imposed by the landslide.

This approach enables the evaluation of the increased vulnerability of the turbine due to the contribution of landslide-induced effects, in addition to those produced by seismic loading alone, thereby providing a realistic representation of structural behavior under multi-hazard conditions. The seismic-induced fragility curves of the superstructure, obtained through lognormal regression of the IDA results, are presented in Figure 4.3.3.

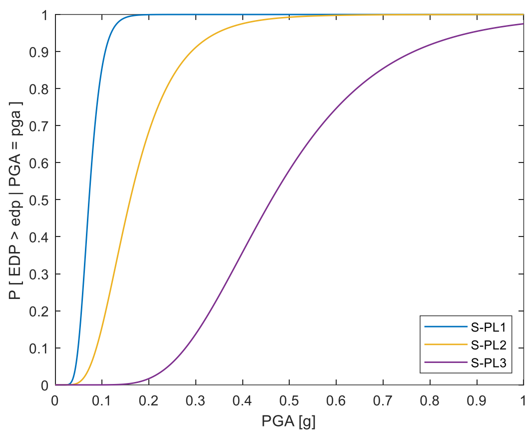

Figure 4.3.3 Fragility curves of the wind turbine superstructure under earthquake-induced landslide conditions (SSI foundation model).

To evaluate the additional contribution of the landslide relative to seismic action alone, Figure 4.3.4 compares earthquake-induced landslide fragility (denoted as EQ+L) with seismic fragility (denoted as EQ), both obtained for the same structural configuration (SSI model). This comparison highlights the increase in vulnerability associated with the kinematic effects of slope deformation, particularly for the most severe performance levels. The corresponding lognormal distribution parameters are reported in Table 4.3.3.

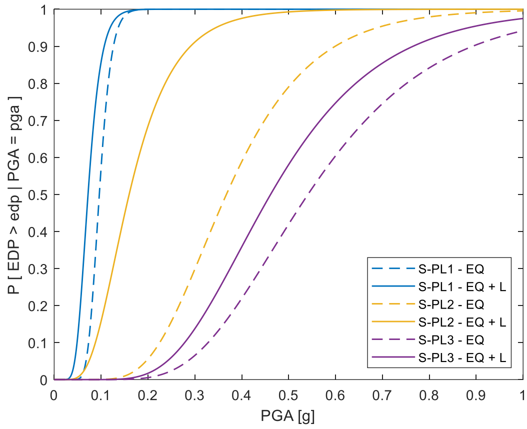

Figure 4.3.4 Comparison between seismic fragility curves (EQ) and earthquake-induced landslide fragility curves (EQ+L) for the wind turbine superstructure (SSI foundation model).

Table 4.3.3 Parameters of the fragility curves for seismic loading (EQ) and combined seismic and landslide actions (EQ+L) for the wind turbine superstructure.

Action	Parameter	S-PL1	S-PL2	S-PL3
EQ	μ [g]	0.09	0.37	0.54
	β	0.21	0.38	0.39
EQ + L	μ [g]	0.07	0.16	0.46
	β	0.30	0.46	0.39

To investigate the influence of the assumptions adopted in defining the settlement profile at the turbine base, a parametric analysis was conducted by varying the ratio between the settlement at the center of gravity of the landslide-affected volume (D_v) and the co-seismic horizontal displacement D. Specifically, amplification coefficients α were introduced such that $D_v = \alpha \cdot D$, considering $\alpha = \{0.1, 0.3, 0.5, 0.7, 1\}$. A distinct set of fragility curves was obtained for each value, as shown in Figure 4.3.5.

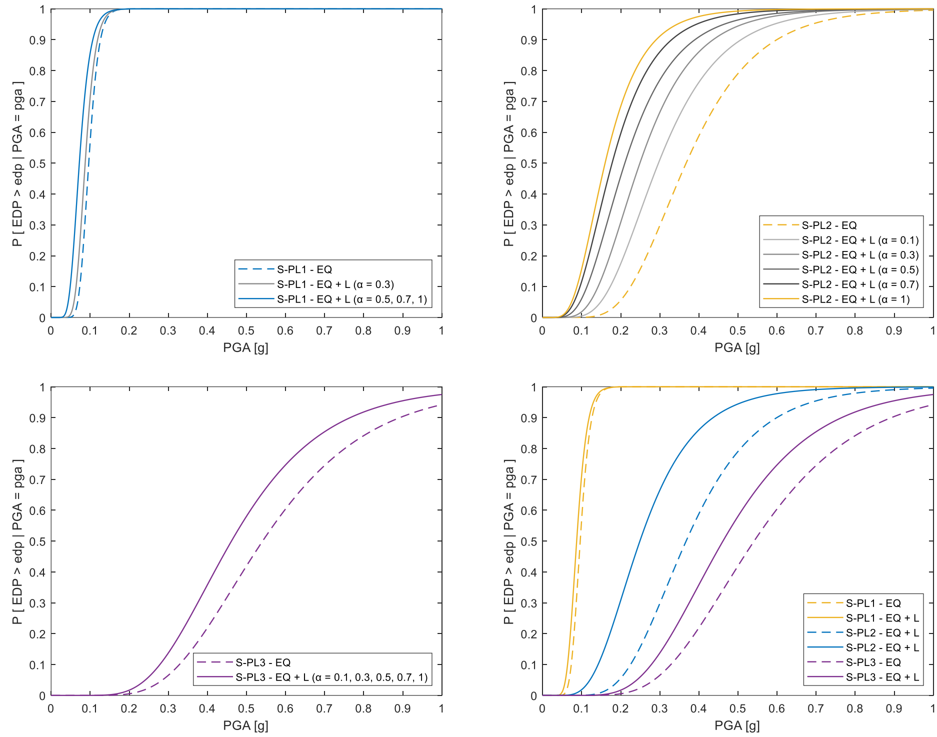

Figure 4.3.5 Comparison of earthquake-induced landslide fragility curves of the wind turbine superstructure for different values of the settlement amplification factor $\boldsymbol{\alpha}$.

The analysis of these curves reveals different trends depending on the performance level considered.

For S-PL1, very low values of the coefficient (α = 0.1) do not introduce appreciable differences compared to the purely seismic case, resulting in overlapping curves. This indicates that, for small settlement values, the kinematic effect of the landslide is insufficient to significantly alter the drift at the tower top. Starting from α = 0.3 the influence of the landslide becomes evident, with a progressive increase in vulnerability for α = 0.5 and α = 0.7, converging towards the curve associated with α = 1.

S-PL2, on the other hand, exhibits greater sensitivity to the α parameter. Each value of α produces a distinct fragility curve, reflecting the highly deformable nature of this performance level, for which even moderate variations in the imposed settlement profile significantly affect the displacement demand at the tower top.

Finally, for S-PL3, all curves corresponding to the different α values are nearly identical to that obtained for α = 1. Although the settlement profile imposed at the base of the turbine varies, the stresses governing the instability threshold do not change sufficiently to alter the exceedance point for this performance level.

Based on these considerations, the last panel in Figure 4.3.5 provides a summary comparison of the three performance levels using $\alpha = 0.3$, selected because it provides an intermediate and realistically consistent estimate of earthquake-induced landslide effects across all performance levels.

This sensitivity analysis enables the assessment of how different assumptions regarding the settlement profile imposed at the turbine base influence the earthquake-induced landslide vulnerability of the structure, highlighting the variability of the resulting fragility curves with respect to these assumptions.

Fragility analysis of underground electrical power pipelines

The schematic model shown in Figure 4.1.1 b, which is representative of a wind turbine located upstream of the slope affected by a landslide, was used to assess the fragility of underground electrical cables. The parameter adopted to evaluate the breakage of underground electrical cables is the average cable strain, ε_m, induced by slope movement. This strain was estimated as the ratio between the co-seismic displacement (D) calculated using Eq. (6) and a conventional turbine-slope distance (x_T). The IDA was also carried out for this component by comparing the deformation demand with the material capacity, expressed as the yield strain ε_y, to obtain the probability of exceeding the damage threshold.

To analyze the performance of the underground electrical cables, a fragility analysis was conducted by varying the critical acceleration k_y, a parameter characterizing the slope. Values of k_y in the range $0.05g \leq k_y \leq 0.25g$ were considered, representing increasingly stable geotechnical conditions. For each value of k_y the co-seismic displacement of the slope was calculated using Eq. (6). The resulting response was then compared with the yield strain ε_y, obtaining the probability of exceeding the damage threshold as a function of PGA. The corresponding fragility curves are shown in Figure 4.3.6.

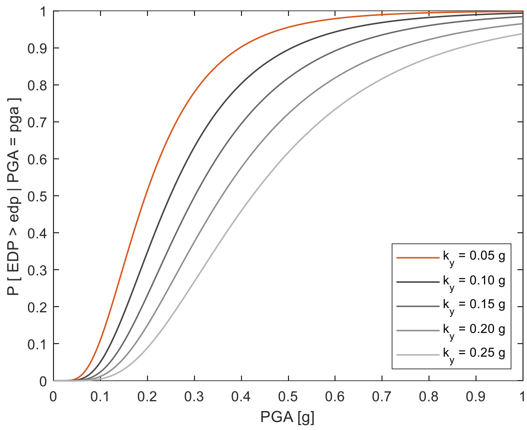

Figure 4.3.6 Fragility curves of underground electrical cables under earthquake-induced landslide conditions for different values of the critical acceleration $\boldsymbol{k_y}$.

The analysis demonstrates that the fragility of underground electrical cables is strongly influenced by the critical acceleration of the slope. For low values of k_y (i.e. more unstable slopes), the calculated co-seismic displacements are larger, resulting in fragility curves that indicate a higher probability of damage at lower PGA levels. As k_y increases, the slope response becomes less sensitive to seismic shaking and the fragility curves shift toward higher PGA values, indicating a reduced likelihood of exceeding the cable deformation threshold.

In addition to the variation of the critical acceleration k_y, a further parametric evaluation was conducted to investigate the influence of the turbine-slope distance on the fragility of underground electrical cables. This distance, denotes as Δ, was assumed to be $40\ \mathrm{m}, 80\ \mathrm{m}$ and $120\ \mathrm{m}$. For each case, the full IDA procedure was performed, producing the fragility curves shown in Figure 4.3.7.

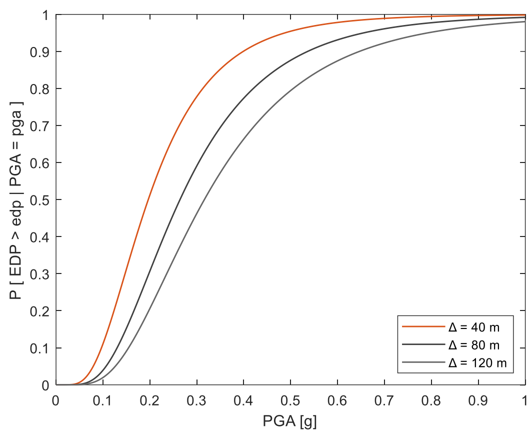

Figure 4.3.7 Effect of turbine–slope distance (**Δ**) on the earthquake-induced landslide fragility of underground electrical cables.

The results indicate that the distance between the turbine and the slope is a highly influential parameter governing electrical cable vulnerability. When the turbine is located close to the slope, as in the case of a 40 m distance, the average deformation imposed on the cable is greater, leading to damage at lower PGA levels. This results in significantly more unfavorable fragility curves, with a high probability of exceeding the yield threshold even under moderate seismic events.

Increasing the distance to 80 m reduces the vulnerability of the system: the deformation demand decreases and the fragility curves shift to the right, indicating a greater capacity to withstand landslide-induced movements. For even larger distances, such as 120 m, the kinematic effects of the slope become less significant. Consequently, the probability of exceeding the yield threshold is lower and the fragility curve shows a less pronounced slope.

These analyses underline the importance of carefully considering site-specific characteristics and the location of electrical infrastructure during the design and optimization of wind farm layouts, especially in areas susceptible to earthquake-induced landslides.

In conclusion, the fragility curves developed for structural performance levels are complemented here by the assessment of the earthquake-induced fragility of underground electrical cables, which are essential for maintaining operational continuity of the wind turbine system. The figure below (Figure 4.3.8) provides an overall summary of the multi-hazard vulnerability of the wind turbine, including both the superstructure fragility, obtained using the representative value $\alpha = 0.3$ for the landslide-induced settlement profile, and the fragility of the electrical cables. All curves were derived for a reference configuration characterized by a critical slope acceleration of $k_y = 0.5\,g$ and a turbine-slope distance of 40 m.

This integrated representation highlights how the overall vulnerability of the system derives from the combined effects of ground shaking and slope movements acting on both superstructure and electrical infrastructure.

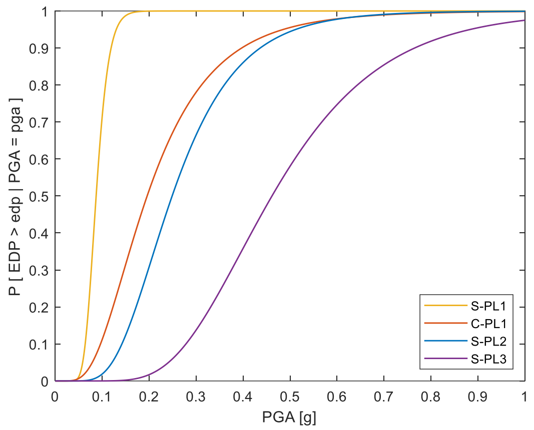

Figure 4.3.8 Earthquake-induced landslide fragility curves of the wind turbine: structural performance levels (S-PL) and underground electrical cables (C-PL).

4.4 Exposure

In the context of risk assessment for a wind turbine installed upstream of a slope potentially subject to second-order seismic effects, such as earthquake-induced landslides, exposure represents the set of elements susceptible to economic and functional losses as a consequence of the damaging event. In the present case, exposure mainly concerns the turbine superstructure (tower, nacelle and rotor), the underground electrical cables used to transport the energy produced and, indirectly, the continuity of service of the entire system.

Each performance level defined in the fragility analysis entails different operational and economic consequences, which constitute the measure of the system's exposure. Depending on the exceeded PL, the turbine may experience temporary service interruptions, efficiency reductions, reversible structural damage or irreversible damage requiring the replacement of structural components or the entire machine. In the analysed configuration, the first three performance levels, S-PL1, C-PL1 and S-PL2, result in loss of operation, whereas exceeding S-PL3 represents the most severe scenario, requiring complete turbine replacement.

A significant aspect of the exposure concerns the downtime of the system, which directly affects the economic losses due to reduced energy production [59].

According to the literature on maintenance and repair strategies for wind turbines, downtime can be decomposed into three fundamental components: Reaction Time (RT), i.e. the time required to activate the intervention procedure after the occurrence of failure; Travelling Time (TT), the time required for the maintenance team to reach the site; and Time to Repair (TR), the duration of inspection, repair or replacement activities. The sum of these components defines the total turbine *downtime*. The sequence of these operations is summarised in Figure 4.4.1, which provides an overview of the stages between the occurrence of the failure and the complete restoration of system functionality.

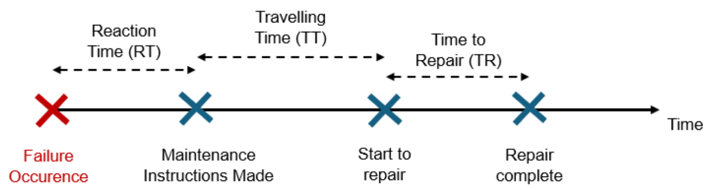

Figure 4.4.1 Timeline of maintenance operations following a failure event, which determine the overall turbine downtime.

The values of these downtime components vary according to the exceeded performance level, as described below.

In particular, exceeding S-PL1, associated with excessive rotation at the tower top, results in the automatic shutdown of the rotor and requires technical inspections within 48 hours. These inspections may lead to immediate restoration or may highlight the need for additional checks, extending the outage (+72 hours). Exceeding C-PL1, relating to the yield strength of underground electrical cables, can lead to a reduction in the cable diameter and a decrease in the power output. Again, the outcome ranges from extended inspection activities to the full replacement of the damaged cable. S-PL2, associated with excessive displacement at the tower top, causes rotor locking and requires approximately 96 hours of downtime for technical inspections. As with S-PL1, the outcome may be immediate restoration or the need for further investigation. Finally, S-PL3 represents the structural collapse of the turbine, which involves the disposal of the damaged machine and the subsequent installation of a new unit, with significant impacts in terms of costs, restoration times and loss of energy production.

The positive and negative scenarios considered for each performance level are reported in Table 4.4.1. These scenarios allow for the systematic quantification of the operational impact associated with exceeding each PL, providing a consistent basis for subsequent risk assessment and for the potential development of mitigation and business continuity strategies.

Table 4.4.1 Operational consequences associated with the exceedance of performance levels.

PL	Description	Immediate effect	Positive outcome	Negative outcome
S-PL1	Large chord rotation on tower top	Rotor shutdown; 48 h inspection	Rotor back in operation	Additional inspections required (+72 h)
C-PL1	Yielding of electrical cable	Power loss due to cable cross-section reduction	Inspection time + reduced power production	Replacement of the electrical cable
S-PL2	Large top displacement	Rotor shutdown; 96 h inspection	Rotor back in operation	Additional inspections required (+72 h)
S-PL3	Structural collapse	Total loss of structure	—	Decommissioning + installation of a new turbine

This information is an essential element in risk assessment, as it allows the exceeding of each PL, quantified by the fragility curves, to be translated into an expected loss.

In the classic seismic risk framework, exposure provides a measure of the “value at risk”, while fragility defines the probability that this value will be damaged. The combination of these two aspects, together with the site-specific hazard level, enables the estimation of annual loss rate, a parameter useful for asset management as well as for planning mitigation measures or business continuity strategies.

4.5 Risk assessment

Risk assessment represents the final step of the analysis process and enables the quantitative integration of site hazard, system vulnerability and exposure in order to estimate the expected consequences.

By integrating vulnerability with hazard, the annual failure rate of the system is determined, understood as the average frequency with which the turbine exceeds a given performance level. Multiplying this frequency by the loss associated with each performance level gives the expected annual loss, the primary risk indicator, which helps identify the most critical components of the system.

To make the loss quantification process explicit, the number of cases associated with each performance level is considered and a percentage of positive and negative outcomes is assigned to each. For example, for S-PL1 it is assumed that 80% of cases correspond to positive outcomes, while the remaining 20% correspond to negative ones. Figure 4.5.1 shows the distribution of cases for each performance level, distinguishing between positive and negative outcomes.

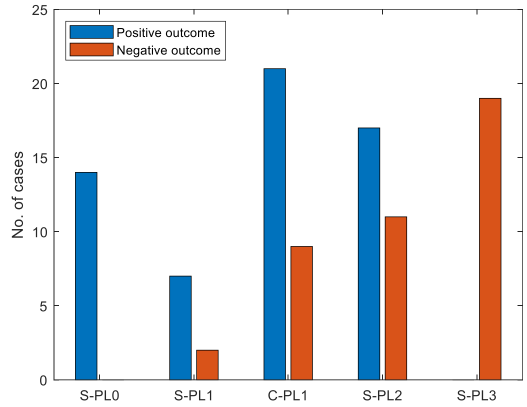

Figure 4.5.1 Distribution of cases by performance level (positive outcome / negative outcome).

Once the unit cost associated with each scenario is defined, the total economic loss is obtained by multiplying the number of cases by the corresponding loss value, again distinguishing between positive and negative outcomes. The result is shown in Figure 4.5.2, which illustrates the total economic losses associated with each performance level.

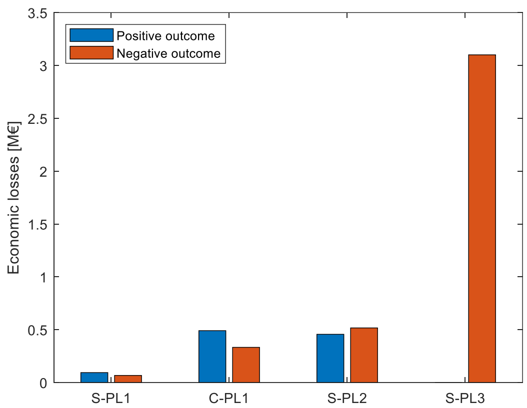

Figure 4.5.2 Economic losses for different performance levels.

The graphs indicate that, although the most frequent cases are associated with intermediate performance levels, the dominant contribution to economic losses arises from the most severe scenarios, in particular exceeding S-PL3, for which turbine replacement generates substantially higher costs than those linked to operational performance levels. This highlights how low-frequency but high-consequence events can significantly influence the overall risk of the system.

The resulting risk estimate constitutes a fundamental decision-making tool for system management, as it enables the identification of the most vulnerable configurations and the evaluation of the effectiveness of potential mitigation strategies. Examples include optimising the turbine–slope distance, adopting more rigid foundations, implementing protective systems for underground electrical cables or introducing monitoring procedures to reduce downtime. Moreover, risk assessment provides useful information during the planning phase, as it allows for the comparison of different potential installation sites and contributes to improving operational continuity in areas exposed to multiple hazards.

4.6 Discussion of results

The results presented in this chapter highlight the central role of a fully integrated approach to multi-hazard risk in assessing the reliability of onshore wind turbines installed in seismically active and morphologically complex contexts. Compared to traditional single-hazard analyses, the proposed framework demonstrates that failure to consider secondary seismic effects, such as earthquake-induced landslides, can lead to a significant underestimation of both the structural vulnerability and the overall risk of the system.

A particularly significant result concerns the quantification of the different contributions made by seismic shaking and co-seismic ground displacement on turbine performance. While pure seismic action mainly governs the exceeding of the most severe structural performance levels, associated with global instability and local instability phenomena of the tower, the inclusion of seismically induced landslides leads to a marked increase in the probability of loss of plant functionality, in particular due to damage to underground electrical cables. This represents a significant advance over the state of the art, in which the vulnerability of auxiliary infrastructure is rarely integrated into turbine-scale risk analyses. The results show that, for installations near the edge of slopes, the contribution of electrical cables can become dominant in defining the annual failure rate, even when structural demand is below the critical thresholds for the tower.

The comparison between the rigid base model and the one that includes soil-structure interaction also confirms that the deformability of the foundation soil and the displacements induced by landslides significantly influence the dynamic response of the turbine, amplifying displacements and rotations at the top. This highlights the need for modeling strategies that coherently integrate structural and geotechnical aspects. Overall, the framework developed provides a quantitative basis for identifying dominant hazards at the site scale and is an effective tool for supporting risk-oriented design and siting criteria for onshore turbines, contributing to greater resilience of wind farms in mountainous areas.

Moreover, the onshore analyses performed using OpenSees were characterized by a limited computational cost, with each nonlinear simulation requiring only a few seconds on a standard workstation, due to the reduced model complexity and the adopted modelling assumptions.

Chapter 5

Offshore Wind Turbines

What we know is a drop, what we don't know is an ocean.

Isaac Newton

The analysis of offshore wind turbines represents the second application domain of the multi-hazard assessment framework developed in this thesis. In contrast to onshore wind turbines, which were examined in the preceding chapters, offshore turbines operate in a substantially more complex environment characterized by extreme environmental conditions. The simultaneous presence of wind, waves and currents induces strongly non-linear system behaviour, thereby necessitating advanced design methodologies and high-fidelity modelling approaches.

The fundamental aspects of offshore wind turbine design are investigated, with particular emphasis on the relevant international standards, performance requirements and differences with respect to onshore turbine design. The main foundation typologies, encompassing both fixed-bottom and floating support structures, are also reviewed, highlighting the influence of the support system on the global dynamic response of the turbine. Therefore, the reference structural model adopted in this study is introduced and the environmental actions governing offshore conditions are described. In particular, wind and wave loads are examined, with reference to the main stochastic generation models and load formulations commonly employed in current design codes. These aspects provide the methodological foundation for evaluating the structural response of offshore wind turbines and for defining appropriate performance criteria under both operational and ultimate design conditions.

In view of recent technological developments, special attention is devoted to floating foundations systems, which currently represent one of the most relevant and discussed solutions in the offshore wind energy sector. Accordingly, the analysis focuses on floating wind turbine technology, examining its defining features and their implications for the dynamic response of the system.

Furthermore, the discussion builds upon the methodological framework previously established for onshore wind turbines, enabling a systematic comparison between onshore and floating offshore configurations. This comparison is conducted in terms of structural modelling strategies, environmental loading conditions, and operational performance, thereby highlighting the distinctive challenges and response characteristics associated with offshore floating wind turbine systems.

5.1 Design of offshore wind turbines

The design of offshore wind turbines is inherently complex due to the wide range of design parameters, diverse operational requirements and harsh environmental conditions involved. The service life of offshore wind turbines is typically assumed to be 50 years, although the foundation is designed to last longer. The tower must be able to withstand static, dynamic and cyclic loads, as well as their critical combinations [60].

Increasing the rated power of wind turbines represents one of the most effective strategies for reducing the cost of electricity generation in offshore wind farms. To this end, manufacturers generally prefer the installation of a single large-capacity turbine rather than multiple smaller units producing the same total output, thereby reducing the cost per kilowatt of installed capacity [61]. In offshore markets, it is common practice among Original Equipment Manufacturers (OEMs) to increase the power output of an existing turbine by upgrading the generator and drivetrain capacity while maintaining the same rotor. This approach allows for higher energy production on the same support structure without requiring modifications to the blade design [62].

As discussed in Chapter 2, IEC 61400-1 [7] establishes the requirements for the design of onshore wind turbines, while the design requirements for offshore wind turbines are established by IEC 61400-3 [28]. Significant overlap exists between these standards and it is common for IEC 61400-3 to refer to IEC 61400-1 for shared design principles. Moreover, IEC 61400-3 frequently delegates detailed aspects of offshore wind turbine design to other standards, such as those developed by ISO. Owing to the intrinsic complexity of offshore wind turbine systems, design requirements often employ terms such as "appropriate", "reliable" and "adequate", implying that multiple design approaches may be acceptable, provided that their technical validity can be demonstrated and verified by an independent third party.

When designing offshore wind turbines under operational conditions, two primary aspects must be considered: loads and structural response. From a loading perspective, the analysis focuses on the environmental variables that induce actions on the turbine and on their interaction with the structural system. As in the case of onshore turbines, multiple environmental conditions contribute to the overall loading scenario. In offshore environments, these effects manifest through hydrodynamic actions associated with sea states, aerodynamic loads induced by wind and other external environmental or non-environmental actions (e.g. ice loads), as well as their coupled behaviour.

The structural response concerns the analysis of the system's reaction to these loads and, in particular, the assessment of its reliability. The feedback from the structural response is what then determines an electrical response, such as energy production. The control and protection system overlaps over both knowledge areas and their interactions. It can be identified on the system's dynamics by mechanisms such as yaw control, or pitch control; or in the electric system through generation control and also in the environmental variables through protection control strategies such as the shut-down control.

Given this level of complexity, the design of offshore wind turbines typically requires large multidisciplinary teams with complementary expertise across several engineering fields.

A fundamental aspect of the offshore wind turbine design concerns the selection and configuration of the foundation system, which represents the structural interface between the turbine and the marine environment. The foundation plays an essential role in ensuring overall system stability, directly influencing both the dynamic response of the tower and the operational performance of the entire system. Unlike onshore turbines, where soil variability is generally limited, the offshore sites are characterized by highly heterogeneous geotechnical conditions, often involving sandy or stratified deposits extending to depths of several tens of meters. As a result, foundation selection constitutes a particularly critical phase of the design process.

Offshore wind turbine foundations can be classified into two categories: fixed-bottom and floating foundations (see Figure 5.1.1). Fixed-bottom solutions include monopiles, gravity-based foundations, jackets and tripods, which are traditionally employed in water depths up to approximately 50–60 m. These systems are characterized by high structural stiffness and relatively straightforward installation procedures and have therefore dominated the current offshore wind market. However, the increasing demand for larger turbines and deployment in deeper waters has revealed both technical and economic limitations of fixed-bottom solutions, thereby motivating the development of floating foundation concepts.

Floating foundations, which are currently the focus of significant research and industrial interest, enable wind turbine installation in deep waters exceeding 60–70 m, substantially expanding the exploitable offshore wind resource. These systems, which include spar buoy, semi-submersible and tension-leg platforms, require a highly multidisciplinary design approach, in which hydrodynamic and aerodynamic interactions and the dynamics of the mooring system play a central role.

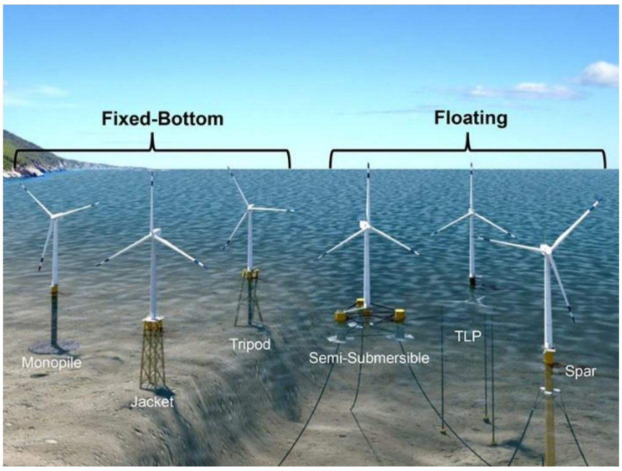

Figure 5.1.1 Main types of offshore wind turbine support structures (fixed-bottom and floating).

Overall, the design of offshore wind turbines requires a complex balance between structural constraints, operational performance, environmental conditions and economic considerations. The following sections introduce the structural model typically adopted for analysis and outline the approach used for modelling environmental loads.

5.2 Structural model

The structural modelling of offshore wind turbines requires a detailed approach capable of representing the simultaneous interaction among aerodynamics, hydrodynamics, structural response and control systems. Unlike onshore turbines, whose behaviour is primarily governed by wind actions and soil-structure interaction, offshore turbines are additionally subjected to loads induced by wave motion and ocean currents and, in the case of floating systems, by platform motions and mooring line dynamics. As a result, offshore wind turbines exhibit a strongly coupled behaviour governed by multi-physical interactions.

Within this framework, the reference to the various environmental and operational actions does not anticipate the subsequent load analysis but is instead intended to define the requirements of the structural modelling. The structural model must therefore be consistent with the level of complexity of the physical system and capable of adequately representing the dominant interactions governing its dynamic response.

For this reason, the structural analysis of offshore wind turbines is typically performed using aero-hydro-servo-elastic simulation codes, which are specifically developed to capture the coupled dynamic response of the system. Among the tools most widely adopted in both industrial practice and academic research are OpenFAST, developed by the National Renewable Energy Laboratory, GH Bladed [63] and HAWC2 [64]. These software packages incorporate dedicated modules for the flexible multi-body structural modelling of the turbine, wind field generation, aerodynamic load computation based on Blade Element Momentum (BEM) theory, hydrodynamic force evaluation using Morison-type formulations, mooring line modelling, and the implementation of turbine control strategies. The general architecture of the simulation framework adopted in modern aero-hydro-servo-elastic codes and specifically in OpenFAST, is illustrated in Figure 5.2.1. The figure highlights the information flow between environmental conditions, load models and the dynamic response of the structural and electromechanical subsystems of the turbine [65].

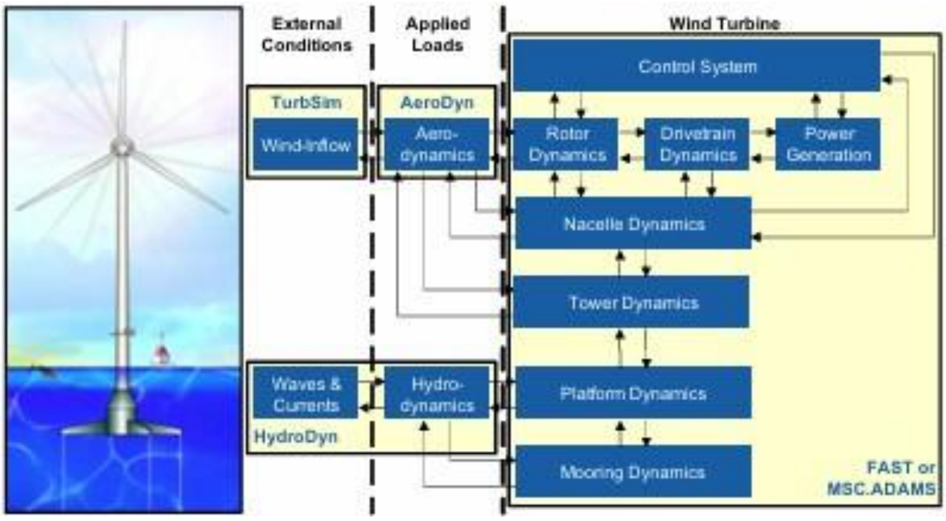

Figure 5.2.1 Interfacing modules to achieve aero-hydro-servo-elastic simulation [66].

From a structural standpoint, the offshore wind turbine is modelled as a flexible multi-body system. The blades and the tower are represented as flexible beam elements using a modal-based approach. Structural deformations are described through a finite number of bending and torsional mode shapes, assuming small deformations and linear elastic behaviour. In the case of floating foundations, the platform is treated as a rigid body with six degrees of freedom and interacts with the mooring system, which introduces additional non-linear effects related to line geometry, initial pretension and water depth.

In this work, particular attention is focused on floating offshore wind turbines (FOWTs), which represent one of the most promising technological solutions for deep-water installations. Floating platforms enable wind turbine deployment in areas characterized by higher and more consistent wind resources. In recent years, several floating platform concepts have been developed, including spar-buoy, tension-leg platform and semi-submersible systems. Although these configurations differ in terms of hydrodynamic response, stability characteristics and mooring system requirements, but share the need for a detailed representation of the coupled platform–mooring–tower dynamics [67].

5.3 Load modelling

The offshore environment is characterized by the combined action of wind, waves and currents, which represent the main sources of loading for offshore wind turbines. An accurate representation of these external agents is a fundamental aspect of the aero-hydro-elastic modelling of floating wind turbine systems, as they directly govern the structural response and overall dynamic behaviour of the system.

Figure 5.3.1 schematically illustrates the typical environmental contributions and the related physical models employed in the simulation of offshore wind turbine behaviour, highlighting the modular architecture adopted in modern aero-hydro-servo-elastic simulation codes. The actions considered exhibit pronounced temporal and spatial variability, which must be adequately represented in order to obtain a realistic description of the environmental conditions acting on the system and the resulting structural response.

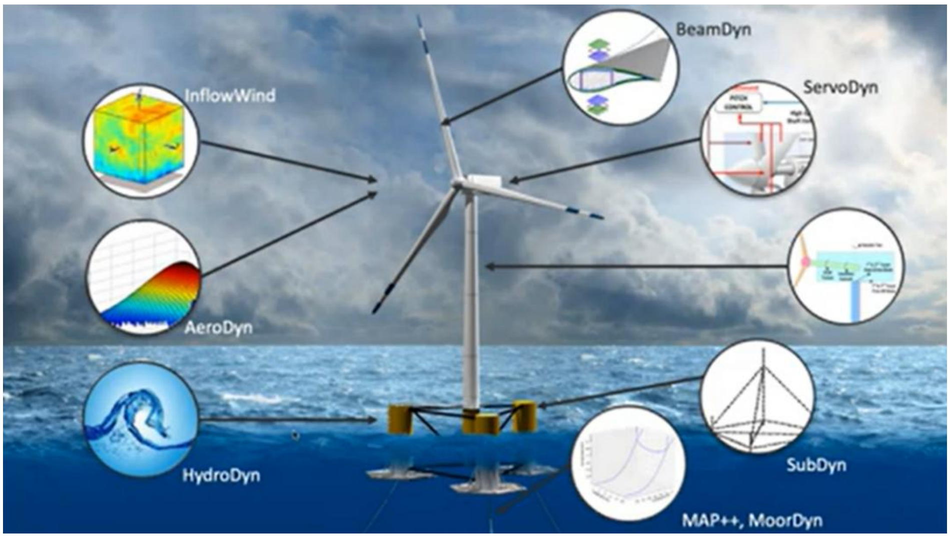

Figure 5.3.1 Schematic representation of the environmental and structural models involved in the aero-hydro-servo-elastic simulation of a floating offshore wind turbine.

Within this framework, wind action is modelled by accounting for its turbulent nature and the aerodynamic theories applicable to rotating rotors. The wind field is generated using stochastic models capable of reproducing the spatial and temporal coherence of speed fluctuations, while the interaction between the flow and the blades is described using aerodynamic models based on Blade Element Momentum theory. These models enable an efficient evaluation of aerodynamic loads distributed along the blades and their variations over time.

Wave action is represented through spectral models capable of reproducing the inherently irregular nature of real sea states. Starting from the assigned wave spectrum, the wave motion is reconstructed in the time domain and associated with the kinematics of fluid particles, which constitute the input for the evaluation of the hydrodynamic forces acting on the structure. These forces are generally computed using Morison-type formulations for slender structural elements, while more advanced modelling approaches may be adopted in the presence of complex geometries.

An additional environmental contribution is provided by marine currents, which can significantly modify the relative velocity between the fluid and the structure, particularly affecting the drag component of the hydrodynamic forces. Currents are typically described by depth-dependent velocity profiles consistent with the oceanographic conditions of the installation site and are combined with wave-induced kinematics in the assessment of the overall hydrodynamic loading.

From a numerical standpoint, each of these environmental contributions is handled within dedicated modules that interact according to a strongly coupled approach. The environmental models supply the aerodynamic and hydrodynamic loads, which are transferred to the structural model of the turbine and its foundation, while the control system acts by modulating the dynamic response through pitch, yaw and power control strategies. The exchange of information among the different modules enables a consistent time-domain simulation of the global system behaviour.

The following subsections present the theoretical background of the main load contributions and physical models adopted, whereas their numerical implementation and specific modelling choices are discussed in the next chapter.

5.3.1 Wind action

The wind loads acting on a FOWT depend on the wind velocity and on the operational condition of the turbine, namely whether it is parked or operating under normal conditions. When the turbine is parked, wind-induced loads are generally limited due to the relatively small projected area of the structural components and the reduced relative velocity between the structure and the airflow. Conversely, under normal operating conditions, the rotating blades sweep a large area and generate significant aerodynamic forces on the rotor. In this case, wind loads are influenced by wind speed, turbine control strategies, blade pitch angle, and rotor yaw misalignment.

As for onshore applications, offshore wind action is commonly decomposed into a mean component and a fluctuating (turbulent) component. The mean wind profile is typically described using a power-law formulation, which is suitable for representing wind speed variations even in offshore environments, where surface roughness is extremely low. The turbulent component, responsible for short-term fluctuations, plays a fundamental role in the generation of non-stationary aerodynamic loads.

To describe the distribution of turbulent energy in the frequency domain, one of the most widely adopted models is the Kaimal spectrum (Eq. (15)), originally proposed to describe velocity fluctuations within the atmospheric boundary layer and subsequently adopted into international standards for wind energy applications. This spectrum forms the basis for the numerical generation of three-dimensional turbulent wind fields. In specific software tools such as TurbSim, the Kaimal formulation is used to generate wind fields that are spatially and temporally coherent, which are then employed in aeroelastic simulations [68].

The interaction between the wind and the rotor is traditionally modelled using BEM theory [69], which combines the momentum balance across an actuator disc with the local aerodynamic behaviour of the individual blade elements. In this framework, the rotor is represented as a permeable actuator disc enclosed within a control volume defined by two cross-sections located far upstream and far downstream of the disc (see Figure 5.3.2). The actuator disc extracts energy from the flow, producing a pressure drop in the fluid downstream.

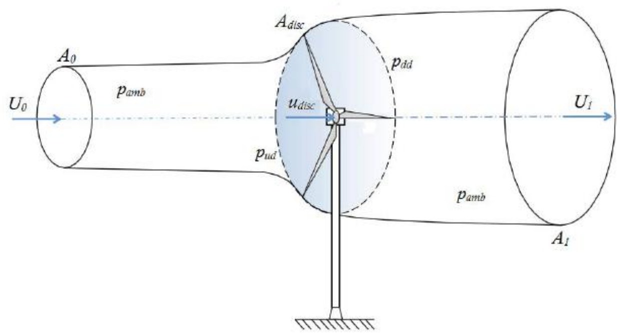

Figure 5.3.2 Rotor represented as an actuator disc and definition of the control-volume streamtube used in the BEM formulation (adapted from [70]).

Denoting U_0 as the free-stream flow velocity, U_1 as the downstream flow velocity and u_{disc} as the velocity on the actuator disc, the axial induction factor is defined as:

$$a = \frac{U_0 - u_{\text{disc}}}{U_0} \tag{16}$$

From this definition, the thrust force exerted by the flow on the rotor can be expressed as:

$$F_A = \frac{1}{2}\,\rho_a A_{\text{disc}} U_0^2\, 4a(1-a) \tag{17}$$

where ρ_a is the air density and A_{disc} denotes the actuator disc area, corresponding to the rotor swept area.

To extend the theory to real wind turbines, the rotor is discretized into a series of concentric annular elements, following the approach originally proposed by Glauert [71]. At each blade section, the aerodynamic behaviour is described by lift and drag forces, which depend on the blade geometry and the aerodynamic characteristics of the airfoil profile:

$$F_L = \frac{1}{2}\rho c W^2 C_L \tag{18}$$

$$F_D = \frac{1}{2}\rho c W^2 C_D \tag{19}$$

where c is the local blade chord length, W is the relative velocity at the blade section and C_L, C_D are the lift and drag coefficients of the aerodynamic profile. The balance between the aerodynamic forces acting on each annular element and the momentum balance in the flow allows the induction factors to be determined, and consequently the distribution of aerodynamic loads along the blade span.

This formulation, which complies with the Danish Design Guidelines [8], constitutes the basis of the aerodynamic models implemented in the AeroDyn module used in aero-hydro-elastic simulations [72]. Starting from the turbulent wind fields generated by TurbSim, AeroDyn computes the aerodynamic forces along the blades, which represent one of the dominant contributions to the global response of floating wind turbines.

5.3.2 Wave action

Wave-induced loads acting on floating foundations depend on water depth and on the characteristics of the prevailing sea states. Since real sea waves are inherently irregular and stochastic in nature, wave motion is typically described through spectral models capable of reproducing the distribution of wave energy across frequency bands. Among these, the Jonswap spectrum is widely adopted for sea states that are not fully developed, a condition frequently encountered in European offshore environments [73]. Compared to the Pierson–Moskowitz spectrum, the Jonswap formulation introduces a peak enhancement factor that enables a more accurate representation of wind-generated or fetch-limited sea states.

The Jonswap spectrum is expressed as:

$$S(\omega) = \alpha g^2 w^{-5} \exp[-\frac{5}{4}(\frac{w_p}{w})^4]\gamma^{\exp\,[-\frac{(w-w_P)^2}{2\sigma^2 w_P{}^2}]} \tag{20}$$

where α is a scale parameter, typically expressed as a function of the significant wave height H_s and the peak frequency ω_p, and g denotes the gravitational acceleration. The angular frequency ω is the independent variable over which the spectral energy is distributed, while ω_p identifies the peak frequency at which the spectrum attains its maximum value. The parameter γ, referred to as the peak enhancement factor, amplifies the spectral peak relative to the Pierson–Moskowitz spectrum to account for non-fully developed sea conditions. The spectral width parameter σ assumes different values depending on whether $\omega \leq \omega_p$ or $\omega > \omega_p$, with typical values of $\sigma = 0.07$ and $\sigma = 0.09$, respectively.

Once the wave spectrum has been defined, time-domain wave kinematics are generated through random wave synthesis, obtained as a superposition of independent harmonic components with amplitudes consistent with the target spectrum. The resulting kinematic quantities, namely the velocities and accelerations of fluid particles, constitute the input for the evaluation of hydrodynamic loads acting on the structure. For slender structural members, wave-induced forces are commonly modelled using Morison's equation [74], which combines an inertia term proportional to the fluid particle acceleration and a drag term dependent on the relative velocity between the fluid and the structure. This formulation is particularly appropriate for cylindrical elements whose characteristic diameter is small compared to the wavelength, a condition typically satisfied by most floating wind turbine support structures.

Wave generation and hydrodynamic load calculations are performed using the HydroDyn module of OpenFAST [75]. HydroDyn analytically generates irregular waves for finite water depths based on linear wave theory and the prescribed input spectrum, and evaluates wave-induced loads through strip theory combined with Morison-type formulations. This modelling approach enables a realistic and computationally efficient representation of the hydrodynamic excitation acting on floating offshore wind turbine platforms.

5.3.3 Current action

In addition to wind and wave actions, offshore structures are also subjected to sea currents. Currents commonly occur in the open sea as a result of wind action on the free surface, tidal motions and density gradients associated with variations in temperature and salinity. From a physical standpoint, sea currents can therefore be classified into wind-generated currents, tidal currents and thermohaline currents. In the context of offshore wind applications, particularly for floating systems installed in deep water, wind-generated currents often constitute the predominant contribution and are thus the most relevant for the assessment of global hydrodynamic loads.

Marine currents influence hydrodynamic forces primarily by modifying the relative velocity between the fluid and the structure. As highlighted by Chakrabarti [76], currents do not introduce significant inertial contributions, but mainly affect the drag component of hydrodynamic forces. Consequently, current-induced loads can be regarded, as a first approximation, as quasi-stationary when compared to wave-induced loads. Nevertheless, the presence of currents may significantly influence the overall response of floating structures, affecting the mean platform offset, the tensions in the mooring lines, and the low-frequency response of the system.

From a modelling perspective, the vertical distribution of current velocity is strongly influenced by the marine boundary layer, resulting in maximum velocities near the free surface and a gradual attenuation with increasing depth. In engineering practice, this behaviour is commonly represented through simplified depth-dependent velocity profiles, such as linear, exponential, or power-law formulations. The adoption of such profiles allows the dominant effects of the current on the structural response to be captured while maintaining an appropriate balance between physical accuracy and computational efficiency. This modelling approach is supported by numerous experimental and numerical studies in the literature, including Nagavinothini and Chandrasekaran [77], which demonstrate that the vertical distribution of current velocity has a significant impact on the hydrodynamic response of floating structures.

In light of these theoretical considerations, attention is focused primarily on wind-generated currents. The speed of the wind-induced current is assumed to vary linearly with depth, reaching its maximum value near the free surface and gradually decreasing toward the seabed. Specifically, a current velocity of 0.50 m/s is applied down to a depth of 60 m; below this depth, the velocity is progressively reduced until it reaches a value of 0.10 m/s at a depth of 90 m, which is then maintained constant down to a depth of 200 m.

Chapter 6

Multi-Hazard Fragility Analysis of Offshore Wind Turbines

Simulation is the imitation of the operation of a real-world process or system over time.

Jerry Banks

The numerical analysis of offshore wind turbines constitutes the final application phase of the methodology developed in this thesis and represents the basis for the multi-hazard fragility assessment presented in this chapter. After analyzing the fundamental design aspects of offshore turbines, their structural peculiarities, and the main environmental actions that govern their behaviour in Chapter 5, this chapter is dedicated to the dynamic simulation of a floating wind turbine using the OpenFAST aero-hydro-servo-elastic code developed by the National Renewable Energy Laboratory (NREL).

OpenFAST allows a fully coupled representation of the interactions between aerodynamics, hydrodynamics, structural dynamics, and control systems, making it a particularly suitable tool for evaluating the overall response of complex systems such as floating offshore wind turbines (FOWTs). Therefore, in this chapter, a representative case study is selected, turbulent wind conditions are generated using TurbSim software, and the structural response of the turbine subjected to the combined action of wind, waves, and currents is analyzed.

The analyses conducted aim to characterize the dynamic response of the system under multiple hazards and to provide the necessary information for the derivation of fragility relationships. This lays the foundation for the probabilistic assessment of structural performance and for future extensions to risk assessment methodologies in offshore environments.

6.1 Selection of case study

The choice of case study is guided by two main criteria: on the one hand, the need to ensure methodological consistency with the analyses conducted for onshore turbines in the previous chapters; on the other hand, the interest in exploring an offshore technology that represents a significant challenge from both an industrial and scientific point of view.

As regards the superstructure, the NREL 5 MW baseline wind turbine, already used in the onshore analyses, was adopted. This choice allows a common basis to be maintained between the two application contexts and makes the comparison between the structural behavior of turbines installed on land and those in an offshore environment more meaningful, isolating the effect of the different foundation configuration and environmental actions.

For the offshore context, the NREL 5 MW turbine was therefore coupled with an OC4-DeepCwind semi-submersible floating foundation, which is one of the most advanced technologies and currently the subject of intense interest in the scientific and industrial community. Floating foundations allow turbines to be installed in deep waters, significantly expanding the potential for exploiting wind resources, but at the same time introducing high levels of complexity in structural modeling and dynamic response assessment.

Despite the growing interest in this technology, the studies available in the literature are still limited, particularly with regard to the analysis of the coupled behavior between the floating platform, mooring system, and superstructure, as well as the assessment of uncertainties associated with environmental loads and the nonlinear response of the system. In this sense, the OC4 floating foundation is a particularly significant case study for the analysis of multi-hazard risk in the offshore environment. The overall configuration of the system analyzed is shown in Figure 6.1.1 a, while the structural layout of the OC4 floating platform is shown in Figure 6.1.1 b.

From a construction point of view, the OC4 floating platform consists of three vertical columns arranged at the vertices of a triangle and connected to each other by horizontal elements and bracing. The turbine tower is installed on a central column, integral with the floating structure. This structural configuration ensures adequate overall stability and achieves natural periods compatible with the main energy components of the dynamic actions acting on the system, such as wind and wave motion. The geometry of the platform and the distribution of masses are designed to limit dynamic amplification and ensure a controlled structural response under the design operating conditions. The main geometric and structural properties of the NREL 5 MW turbine and the OC4-DeepCwind floating platform adopted as a case study are shown in Table 6.1.1.

Ultimately, the choice of OC4 technology provides a representative and widely validated case study, thanks to the availability of technical data sheets [78]. At the same time, it ensures methodological consistency with the analyses carried out for onshore turbines and allows the differences in structural response between ground-based configurations and floating structures operating in an offshore environment to be clearly highlighted.

(a) (b)

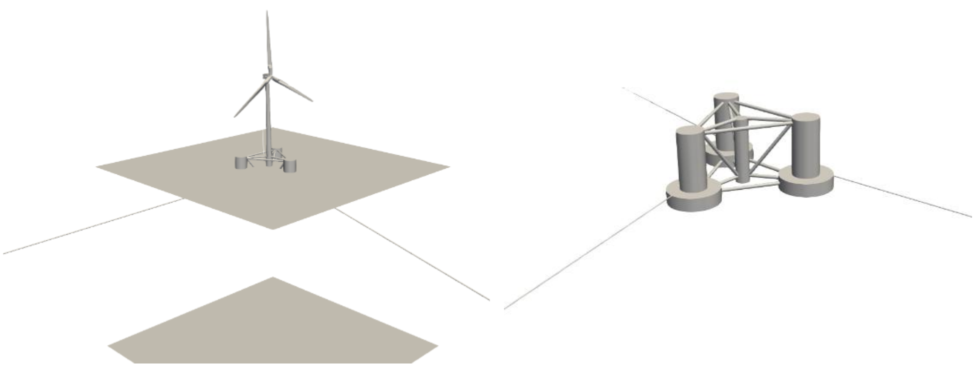

Figure 6.1.1 (a) Schematic representation of the wind turbine with the rotor modelled as an aerodynamic actuator. (b) Structural layout of the OC4 semi-submersible floating platform.

Table 6.1.1 Main structural properties of the NREL 5 MW floating wind turbine (OC4-DeepCwind).

Subsystem	Wind Turbine	OWT semi-submersible
Rotor	Hub height	90 m
	Rotor diameter	126 m
	Blade length	61.5 m
	Cut-in, rated and cut-out wind speed	3 m/s, 11.4 m/s, 25 m/s
	Cut-in and rated rotor speed	6.9 rpm, 12.1 rpm
	Rotor mass	110000 kg
Nacelle	Nacelle mass	240000 kg
Tower	Tower top height	87.6 m
	Tower base height	10 m
	Top outer diameter and wall thickness	3.87 m, 0.019 m
	Bottom outer diameter and wall thickness	6.5 m, 0.027 m
Substructure	Transition piece height	10 m above SWL
	Platform mass	$13.47 \cdot 10^6$ kg
	Outer diameter and wall thickness (main column)	6.5 m, 0.03 m
	Outer diameter and wall thickness (offset columns)	12 m, 0.06 m
	Mass density (steel)	7850 kg/m^3
	Water depth	200 m

6.2 Wind simulation using TurbSim

Wind action on offshore wind turbines is modeled using a stochastic description of atmospheric turbulence. In common practice for the analysis of offshore structures, the wind field is generated using TurbSim [79], a turbulent wind simulator developed by the National Renewable Energy Laboratory (NREL) and widely used within the OpenFAST framework.

TurbSim is based on a statistical approach, in which atmospheric turbulence is described in terms of velocity spectra and spatial coherence functions, rather than by directly solving fluid dynamics equations. In this context, wind is treated as a stationary random process, and the temporal evolution of the velocity components is obtained through an inverse Fourier transform from the frequency domain to the time domain.

The code generates time series of the three components of wind speed at a set of points distributed on a two-dimensional vertical grid, fixed in space and centered at the height of the turbine hub. This “full-field” representation allows explicit consideration of the spatial variability of the wind over the area swept by the rotor, which is essential for the correct evaluation of non-uniform aerodynamic loads and asymmetric load conditions. A schematic representation of the wind field generated by TurbSim is shown in Figure 6.2.1.

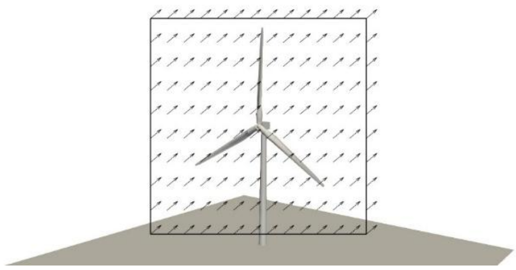

Figure 6.2.1 Full-field wind representation generated by TurbSim: wind velocity vectors defined on a vertical two-dimensional grid centered at hub height and covering the rotor swept area.

The grid size must be chosen very carefully. The spatial extent and resolution of the wind grid are chosen so as to cover the entire area swept by the rotor, with dimensions consistent with the rotor diameter and centered at hub height. The spatial discretization of the wind field is defined in such a way as to ensure a correct representation of turbulent variability and to be compatible with the aerodynamic discretization adopted in the AeroDyn module of OpenFAST. An inadequate definition of the grid could in fact lead to an inaccurate estimate of the non-uniform aerodynamic loads acting on the blades.

The wind field generated by TurbSim is then fed into the AeroDyn module, which calculates the local velocities acting on the blade elements using Taylor's frozen turbulence hypothesis. According to this assumption, turbulent structures are transported along the direction of the average wind at the average hub speed, allowing the wind speed perceived by the rotating blades to be reconstructed by means of appropriate spatial and temporal interpolations of the generated wind field.

TurbSim allows the use of different spectral turbulence models, including those defined by IEC standards, as well as site-specific models. In addition, different vertical wind speed profiles can be assigned, such as the power law profile or the logarithmic profile, allowing the effect of wind shear along the height of the rotor to be represented realistically.

It should be noted that the wind fields generated by TurbSim are based on certain simplifying assumptions, including the stationarity of the wind field, the spatial homogeneity of turbulence, and the validity of the frozen turbulence assumption. Despite these assumptions, TurbSim is a well-established and computationally efficient tool for generating wind actions and is currently considered the benchmark for most numerical analyses of offshore wind turbines.

From a structural engineering perspective, this approach provides a consistent and sufficiently accurate description of the aerodynamic actions required for the analysis of the coupled dynamic response of the turbine-support structure system, while ensuring an adequate balance between modeling realism and computational burden.

6.3 Failure modes for offshore wind turbines

Compared to onshore wind turbines and fixed-foundation offshore turbines, floating configurations are subject to additional sources of uncertainty related not only to the combined action of wind, waves, and currents, but also to the dynamic behavior of the floating platform and mooring system. These aspects significantly influence failure modes and overall system reliability.

Several studies have analyzed the failure modes of offshore and floating wind turbines based on past events and maintenance records. Li et al. ([80]) showed that the parts most prone to failure are electrical systems, pitch and yaw systems, and cooling and hydraulic systems. They also highlight that the failure rate of floating offshore wind turbines is approximately 28.6% higher than that of onshore turbines, mainly due to harsher environmental conditions, greater system complexity, and difficulties in accessing the turbines for maintenance operations.

A more detailed analysis of FOWT failure modes was conducted by Sun et al. ([81]), who examined the maintenance records of four offshore wind farms. A significant finding from this study is that failures cannot be considered independent, but are often correlated due to the sharing of common subsystems, such as cooling and control systems. This correlation can lead to cascading phenomena, in which an initially limited failure evolves into more severe consequences at the system level.

From a functional and structural point of view, the failure modes of floating offshore wind turbines can be divided into several main categories. The first category concerns the components of the wind turbine itself, such as blades, drivetrain, gearbox, generator, and control systems, which are frequently subject to problems related to abnormal vibrations, overheating, bearing wear, and electrical malfunctions. A second category concerns the tower and connecting elements, for which corrosion and welding defects are critical. A third category is associated with the floating foundation, which can be subject to structural damage due to hydrodynamic actions, corrosion, or accidental impacts. Finally, the mooring system is one of the most critical elements for FOWTs, as it is subject to corrosion and line overvoltage, which can compromise its ability to maintain position and lead to systemic collapse scenarios. In particular, Sun et al. ([81]) have highlighted how the mooring system and floating foundation play a key role in the overall safety of the turbine, as exceeding certain tension or displacement thresholds can trigger mechanisms of global instability and loss of balance. The occurrence of abnormal stresses is therefore a major cause of failure, especially in extreme environmental conditions.

From a regulatory point of view, the DNV guidelines ([82], [83]) indicate that offshore wind turbines must be verified in terms of both Serviceability Limit States (SLS) and Ultimate Limit States (ULS). SLS are associated with tolerance criteria related to normal turbine operation and include excessive deformation, vibration, and displacement that can compromise the operation of non-structural components or lead to turbine shutdown. ULS, on the other hand, are related to the loss of load-bearing capacity or stability of the system and can manifest themselves through phenomena such as global instability, local instability, buckling, or structural component failure.

However, defining parameters that represent the achievement of performance levels is not straightforward, especially with regard to the temporary outage of offshore turbines. De Risi et al. ([84]) highlighted the difficulty of identifying a single indicator for this condition and proposed the use of structural response parameters, such as maximum chord rotation and bending moment at the base of the tower, as proxies for exceeding SLS and ULS, respectively. Although their study focuses on fixed-foundation offshore turbines, the failure mechanisms identified, such as excessive vibrations, large rotations, and local instability governed by bending moment, are also relevant for floating configurations.

More recent studies have extended these concepts to floating offshore wind turbines subject to combined aero-hydrodynamic loads. Sheng et al. ([85]) showed that the systemic collapse of FOWTs is frequently governed by excessive bending demand at the base of the tower. Consequently, failure modes related to global instability, local buckling, and loss of mooring system efficiency emerge as dominant mechanisms under severe environmental conditions.

Overall, the literature highlights how the failure modes of floating offshore wind turbines are strongly influenced by the interaction between aerodynamic and hydrodynamic loads and the dynamic response of the system ([86]). The recurrence of failure mechanisms associated with excessive deformation and vibration, as well as global instability phenomena, suggests the need for a performance-based approach, in which appropriate engineering response parameters are able to describe both performance degradation during operation and structural collapse. These considerations constitute the conceptual reference for the definition of the performance levels adopted in the following paragraphs.

6.4 Sensitivity analysis under combined loads

Based on the failure modes discussed in Section 6.3, it is possible to identify a set of Engineering Demand Parameters (EDP) that describe the structural and functional behavior of floating offshore wind turbines under the combined action of wind, waves, and currents. In particular, quantities such as drift at the top of the tower, nacelle acceleration, bending moment at the base of the tower, and mooring line stresses are directly related to the performance degradation and systemic collapse mechanisms identified in the literature.

Figure 6.4.1 shows a representative sample of the time histories of the environmental loads and the corresponding Engineering Demand Parameters adopted in the sensitivity analysis.

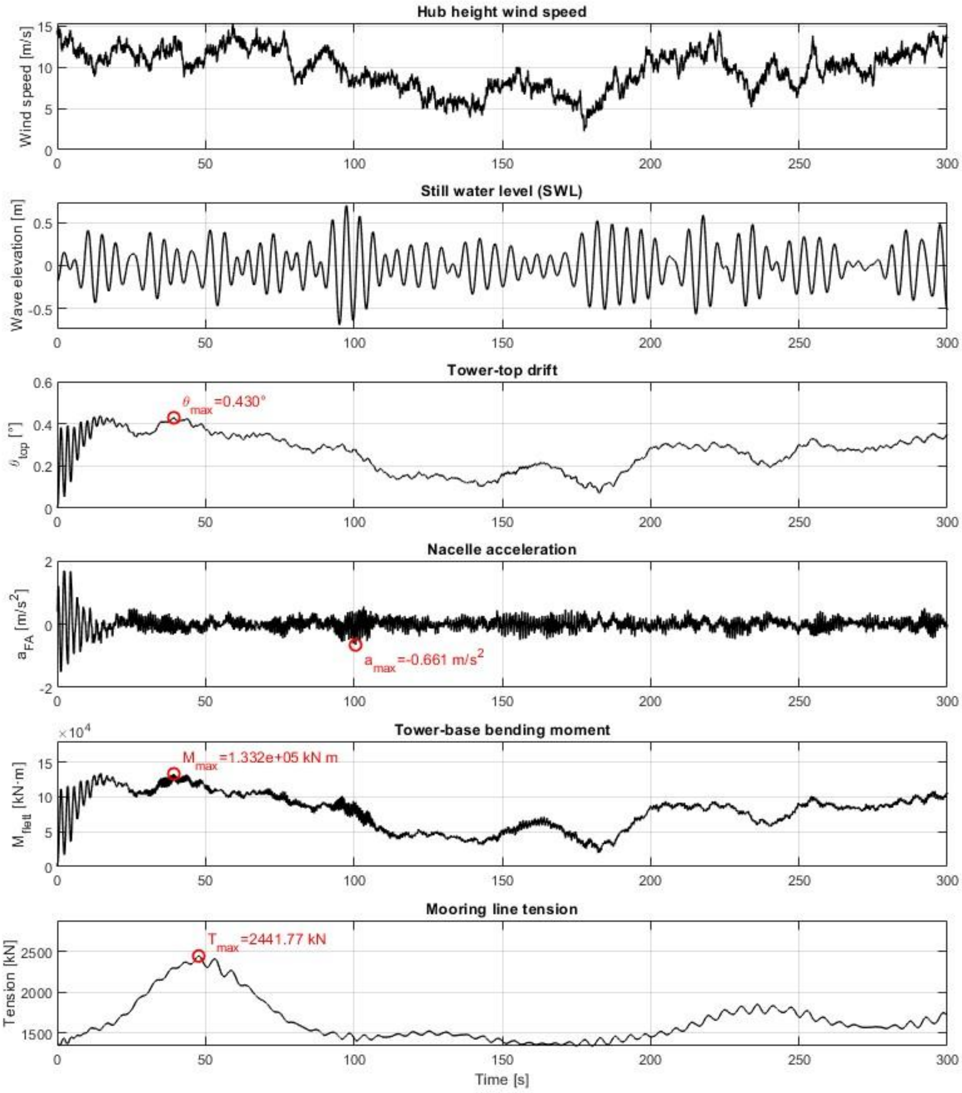

Figure 6.4.1 A sample of the time histories of wind speed, wave height and structural response obtained from OpenFAST simulations for the OC4 floating wind turbine under $[\boldsymbol{V_{hub}}, \boldsymbol{H_s}]$ = [10 m/s, 1.2 m]: a) along-direction wind speed at hub height; b) wave elevation at the still water level; c) tower top drift; d) nacelle acceleration; e) tower base bending moment and f) mooring line tension force.

The sensitivity analysis is therefore aimed at assessing how these EDPs vary as the intensity of the environmental loads considered increases and at understanding which actions are dominant in controlling the response of the system. This analysis represents a fundamental intermediate step between the identification of failure modes and the subsequent definition of performance levels.

To this aim, selected results of the sensitivity analyses are discussed in the following, highlighting the dependence of the main EDPs on wind, wave and current loading.

The adopted approach is parametric: the intensity of one environmental action is incrementally varied while keeping the others constant, in order to isolate the contribution of each load (wind, wave and current) to the structural response.

Wind sensitivity

The first series of sensitivity analyses concerns wind action, considered the main load acting on the wind turbine. Wind speed is progressively increased, analyzing the system's response in terms of the various EDPs. The simulations show how an increase in wind speed leads to a significant increase in all the EDPs considered, highlighting a strong dependence of the overall system response on aerodynamic action (see Figure 6.4.2).

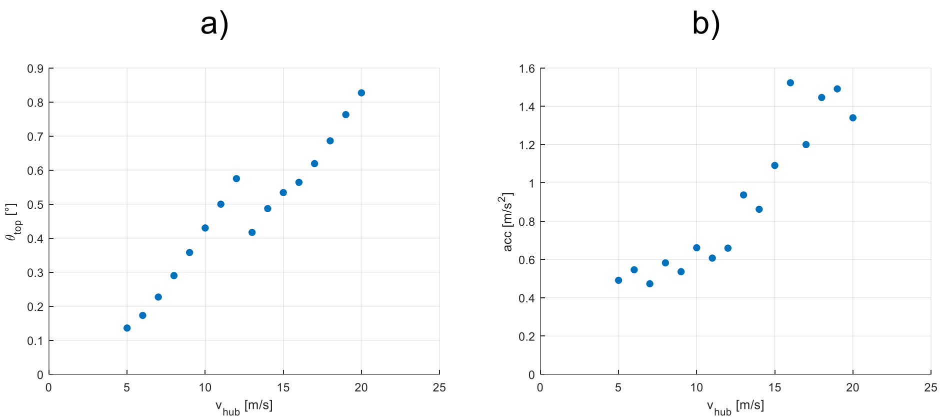

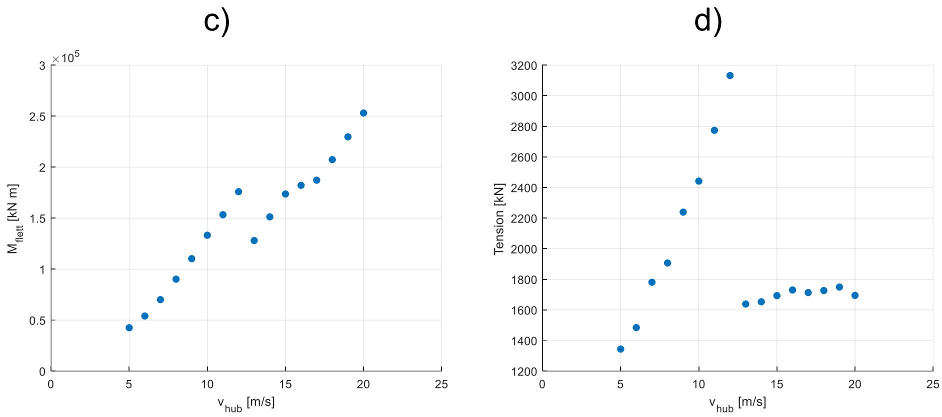

Figure 6.4.2 Sensitivity of selected Engineering Demand Parameters to hub-height wind speed for the OC4 floating wind turbine: a) tower top drift; b) nacelle acceleration; c) tower base bending moment and d) mooring line tension force.

When the rated speed is about to be exceeded, it is necessary to modify the initial operating conditions of the turbine in order to take into account the intervention of the control systems. This aspect is particularly relevant, as it directly affects the trend of the EDPs and their evolution with load intensity, confirming the key role of aeroelastic interaction in the behaviour of wind turbines.

Sensitivity to wave motion

The second series of sensitivity analyses focuses on wave motion. The intensity of wave action is varied through the significant wave height, while keeping other environmental conditions constant. The results show that wave motion has a significant effect on the dynamic response of the system, particularly on the drift at the top of the tower, the bending moment at the base and the tensions in the mooring lines (see Figure 6.4.3).

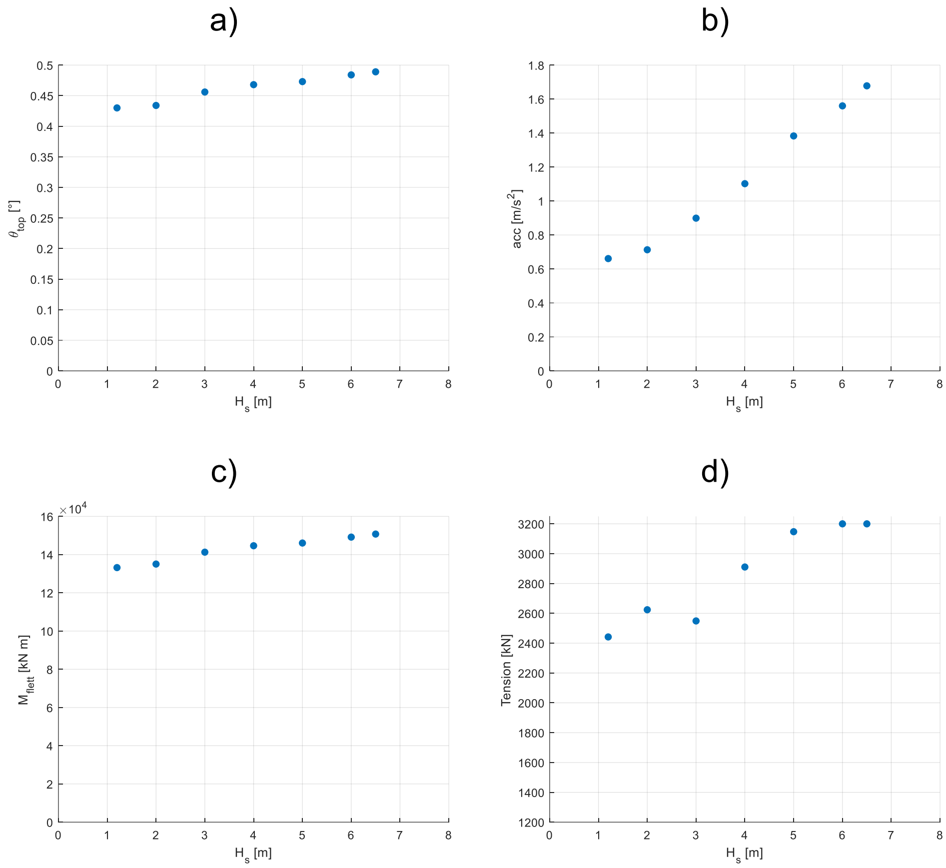

Figure 6.4.3 Sensitivity of selected Engineering Demand Parameters to significant wave height for the OC4 floating wind turbine: a) tower top drift; b) nacelle acceleration; c) tower base bending moment and d) mooring line tension force.

Compared to wind action, wave motion is more closely related to the global oscillation phenomena of the floating platform, with amplified effects on the low-frequency structural response. These results are in agreement with what is reported in the literature for floating offshore turbines subject to combined aerodynamic and hydrodynamic loads and confirm the need to include wave motion action in the assessment of the structural performance of the system.

Sensitivity to current

Finally, a sensitivity analysis was conducted with respect to the action of the marine current. The current is modeled as wind-generated, with maximum velocity near the sea surface and decreasing with depth, according to a standard profile implemented in the HydroDyn module of OpenFAST. The parameters of the current profile are defined on the basis of studies in the literature and appropriately adapted to the case in question.

The results indicate that the current has a generally limited influence on the response parameters associated with operating conditions, such as drift at the top of the tower and acceleration of the nacelle. However, its contribution becomes more significant in terms of mooring line stresses, especially in combination with wind and wave motion (see Figure 6.4.4).

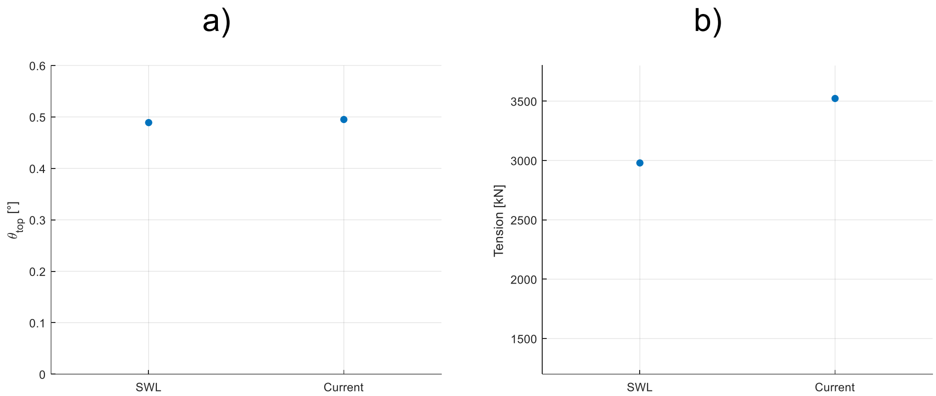

Figure 6.4.4 Comparison of selected Engineering Demand Parameters for still water level (SWL) and current loading conditions for the OC4 floating offshore wind turbine: a) tower top drift; b) mooring line tension force.

This suggests that, while not dominant in controlling operational performance, current can play a significant role in the assessment of ultimate limit states and systemic collapse mechanisms.

In addition to the sensitivity analyses on environmental loading parameters, a preliminary assessment was also performed to evaluate the influence of the simulation length on both the structural response and the associated computational cost. Three different analysis durations were considered, namely 150 s, 300 s and 600 s. The results indicate that reducing the simulation length from 600 s to 300 s leads to variations below 5–10% in the main response parameters, while approximately halving the overall computational time. Conversely, a further reduction to 150 s results in a more pronounced loss of accuracy. On this basis, a simulation length of 300 s was adopted for the subsequent analyses, representing an effective compromise between result accuracy and computational efficiency.

Overall, sensitivity analysis allows the identification of the environmental actions that most influence the structural response of floating offshore turbines and highlights the response parameters that are most representative of performance degradation and collapse mechanisms. These results form the basis for defining the performance levels adopted in the following paragraph.

6.5 Definition of performance levels for FOWTs

The definition of performance levels is supported by the results of the sensitivity analysis. Performance levels (PLs) represent a key component in the assessment of the structural vulnerability of floating offshore wind turbines, as they provide a direct link between the system response, expressed through Engineering Demand Parameters (EDPs) and physically interpretable damage states.

In accordance with the reference literature and the main regulatory guidelines for offshore structures, in particular those proposed by DNV, the performance levels of offshore wind turbines are generally defined with reference to the structural serviceability limit states and ultimate limit states.

Based on the failure modes discussed in Section 6.3 and the results of the sensitivity analysis presented in Section 6.4, this study defines three performance levels, characterized by exceeding thresholds assigned to specific EDPs. Table 6.5.1 summarizes the performance levels adopted, the associated damage level, and the engineering response parameters used for their definition.

Table 6.5.1 Performance levels considered for fragility analysis of offshore wind turbines.

Category	PL	Description	EDP	Threshold
SLS	PL1	Temporary shutdown without need for intervention	θ_{top}	θ_{max}
SLS	PL2	Shutdown requiring maintenance actions	a	a_{max}
ULS	PL3	Systemic collapse	M, T	M_u, T_{lim}

The first performance level (PL1) is associated with minor damage and represents temporary turbine shutdown conditions without the need for intervention. This level is linked to excessive drift at the top of the tower (θ_{top}), which can compromise operational stability and control system efficiency, even in the absence of significant structural damage. Exceeding PL1 is therefore assessed in terms of rotation or displacement at the top of the tower, a parameter widely used in the literature as an indicator of loss of operability for wind turbines.

The second performance level (PL2) represents a more severe state of damage, associated with turbine shutdown conditions requiring maintenance intervention. In this case, the damage is mainly related to high levels of nacelle acceleration (a), which can cause malfunction or damage to electromechanical components and auxiliary systems. Exceeding PL2 is therefore assessed by means of nacelle acceleration, considered a key parameter for assessing the operational safety of offshore turbines.

The third performance level (PL3) is associated with systemic collapse and loss of the turbine's overall load-bearing capacity. In the case of floating offshore wind turbines, such collapse conditions may involve both the structural components of the tower and the mooring system responsible for maintaining the platform's position. In particular, structural collapse can manifest itself through local instability phenomena at the base of the tower, such as local buckling, which are indirectly evaluated here by means of the bending moment at the base of the tower. However, in floating offshore wind turbines, exceeding the capacity of the mooring lines represents an additional and independent mechanism of collapse. In particular, the attainment of high tensile forces, often associated with the most stressed mooring line, can cause the platform to lose its correct trim and lead to systemic collapse. For this reason, performance level PL3 is defined by exceeding two engineering response parameters: the bending moment at the base of the tower (M) and the tension in the mooring lines (T).

For the case study analyzed in this work, the thresholds associated with the different performance levels are defined as follows. Level PL1 is considered exceeded when the drift at the top of the tower reaches a value of 0.25°, in line with values commonly adopted in the literature for offshore turbines [84]. Level PL2 is associated with a nacelle acceleration threshold of 1 m/s², beyond which turbine operation is considered unsafe and requires maintenance [86]. Finally, level PL3 is considered exceeded when at least one of the two parameters exceeds its respective capacity threshold, represented by the ultimate bending moment M_u or the limit stress T_{lim} [85].

The performance levels form the basis for the subsequent formulation of the fragility curves and surfaces presented in Section 6.6.

6.6 Fragility analysis framework for FOWTs

The definition of structural vulnerability for wind turbines was introduced in Section 4.3. In a probabilistic context, vulnerability quantifies the sensitivity of the structural response to increased external loads and is a fundamental element in the risk assessment of infrastructure, in this case offshore. Accordingly, and in line with approaches commonly adopted in performance-based seismic engineering and in the vulnerability assessment of onshore wind turbines, the vulnerability of floating offshore wind turbines is described through the relationship between structural demand and capacity, expressed in terms of EDPs and corresponding performance thresholds. This relationship is formalized through fragility functions, which express the conditional probability of reaching or exceeding a given performance level for assigned values of the intensity measures characterizing the external actions.

In the case of floating offshore wind turbines, the definition of fragility functions is particularly complex due to the strongly coupled aero-hydro-servo-elastic behaviour of the system. The structural response is not governed exclusively by wind action, but is influenced by the concomitant presence of wave motion and sea currents, which interact with the dynamics of the floating platform and the turbine control systems. Consequently, the vulnerability of FOWTs cannot always be comprehensively represented by one-dimensional fragility curves, making a multidimensional description using fragility surfaces necessary in many cases.

In this study, the fragility analysis is performed using the Incremental Dynamic Analysis (IDA) approach. This methodology consists of a sequence of nonlinear time-domain dynamic analyses in which the intensity of the considered environmental actions is progressively increased, while monitoring the evolution of selected EDPs. For each intensity level, the structural response is compared against the thresholds defining the performance levels introduced in Section 6.5.

The proposed fragility framework is divided into four main phases. First, the main sources of uncertainty affecting structural response and environmental loads are explicitly modelled. Subsequently, fragility curves associated with wind action considered individually are derived, assuming the hub-height wind speed as the reference intensity measure. The analysis is then extended to combined loading conditions, including wind–wave and wind–current interactions, through the definition of fragility surfaces that capture the joint effect of multiple environmental actions.

When multiple concurrent environmental actions are considered, fragility is formulated in a bivariate framework by expressing the probability of exceeding a given performance level as a function of two intensity measures. The median structural demand is modelled through a multiplicative power-law relationship, calibrated by linear regression in log-space:

$$\ln(EDP) = \ln(a) + b\ln(IM_1) + c\ln(IM_2) \tag{21}$$

Assuming a lognormal distribution of EDP with logarithmic dispersion β, the bivariate fragility surface for a threshold edp is given by:

$$\mathrm{P}\,[\,\mathrm{EDP} > \mathrm{edp} \mid \mathrm{IM}_1, \mathrm{IM}_2\,] = \,\phi\left(\frac{\ln(EDP) - \ln\,(edp)}{\beta}\right) \tag{22}$$

where IM_1 and IM_2 denote two intensity measures that describe the combined environmental loading acting on the system. In this study, IM_1 is assumed to be the wind speed at hub height, while IM_2 represents either the significant wave height or the sea current velocity, depending on the specific load combination under consideration. The parameters a, b, and c are obtained through regression analysis of the structural demand and quantify the relative influence of the two intensity measures, whereas β represents the total logarithmic dispersion, accounting for demand variability, capacity uncertainty, and modelling uncertainties.
The function $\Phi(\cdot)$ denotes the cumulative distribution function of the standard normal distribution, consistent with the lognormal fragility assumption.

Starting from the bivariate fragility surface, the conditional fragility function associated with a given environmental state can be obtained through probabilistic integration. In particular, conditioning on the second intensity measure IM_2, the probability of exceeding the selected performance level can be expressed as:

$$\begin{aligned} &\mathrm{P}\,[\,\mathrm{EDP} > \mathrm{edp} \mid \mathrm{IM}_2\,] \\ &\qquad = \int \mathrm{P}\,[\mathrm{EDP} > \mathrm{edp} \mid \mathrm{IM}_1 = v, \mathrm{IM}_2]\; \mathrm{f}_{\mathrm{IM}_1 | \mathrm{IM}_2}(v)\; dv \end{aligned} \tag{23}$$

where v is a dummy integration variable representing a generic realization of the hub-height wind speed and $\mathrm{f}_{\mathrm{IM}_1|\mathrm{IM}_2}(v)$ denotes its conditional probability density function.

Under the assumption of lognormal structural demand and of a lognormal conditional distribution of the hub-height wind speed, the above expression admits a closed-form solution, leading to the following conditional fragility function:

$$\mathrm{P}\left[\,\mathrm{EDP} > \mathrm{edp}\mid \mathrm{IM}_2\,\right] = \phi\left(\frac{\ln(IM_1) - \ln\big(\mu(IM_2)\big)}{\beta(IM_2)}\right) \tag{24}$$

where $\mu(IM_2)$ and $\beta(IM_2)$ denote the median and the logarithmic dispersion of the conditional fragility function, respectively, expressed as functions of the second intensity measure. This expression highlights that the conditional fragility function represents the analytical integration of the bivariate fragility surface over the conditional distribution of the hub-height wind speed given the environmental state. The conditional formulation therefore enables the influence of secondary environmental actions to be consistently incorporated, while preserving a continuous probabilistic description of performance exceedance in the space of load intensities.

6.6.1 Modelling of uncertainties

The assessment of the fragility of floating offshore wind turbines requires an explicit representation of the main sources of uncertainty. In a probabilistic context, these uncertainties arise both from the modeling of the structural system and its components, and from the description of environmental actions and operating conditions of the turbine. Their correct characterization is particularly relevant in the case of FOWTs, due to their strongly coupled aero-hydro-servo-elastic behavior and the marked variability of metocean conditions.

Several studies in the literature have shown that the inclusion of model, material, and environmental uncertainties has a significant impact on vulnerability estimates. In particular, Wilkie and Galasso ([87], [88]) have shown that the uncertainty associated with dynamic modeling and structural capacity can substantially influence the probability of exceeding performance levels, even in the presence of well-characterized environmental actions. Other contributions have focused mainly on the variability of environmental actions, highlighting how the stochastic nature of wind and wave motion represents one of the main sources of dispersion in the response of offshore turbines. In these studies, the uncertainty associated with loads is often modeled through the variability of spectral parameters, characteristic intensities, and environmental signal generation processes, showing how different realizations of the same meteo-ocean scenario can lead to significantly different structural responses ([89], [90]).

Based on these considerations, in this work, uncertainties are modeled by introducing random variables that act on the main parameters of the numerical model and on the environmental input quantities. In particular, model uncertainties take into account approximations in the description of structural dynamics, in the definition of the material model, and in the evaluation of critical loads associated with collapse mechanisms, such as local instability at the base of the tower. The properties of structural materials, such as the elastic modulus and yield strength of steel, are also treated as random variables, in accordance with what is commonly adopted in the literature on the fragility of offshore structures.

Additional sources of uncertainty are associated with the operating conditions of the rotor and the description of environmental loads. In particular, the orientation of the rotor and the angular position of the blades are modeled as uniformly distributed random variables in order to represent the variability of the dynamic response. Similarly, the stochastic nature of wind and wave motion is represented by the variability of the seeds used to generate turbulent wind fields and wave motion signals.

The probability distributions and statistical parameters adopted for modeling uncertainties are defined based on the information provided in the literature and are summarized in Table 6.6.1.

Table 6.6.1 Random variables adopted for uncertainty modelling in the fragility analysis.

Type	Parameter	Mean	CoV	Distribution
Model uncertainty (structural dynamics)	Structural response parameters (displacement, velocity, acceleration)	1	0.05	Lognormal
Model uncertainty (material)	Material model factor	1	0.05	Lognormal
Model uncertainty (critical load)	Buckling factor	1	0.10	Lognormal
Material	Steel Young's modulus	1	0.02	Lognormal
	Steel yield strength	1	0.05	Lognormal
Rotor	Yaw angle	[-8°, 8°]		Uniform
	Blade azimuth angle	[0°, 180°]		Uniform
Environmental	Wind seed	[0, 1]		Uniform
	Wave seed	[0, 1]		Uniform

The explicit introduction of these uncertainties allows us to take into account the dispersion observed in the structural response for the same intensity of environmental action and is a fundamental element in the construction of the fragility curves and surfaces presented in the following paragraphs. In this way, the fragility of FOWTs is assessed not as a deterministic relationship between demand and capacity, but as a probabilistic measure that consistently incorporates the intrinsic variability of the system and the offshore environment.

6.6.2 Fragility curves for Wind Loading

The analysis of fragility with respect to wind action represents the first step in the probabilistic assessment of the vulnerability of floating offshore wind turbines, as wind is the main environmental load during the operational life of the system. Unlike the onshore case, where the turbulent component of the wind was modeled using a spectral representation, in this study the wind fields are generated using the

TurbSim code, as described in Section 6.2. This approach allows for a more realistic description of atmospheric turbulence and its interaction with the dynamics of the rotor and the floating structure.

The assessment of wind vulnerability is conducted using Incremental Dynamic Analysis (IDA). The intensity measure adopted is the average wind speed at the hub, V_{hub}, which is progressively increased within the turbine's operating range. For each intensity level, nonlinear dynamic analyses are performed in the time domain, and the engineering response parameters associated with the performance levels defined in Section 6.5 are extracted.

For each value of V_{hub}, exceeding the different performance levels is assessed by comparing the maximum EDP values with the corresponding capacity thresholds. The set of simulations allows the probability of exceeding each performance level to be estimated for each wind intensity level.

In order to take into account the uncertainty associated with the numerical sampling strategy, the fragility curves are initially derived using the Latin Hypercube Sampling (LHS) method and then corrected by comparison with reference solutions obtained using Monte Carlo (MC) simulations. For each performance level, correction factors are defined for the median and logarithmic dispersion of the fragility function, calculated as the ratio between the parameters obtained with the MC method and those derived with the LHS method. This procedure allows the computational efficiency of the LHS method to be maintained, while reducing the bias introduced by a limited number of simulations.

In accordance with scientific literature, the probability of exceeding each performance level is modeled using a lognormal distribution. The corrected fragility curves describe the conditional probability of exceeding performance levels as a function of the average hub wind speed and provide a summary representation of the vulnerability of the floating offshore turbine to wind action.

The wind fragility curves obtained for the different performance levels are shown in Figure 6.6.1, while the corresponding statistical parameters of the lognormal distribution are summarized in Table 6.6.2.

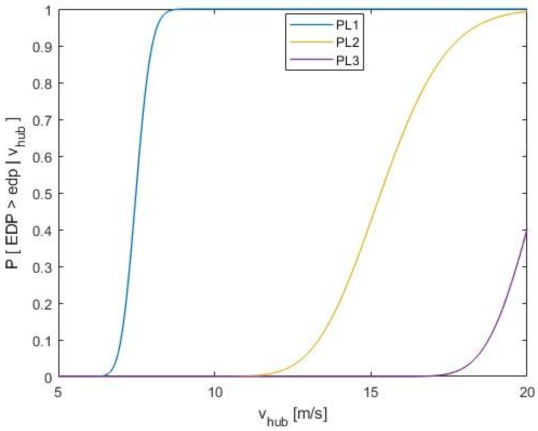

Figure 6.6.1 Wind fragility curves of the offshore wind turbine.

Table 6.6.2 Parameters of wind fragility curves for the offshore wind turbine.

Fragility curve	μ [m/s]	β
S-PL1	7.48	0.05
S-PL2	15.32	0.11
S-PL3	20.31	0.06

6.6.3 Fragility surfaces under combined Wind and Wave effects

The structural response of floating offshore wind turbines is governed by the combined action of wind and wave loading, due to the strong coupling between aerodynamic excitation, hydrodynamic forces acting on the floating platform and the global aero–hydro–servo–elastic behaviour of the system. As highlighted by the sensitivity analysis presented in Section 6.4, wave motion plays a relevant role in modulating the overall response of the structure, particularly in terms of platform oscillations and load transfer to the tower and mooring system. Consequently, a vulnerability representation based exclusively on one-dimensional fragility curves is generally insufficient to fully characterize the behaviour of the system under combined environmental actions.

To explicitly account for wind–wave interaction effects, fragility is formulated within a bivariate framework by defining fragility surfaces that express the probability of exceeding a given performance level as a function of two intensity measures: the hub-height wind speed, V_{hub}, and the significant wave height, H_s. The adopted methodology is consistent with the general fragility framework described in Section 6.6 and is based on the execution of nonlinear time-domain dynamic analyses for increasing combinations of wind and wave intensity.

For each performance level, the structural demand was modelled through a bivariate lognormal formulation, allowing the joint influence of wind and wave loading on structural vulnerability to be captured. The resulting bivariate fragility surfaces provide a continuous probabilistic description of performance exceedance in the two-dimensional space defined by wind speed and significant wave height (see Figure 6.6.2).

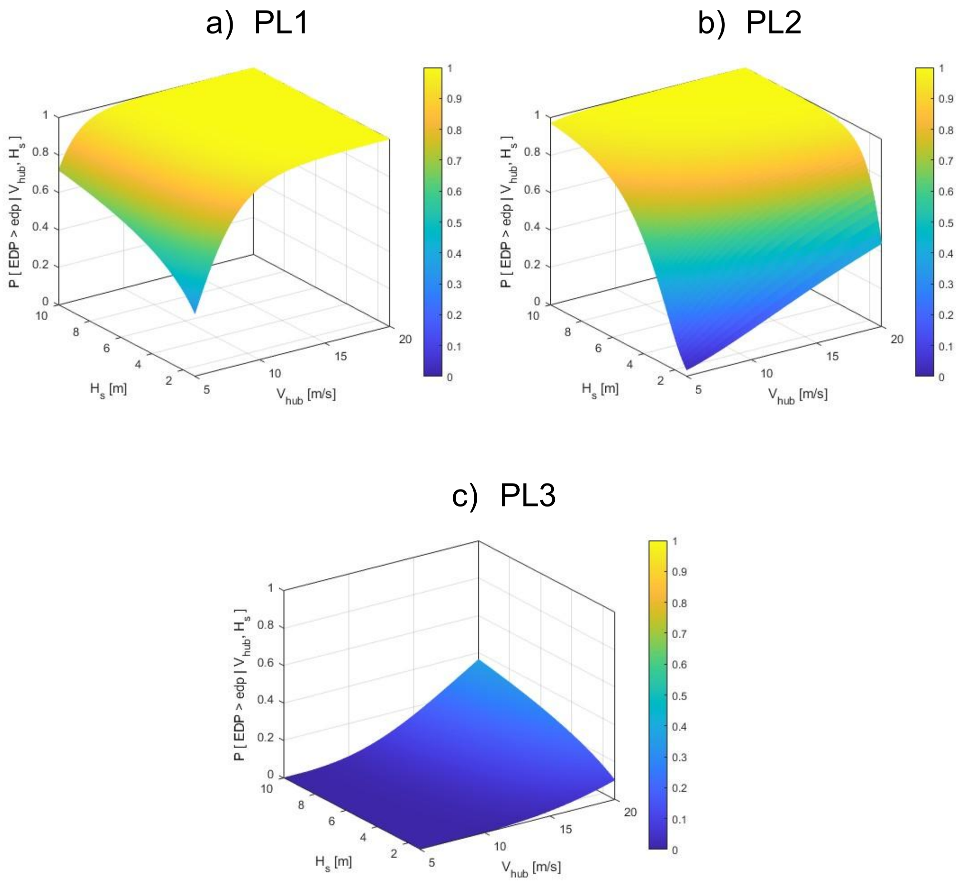

Figure 6.6.2 Bivariate fragility surfaces under combined wind and wave loading for the OC4 floating wind turbine. The probability of exceeding (a) PL1, (b) PL2 and (c) PL3 is shown as a function of hub-height wind speed $\boldsymbol{V}_{\text{hub}}$ and significant wave height $\boldsymbol{H_s}$.

Following the definition of the bivariate fragility surfaces, the parameters of the underlying regression model are reported in Table 6.6.3 for the three performance levels considered. The parameters are obtained from the regression analysis of the structural demand, as described in Section 6.6 (22), and define the probabilistic model on which the fragility surfaces are based.

Table 6.6.3 Parameters of the bivariate lognormal fragility surfaces under combined wind and wave loading for the OC4 floating wind turbine.

Fragility surface	ln(a)	b	c	β	R^2
PL1	-2.48	0.61	0.11	0.23	0.57
PL2	-0.96	0.28	0.41	0.23	0.61
PL3	-2.11	0.59	0.11	0.26	0.50

The parameter $\ln(a)$ represents the scale factor of the demand model, while the coefficients b and c quantify the sensitivity of the fragility to variations in hub-height wind speed and significant wave height, respectively. These coefficients therefore provide a direct measure of the relative influence of wind and wave loading on the probability of exceeding the considered performance levels. The parameter β represents the total logarithmic dispersion of fragility function, accounting for demand variability, capacity uncertainty and modelling uncertainties. The coefficient of determination R^2 is reported to quantify the accuracy of the regression model used to describe the structural demand.

An examination of the regression coefficients highlights that wind loading plays a dominant role for performance levels PL1 and PL3, while the influence of wave motion becomes more significant for PL2. This result is consistent with the physical interpretation of the selected engineering demand parameters and with the trends observed in the corresponding fragility surfaces.

Starting from the bivariate formulation, conditional fragility surfaces were also derived in order to provide a complementary representation of structural vulnerability associated with assigned sea states. In this case, fragility functions were obtained by conditioning the bivariate fragility surface on selected values of the significant wave height, through probabilistic integration over the conditional distribution of the hub-height wind speed.

The resulting conditional fragility surfaces express the probability of exceeding the selected performance levels as a function of wind speed, with the parameters of the fragility function explicitly expressed as functions of the significant wave height. This representation allows a compact and continuous description of the influence of sea state severity on structural vulnerability and facilitates the interpretation of the results (see Figure 6.6.3).

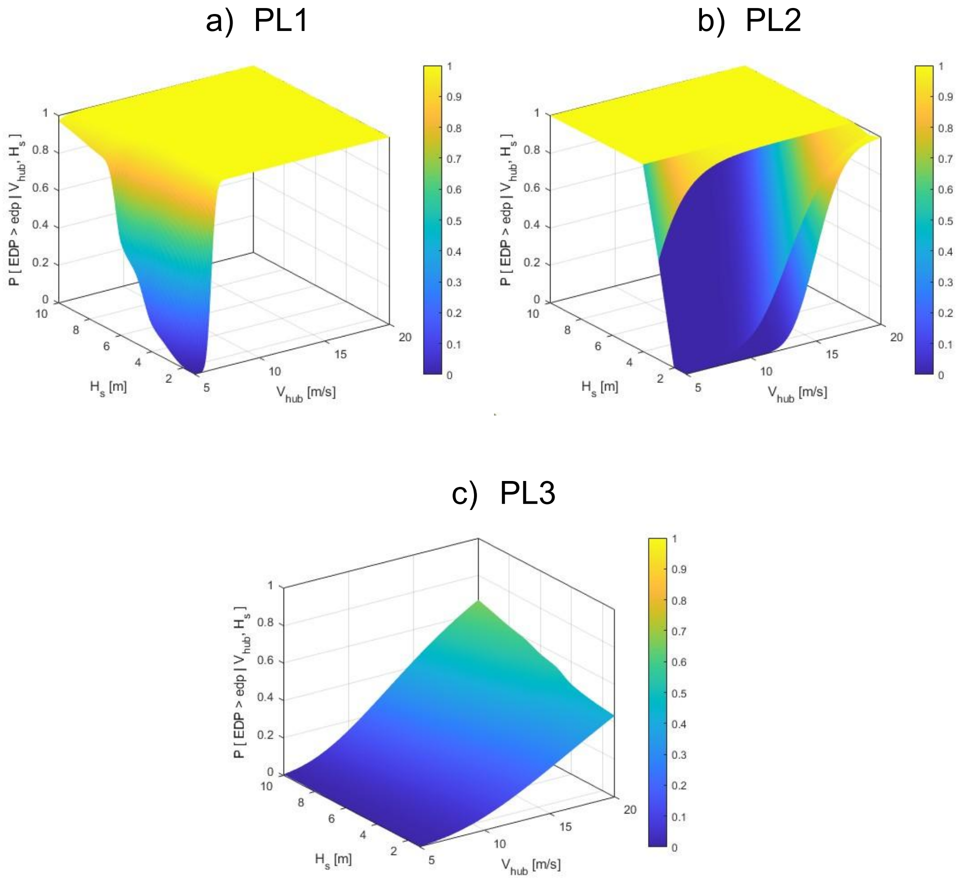

Figure 6.6.3 Conditional fragility surfaces under combined wind and wave loading for the OC4 floating wind turbine. The probability of exceeding (a) PL1, (b) PL2 and (c) PL3 is shown as a function of hub-height wind speed $\boldsymbol{V}_{\text{hub}}$ and significant wave height $\boldsymbol{H_s}$.

Table 6.6.4 Parameters of the conditional lognormal fragility surfaces under combined wind and wave loading for the OC4 floating wind turbine.

Fragility surface	$\mu(H_s)$	$\beta(H_s)$
PL1	-0.08 H_s + 1.99	0.02 H_s + 0.02
PL2	-0.47 H_s + 2.42	0.08 H_s + 0.19
PL3	-0.04 H_s + 3.15	-0.01 H_s + 0.55

It is emphasized that the conditional fragility surfaces do not represent an alternative modelling approach, but are derived from the bivariate fragility surfaces through probabilistic integration. The bivariate formulation therefore remains the baseline probabilistic description of the combined wind–wave effects on the structural response of the floating wind turbine.

The parameters of the conditional fragility functions, expressed in terms of median and logarithmic dispersion as functions of the significant wave height, are summarized in Table 6.6.4.

6.6.4 Fragility surfaces under combined Wind and Current effects

The fragility analysis under combined wind and current loading is developed to investigate the influence of sea currents on the structural vulnerability of floating offshore wind turbines. In line with the approach adopted for the wind–wave combination, vulnerability is described through fragility surfaces, which express the probability of exceeding performance levels as a function of two intensity measures: wind speed at the hub V_{hub} and current speed at the still water level (SWL) $V_{\text{current,SWL}}$.

The fragility analysis is conducted using IDA, progressively increasing the intensity of the wind at hub height, while the action of the sea current is introduced through a prescribed vertical current profile implemented in OpenFAST. For each load combination, the structural response is evaluated in terms of the EDPs associated with performance levels PL1, PL2 and PL3, including the sources of uncertainty described in Section 6.6.1.

For each performance level, the structural demand was modelled using a bivariate lognormal formulation, allowing the joint influence of wind and current loading on structural vulnerability to be captured without assuming a priori dominance of either environmental action. The resulting bivariate fragility surfaces provide a continuous probabilistic description of performance exceedance in the two-dimensional space defined by hub-height wind speed and current velocity at still water level. The bivariate fragility surfaces corresponding to performance levels PL1 and PL2 are shown in Figure 6.6.4 (a – b). Figure 6.6.4 shows that, for performance levels PL1 and PL2, the probability of exceedance is primarily governed by the hub-height wind speed, while variations in current velocity have a limited influence on the fragility surfaces. This behaviour is consistent with the physical nature of the response parameters associated with serviceability-related performance levels and with the trends observed in the sensitivity analysis presented in Section 6.4.

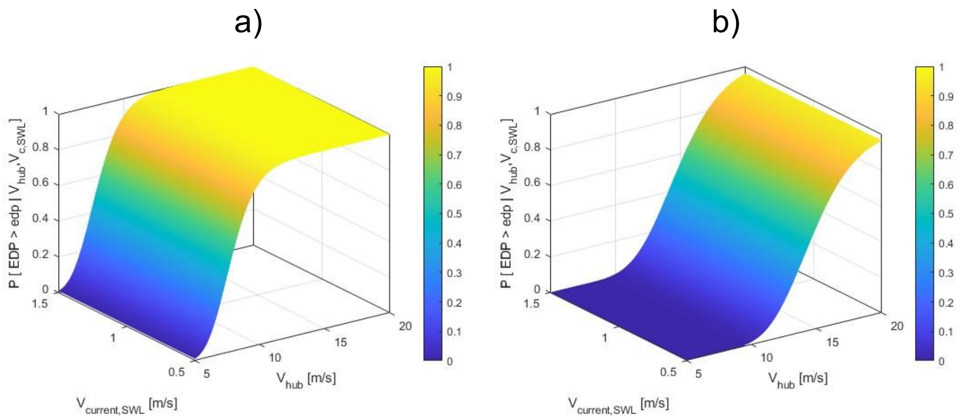

Figure 6.6.4 Bivariate fragility surfaces under combined wind and current loading for the OC4 floating wind turbine. The probability of exceeding (a) PL1 and (b) PL2 is shown as a function of hub-height wind speed $\boldsymbol{V}_{\text{hub}}$ and current speed at still water level $\boldsymbol{V}_{\text{current,SWL}}$.

Conversely, the bivariate fragility surface associated with performance level PL3, shown in Figure 6.6.5, exhibits a more pronounced dependence on current velocity. Performance level PL3 is representative of systemic collapse conditions of the floating offshore wind turbine and may be exceeded through different competing failure mechanisms, including excessive bending demand at the tower base and excessive tension in the mooring lines. In this context, the presence of sea currents contributes to an increase in hydrodynamic loading acting on the platform and the mooring system, resulting in an increase in the overall structural demand. Accordingly, the probability of exceeding PL3 increases systematically with increasing current velocity for a given wind speed.

Following the definition of the bivariate fragility surfaces, the parameters of the underlying regression model are reported in Table 6.6.5 for the three considered performance levels. These parameters are obtained from the regression analysis of the structural demand, as described in the fragility framework introduced in Section 6.6, and define the probabilistic model on which the bivariate fragility surfaces are based.

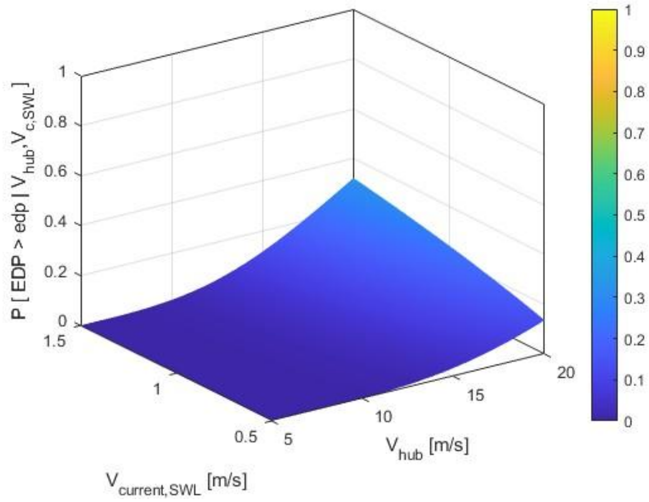

Figure 6.6.5 Bivariate fragility surface under combined wind and current loading for the OC4 floating wind turbine. The probability of exceeding PL3 (systemic collapse) is shown as a function of hub-height wind speed $\boldsymbol{V}_{\text{hub}}$ and current speed $\boldsymbol{V}_{\text{current, SWL}}$.

Table 6.6.5 Parameters of the bivariate lognormal fragility functions under combined wind and current loading for the OC4 floating offshore wind turbine.

Fragility surface	ln(a)	b	c	β	R^2
PL1	-3.68	1.12	-0.01	0.21	0.83
PL2	-2.73	1.02	-0.01	0.18	0.85
PL3	-1.65	0.50	0.12	0.20	0.54

An examination of the regression coefficients indicates a negligible dependence on current velocity for performance levels PL1 and PL2, as reflected by values of the coefficient c close to zero. Conversely, performance level PL3 exhibits sensitivity to both wind and current loading, while remaining more strongly governed by wind action. This interpretation is consistent with the trends observed in the corresponding bivariate fragility surfaces and with the physical nature of the collapse mechanisms associated with PL3. Consistently, the coefficient of determination R^2 associated with the bivariate fragility surface for PL3 is lower than those obtained for PL1 and PL2. This behaviour can be attributed to the composite definition of systemic collapse adopted in this study, whereby PL3 is exceeded through the alternative activation of two distinct failure mechanisms: attainment of the ultimate bending capacity at the tower base and exceedance of the tensile capacity of the mooring lines. The two mechanisms exhibit different sensitivities to the considered intensity measures (V_{hub}, $V_{current,SWL}$). While tower-base bending failure is primarily driven by wind loading, mooring failure is more strongly influenced by current action. As a result, different regions of the intensity-measure space are governed by different dominant failure mechanisms, leading to a regime transition in the structural response. The adoption of a single log-linear regression model to represent a fragility surface associated with a systemic collapse definition based on the alternative activation of multiple failure mechanisms therefore introduces additional residual dispersion and reduces the overall goodness of fit, as reflected by the lower R^2 value. This outcome is physically meaningful and reflects the inherent complexity of systemic collapse in floating offshore wind turbines.

Starting from the bivariate formulation, conditional fragility surfaces were also derived to provide a complementary representation of structural vulnerability associated with assigned current velocities. In this case, fragility functions were obtained by conditioning the bivariate fragility surface on selected values of the current velocity at still water level, through probabilistic integration over the conditional distribution of the hub-height wind speed. The resulting conditional fragility surfaces express the probability of exceeding the selected performance levels as a function of wind speed, with the parameters of the fragility function explicitly expressed as functions of the current velocity.

The conditional fragility surfaces corresponding to performance levels PL1, PL2, and PL3 are shown in Figure 6.6.6, while the parameters of the conditional lognormal fragility functions, expressed in terms of median and logarithmic dispersion as functions of current velocity, are summarized in Table 6.6.6.

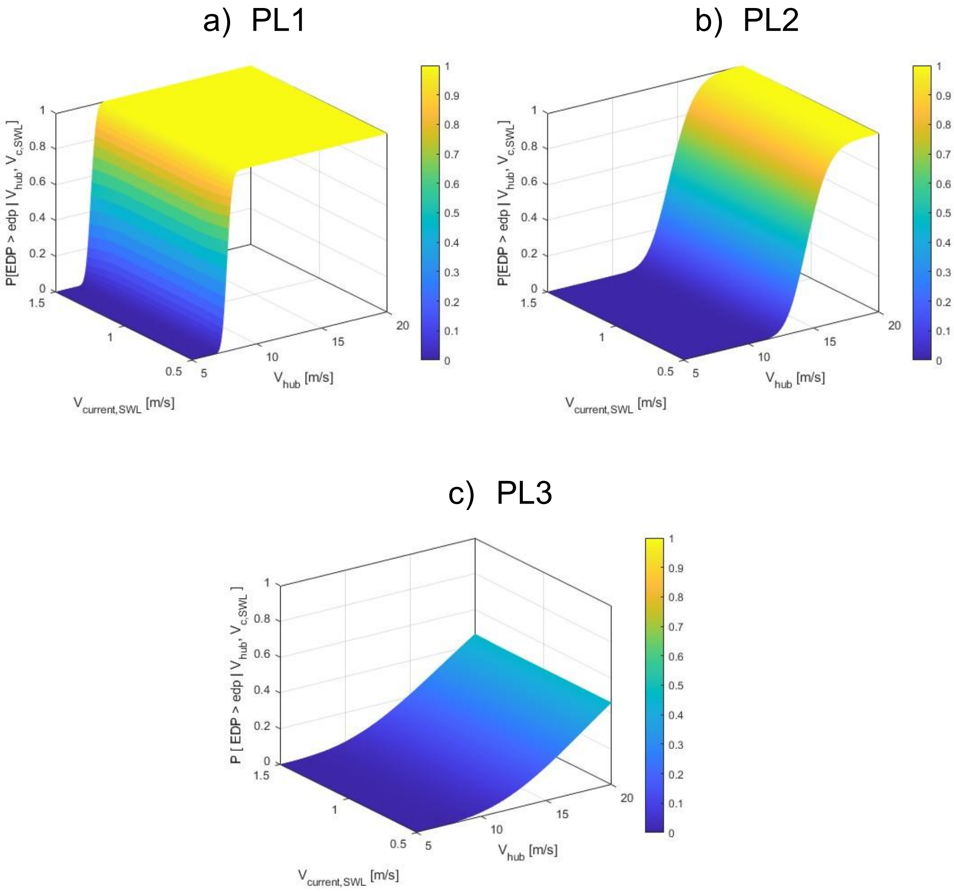

Figure 6.6.6 Conditional fragility surfaces under combined wind and current loading for the OC4 floating wind turbine. The probability of exceeding (a) PL1, (b) PL2 and (c) PL3 is shown as a function of hub-height wind speed $\boldsymbol{V}_{\text{hub}}$ and current speed $\boldsymbol{V}_{\text{current, SWL}}$.

Table 6.6.6 Parameters of the conditional lognormal fragility functions under combined wind and current loading for the OC4 floating wind turbine.

Fragility surface	$\mu(V_{\text{c, SWL}})$	$\beta(V_{\text{c, SWL}})$
PL1	$0.01\, V_{\text{c, SWL}} + 2.04$	$0\, V_{\text{c, SWL}} + 0.04$
PL2	$0\, V_{\text{c, SWL}} + 2.68$	$0.01\, V_{\text{c, SWL}} + 0.08$
PL3	$0\, V_{\text{c, SWL}} + 3.03$	$0.03\, V_{\text{c, SWL}} + 0.36$

Overall, the wind–current fragility analysis highlights that sea currents primarily affect vulnerability through mechanisms associated with global equilibrium and ultimate capacity, whereas their influence on serviceability-related performance levels is limited.

6.7 Discussion of results for OWTs

The numerical analyses conducted for the offshore case study highlight the importance of considering the aero-hydro-structural coupling within a probabilistic framework based on fragility functions. The results confirm that the structural response of offshore wind turbines, particularly for floating configurations, cannot be reliably assessed by considering individual environmental actions separately. On the contrary, it is their interaction that governs the exceeding of operational and collapse performance levels.

The fragility surfaces obtained under combined wind-wave and wind-current actions determine an amplification of the overall response of the structure compared to single hazard scenarios. In fact, the analyses show that, even in the presence of moderate wave conditions, excitation due to turbulent wind is the main mechanism triggering the dynamic response, while hydrodynamic actions act mainly as an amplification factor.

In particular, the results highlight how performance level PL3, associated with systemic collapse conditions, represents the main risk driver for floating offshore turbines, being significantly more sensitive to combined environmental actions than operational performance levels.

It should be noted that the application of a multi-dimensional fragility approach to floating offshore wind turbines is still a relatively unexplored area of research. The use of fragility surfaces, instead of traditional one-dimensional curves, allows for a more realistic understanding of the interaction between different environmental actions and the identification of critical regions in the load intensity space, which are difficult to identify using simplified approaches. The available literature is limited to a small number of studies, often focused on fixed foundation configurations, while probabilistic assessments of the structural vulnerability of FOWTs are still rare. In this context, this paper proposes a methodology capable of coherently integrating the dynamic coupling between wind, waves, and currents within a risk assessment framework.

From a risk assessment perspective, the proposed framework allows for a direct comparison between onshore and offshore configurations in terms of vulnerability mechanisms and dominant hazards. The introduction of fragility surfaces also provides valuable support for the future development of performance- and risk-oriented offshore design criteria, particularly for deepwater installations and floating systems. Looking ahead, these tools can support plant-scale reliability analyses, site-specific risk assessments, and design and management strategies geared towards the resilience of offshore infrastructure.

Chapter 7

Conclusions and future perspectives

The most important thing is not to stop questioning.

Albert Einstein

The study presented in this dissertation addressed the issue of the structural reliability of wind turbines by adopting a multi-hazard risk-based perspective, with the aim of overcoming the limitations of traditional deterministic and single-hazard approaches. The work has focused on both onshore and offshore wind turbines, explicitly characterizing environmental actions and structural response in these different contexts and proposing a framework for vulnerability and risk assessment.

A central contribution of the thesis is the development and application of a coherent probabilistic framework, which integrates natural hazard characterization, structural modelling, fragility analysis and risk quantification. The adoption of engineering-relevant performance levels and the explicit modelling of the main sources of uncertainty enable the evaluation of the probability of exceeding different performance thresholds and loss of function conditions under multiple natural hazards.

With regard to onshore wind turbines, the results highlight how the interaction among different hazards can significantly influence system performance. Analyses show that turbines installed on ridges or slopes in seismically active areas may be strongly affected by the combined effects of wind, seismic ground shaking and earthquake-induced landslides. In particular, permanent ground displacements associated with slope instability are shown to be potentially dominant in governing both structural demand and loss of functionality. The comparison between seismic-only fragility curves and fragility curves including earthquake-induced landslide effects clearly demonstrates that neglecting secondary seismic hazards may lead to a significant underestimation of vulnerability and risk. Moreover, the inclusion of soil–structure interaction effects substantially modifies the dynamic response of the tower, emphasizing the importance of realistic modelling assumptions in multi-hazard analyses.

An additional relevant finding concerns the role of non-structural components, such as underground electrical cables, whose performance may control the system's functionality. This aspect confirms that wind turbines should be considered as complex infrastructure systems and that risk assessment should not be limited to the tower or foundation alone, but should also include auxiliary elements that are essential for energy production and transmission.

For offshore wind turbines, the thesis extended the multi-hazard framework to floating systems installed in deep waters, in which the interaction between wind, waves and marine currents governs the structural behaviour. Time-domain aero–hydro–structural simulations performed using OpenFAST show that environmental load coupling may lead to a significant amplification of structural response. The fragility surfaces derived in this study provide a more realistic representation of offshore wind turbine vulnerability compared to traditional fragility curves, allowing the combined effects of multiple environmental intensity measures to be captured.

The comparison between onshore and offshore configurations shows that, although the dominant hazards and damage mechanisms differ, multi-hazard interaction represents a key factor in governing the response and reliability of wind turbines in both contexts. This finding reinforces the need to adopt integrated, risk-oriented methodologies as a common reference for the assessment of wind energy infrastructure operating in complex environmental conditions.

The proposed framework is inherently flexible and can be adapted to different turbine typologies, foundation systems and site conditions, provided that appropriate modifications are introduced in the hazard characterization and structural modelling phases.

From an engineering perspective, the results of this research demonstrate that the use of fragility curves and surfaces, combined with risk metrics such as annual exceedance rates of performance levels and expected economic losses, provides valuable information to support design decisions. These indicators may be employed within reliability-based design approaches, in the prioritization of mitigation measures and in the optimization of inspection and maintenance strategies, contributing to the long-term safety and economic sustainability of wind energy installations.

The results obtained open several perspectives for future developments. Possible extensions of this work include the integration of additional natural hazards, such as icing phenomena, extreme temperature effects or tsunamis, within a life-cycle risk assessment framework. For offshore turbines, integrating real-time monitoring data represents a relevant opportunity to further refine the analyses. In this context, the increasing adoption of structural health monitoring technologies and digital twin approaches offers promising prospects for the development of adaptive, risk-informed design and management strategies for future wind energy infrastructure.

Bibliography

[1] K. R. Rao, 'Wind Energy for Power Generation Meeting the Challenge of Practical Implementation'.

[2] U.S. Department of Energy, 'Trends in the Size and Power of Wind Turbines', 2023.

[3] A. Quilligan, A. O'Connor, and V. Pakrashi, 'Fragility analysis of steel and concrete wind turbine towers', *Eng. Struct.*, vol. 36, pp. 270–282, Mar. 2012, doi: 10.1016/j.engstruct.2011.12.013.

[4] E. C. Edwards, A. Holcombe, S. Brown, E. Ransley, M. Hann, and D. Greaves, 'Evolution of floating offshore wind platforms: A review of at-sea devices', Sep. 01, 2023, *Elsevier Ltd*. doi: 10.1016/j.rser.2023.113416.

[5] S. Liu, S. Ren, and H. Jiang, 'Predictive maintenance of wind turbines based on digital twin technology', *Energy Reports*, vol. 9, pp. 1344–1352, Oct. 2023, doi: 10.1016/j.egyr.2023.05.052.

[6] E. Kandemir, A. Hasan, T. Kvamsdal, and S. Abdel-Afou Alaliyat, 'Predictive digital twin for wind energy systems: a literature review', Dec. 01, 2024, *Springer Nature*. doi: 10.1186/s42162-024-00373-9.

[7] International Electrotechnical Commission, 'IEC 61400-1: Wind Turbines – Part 1: Design Requirements', 2005.

[8] Det Norske Veritas, *Guidelines for design of wind turbines*. DNV; Wind Energy Dept., Risø National Laboratory, 2002.

[9] Youngji Y., 'Looking inside Wind Turbine', 2015.

[10] S. Dilanika Kulatunga, E. Jayamani, K. Heng Soon, P. V. S. Hari Prashanth, S. Jeyanthi, and R. Ravi Sankar, 'Comparative study of static and fatigue performances of wind turbine blade materials', in *Materials Today: Proceedings*, Elsevier Ltd, Jan. 2022, pp. 6848–6853. doi: 10.1016/j.matpr.2022.05.052.

[11] S. Jayswal and A. Bhattu, ‘Structural and modal analysis of small wind turbine blade using three different materials’, in *Materials Today: Proceedings*, Elsevier Ltd, Jan. 2023, pp. 1347–1352. doi: 10.1016/j.matpr.2022.09.329.

[12] David Wagman, ‘GE to Invest in 12 MW Offshore Wind Turbine’, 2018.

[13] MingYang, ‘Sustainability Report’, 2024. Accessed: Dec. 01, 2025. [Online]. Available: www.myse.com

[14] J. S. Chou and W. T. Tu, ‘Failure analysis and risk management of a collapsed large wind turbine tower’, *Eng. Fail. Anal.*, vol. 18, no. 1, pp. 295–313, Jan. 2011, doi: 10.1016/j.engfailanal.2010.09.008.

[15] J. S. Chou, Y. C. Ou, and K. Y. Lin, ‘Collapse mechanism and risk management of wind turbine tower in strong wind’, *Journal of Wind Engineering and Industrial Aerodynamics*, vol. 193, Oct. 2019, doi: 10.1016/j.jweia.2019.103962.

[16] P. Tchakoua, R. Wamkeue, M. Ouhrouche, F. Slaoui-Hasnaoui, T. A. Tameghe, and G. Ekemb, ‘Wind turbine condition monitoring: State-of-the-art review, new trends, and future challenges’, 2014, *MDPI AG*. doi: 10.3390/en7042595.

[17] W. Qiao and D. Lu, ‘A Survey on Wind Turbine Condition Monitoring and Fault Diagnosis - Part II: Signals and Signal Processing Methods’, Oct. 01, 2015, *Institute of Electrical and Electronics Engineers Inc.* doi: 10.1109/TIE.2015.2422394.

[18] Z. Jiang, W. Hu, W. Dong, Z. Gao, and Z. Ren, ‘Structural reliability analysis of wind turbines: A review’, Dec. 01, 2017, *MDPI AG*. doi: 10.3390/en10122099.

[19] C. Bernuzzi *et al.*, ‘Resonance of steel wind turbines: Problems and solutions’, *Structures*, vol. 32, pp. 65–75, Aug. 2021, doi: 10.1016/j.istruc.2021.02.053.

[20] I. Lavassas, G. Nikolaidis, P. Zervas, E. Efthimiou, I. N. Doudoumis, and C. C. Baniotopoulos, ‘Analysis and design of the prototype of a steel 1-MW wind turbine tower’, *Eng. Struct.*, vol. 25, no. 8, pp. 1097–1106, Jul. 2003, doi: 10.1016/S0141-0296(03)00059-2.

[21] M. A. Asareh, W. Schonberg, and J. Volz, ‘Fragility analysis of a 5-MW NREL wind turbine considering aero-elastic and seismic interaction using finite element method’, *Finite Elements in Analysis and Design*, vol. 120, pp. 57–67, Nov. 2016, doi: 10.1016/j.finel.2016.06.006.

[22] Z. Zhang, R. De Risi, and A. Sextos, ‘Multi-hazard fragility assessment of monopile offshore wind turbines under earthquake, wind and wave loads’, *Earthq. Eng. Struct. Dyn.*, vol. 52, no. 9, pp. 2658–2681, Jul. 2023, doi: 10.1002/eqe.3888.

[23] P. Caprari, M. Della Seta, S. Martino, A. Fantini, M. Fiorucci, and T. Priore, ‘Upgrade of the CEDIT database of earthquake-induced ground effects in Italy’, *Italian Journal of Engineering Geology and Environment*, vol. 18, no. 2, pp. 23–39, 2018.

[24] S. Romeo, ‘The rapid survey of earthquake-induced landslides during the 2016–2017 seismic sequence in Central Italy.’

[25] BS EN 1990:2002, *Eurocode – Basis of Structural Design*. British Standards Institution (BSI), London, 2006.

[26] Consiglio Nazionale delle Ricerche, ‘CNR-DT 207 R1/2018 Istruzioni per la valutazione delle azioni e degli effetti del vento sulle costruzioni’.

[27] American Society of Civil Engineers, *Minimum design loads for buildings and other structures*. Structural Engineering Institute, 2010.

[28] International Electrotechnical Commission, ‘IEC 61400-3: Wind Turbines – Part 3: Design Requirements for Offshore Wind Turbines’, p. 263, 2009.

[29] L. Arany, S. Bhattacharya, J. Macdonald, and S. J. Hogan, ‘Design of monopiles for offshore wind turbines in 10 steps’, *Soil Dynamics and Earthquake Engineering*, vol. 92, pp. 126–152, Jan. 2017, doi: 10.1016/j.soildyn.2016.09.024.

[30] P. Frohboese, C. Schmuck, and G. L. G. Hassan, ‘Thrust coefficients used for estimation of wake effects for fatigue load calculation’, in *European Wind Energy Conference*, European Wind Energy Association, 2010.

[31] CEN, ‘Eurocode 8: Design of structures for earthquake resistance, Part 1: General rules, seismic actions and rules for buildings (EN 1998-1)’, 2004.

[32] Ministero delle Infrastrutture e dei Trasporti, ‘Norme Tecniche per le Costruzioni (NTC 2018)’, 2018.

[33] I. Iervolino, C. Galasso, and E. Cosenza, ‘REXEL: Computer aided record selection for code-based seismic structural analysis’, *Bulletin of Earthquake Engineering*, vol. 8, no. 2, pp. 339–362, Apr. 2010, doi: 10.1007/s10518-009-9146-1.

[34] Federal Emergency Management Agency, ‘Hazus - MH 2.1 Technical Manual’, 2013.

[35] D. K. Keefer, ‘Landslides caused by earthquakes’, *Bulletin of the Geological Society of America*, vol. 95, no. 4, pp. 406–421, 1984, doi: 10.1130/0016-7606(1984)95<406:lcbe>2.0.co;2.

[36] R. W. Jibson, ‘Methods for assessing the stability of slopes during earthquakes-A retrospective’, *Eng. Geol.*, vol. 122, no. 1–2, pp. 43–50, Sep. 2011, doi: 10.1016/j.enggeo.2010.09.017.

[37] S. D. Fotopoulou and K. D. Pitilakis, ‘Predictive relationships for seismically induced slope displacements using numerical analysis results’, *Bulletin of Earthquake Engineering*, vol. 13, no. 11, pp. 3207–3238, Nov. 2015, doi: 10.1007/s10518-015-9768-4.

[38] S. D. Fotopoulou and K. D. Pitilakis, ‘Vulnerability assessment of reinforced concrete buildings at precarious slopes subjected to combined ground shaking and earthquake induced landslide’, *Soil Dynamics and Earthquake Engineering*, vol. 93, pp. 84–98, Feb. 2017, doi: 10.1016/j.soildyn.2016.12.007.

[39] J. Jonkman, S. Butterfield, W. Musial, and G. Scott, ‘Definition of a 5-MW Reference Wind Turbine for Offshore System Development’, 2009. [Online]. Available: http://www.osti.gov/bridge

[40] I. Lavassas, G. Nikolaidis, P. Zervas, E. Efthimiou, I. N. Doudoumis, and C. C. Baniotopoulos, ‘Analysis and design of the prototype of a steel 1-MW wind turbine tower’, *Eng. Struct.*,

vol. 25, no. 8, pp. 1097–1106, Jul. 2003, doi: 10.1016/S0141-0296(03)00059-2.

[41] M. Kitahara and T. Ishihara, ‘Seismic soil-structure interaction analysis of wind turbine support structures using augmented complex mode superposition response spectrum method’, *Wind Energy Science*, vol. 7, no. 3, pp. 1007–1020, May 2022, doi: 10.5194/wes-7-1007-2022.

[42] G. Gazetas, ‘Analysis of machine foundation vibrations: state of the art’, 1983.

[43] G. Gazetas, ‘Formulas and charts for impedances of surface and embedded foundations’, *Journal of geotechnical engineering*, vol. 117, no. 9, pp. 1363–1381, 1991.

[44] T. Ishihara and L. Wang, ‘A study of modal damping for offshore wind turbines considering soil properties and foundation types’, *Wind Energy*, vol. 22, no. 12, pp. 1760–1778, Dec. 2019, doi: 10.1002/we.2401.

[45] F. McKenna, ‘OpenSees: A Framework for Earthquake Engineering Simulation’, *Computing in Science and Engineering 13, 58–66*, 2011.

[46] A. Ali, R. De Risi, and A. Sextos, ‘Seismic assessment of wind turbines: How crucial is rotor-nacelle-assembly numerical modeling?’, *Soil Dynamics and Earthquake Engineering*, vol. 141, Feb. 2021, doi: 10.1016/j.soildyn.2020.106483.

[47] CEN, ‘Eurocode 1: Actions on structures - General actions, Part 1-4: Wind actions (EN 1991-1-4)’, 2004.

[48] CEN, ‘Eurocode 8: Design provisions for earthquake resistance of structures, Part 6: Towers, masts and chimneys (EN 1998-6)’, 2003.

[49] CEN, ‘Eurocode 3: Design of steel structures, Part 1-6: Strength and stability of shell structures (EN 1993-1-6)’, 2004.

[50] CEN, ‘Eurocode 3: Design of steel structures, Part 1-9: Fatigue (EN 1993-1-9)’, 2003.

[51] C. J. White *et al.*, ‘Towards multi-hazard and multi-risk indicators – a review and recommendations for development and

implementation’, *Natural Hazards and Earth System Sciences*, vol. 25, no. 11, pp. 4263–4281, Oct. 2025, doi: 10.5194/nhess-25-4263-2025.

[52] B. D. Lago *et al.*, ‘Experimental tests on shallow foundations of onshore wind turbine towers’, *Structural Concrete*, vol. 23, no. 5, pp. 2986–3006, Oct. 2022, doi: 10.1002/suco.202100655.

[53] R. De Risi, S. Bhattacharya, and K. Goda, ‘Seismic performance assessment of monopile-supported offshore wind turbines using unscaled natural earthquake records’, *Soil Dynamics and Earthquake Engineering*, vol. 109, pp. 154–172, Jun. 2018, doi: 10.1016/j.soildyn.2018.03.015.

[54] J. O. Martin del Campo, A. Pozos-Estrada, and O. Pozos-Estrada, ‘Development of fragility curves of land-based wind turbines with tuned mass dampers under cyclone and seismic loading’, *Wind Energy*, vol. 24, no. 7, pp. 737–753, 2021.

[55] J. O. M. Del Campo and A. Pozos-Estrada, ‘Multi-hazard fragility analysis for a wind turbine support structure: An application to the Southwest of Mexico’, *Eng. Struct.*, vol. 209, p. 109929, 2020.

[56] L. Wang and T. Ishihara, ‘Failure-mechanism for wind turbines supported by pile groups at the Kugino wind farm in the Kumamoto earthquake’, in *Structures*, Elsevier, 2024, p. 107201.

[57] D. Vamvatsikos and C. Allin Cornell, ‘Incremental dynamic analysis’, *Earthq. Eng. Struct. Dyn.*, vol. 31, no. 3, pp. 491–514, 2002, doi: 10.1002/eqe.141.

[58] Jack W Baker, ‘Efficient Analytical Fragility Function Fitting Using Dynamic Structural Analysis’, *Earthquake Spectra*, vol. 31, no. 1, pp. 579–599, Feb. 2015, doi: 10.1193/021113EQS025M.

[59] H. Li, W. Peng, C. G. Huang, and C. Guedes Soares, ‘Failure Rate Assessment for Onshore and Floating Offshore Wind Turbines’, *J. Mar. Sci. Eng.*, vol. 10, no. 12, Dec. 2022, doi: 10.3390/jmse10121965.

[60] S. Basack, S. Dutta, D. Saha, and G. Das, 'Power generation by offshore wind turbines: An overview on recent research and developments', *WSEAS Trans. Power Syst*, vol. 16, pp. 254–261, 2021.

[61] M. Shields, P. Beiter, J. Nunemaker, A. Cooperman, and P. Duffy, 'Impacts of turbine and plant upsizing on the levelized cost of energy for offshore wind', *Appl. Energy*, vol. 298, Sep. 2021, doi: 10.1016/j.apenergy.2021.117189.

[62] W. Musial *et al.*, 'Offshore Wind Market Report: 2021 Edition', 2015.

[63] E. A. Bossanyi, 'GH bladed theory manual', *GH & Partners Ltd*, vol. 2, pp. 56–58, 2003.

[64] T. J. Larsen and A. M. Hansen, *HAWC2, the user's manual*. Risø National Laboratory, 2007.

[65] J. Jonkman and M. Sprague, 'OpenFAST documentation', *URL: https://openfast. readthedocs. io/en/main*, 2021.

[66] J. Jonkman, 'The New Modularization Framework for the FAST Wind Turbine CAE Tool Preprint', 2013. [Online]. Available: http://www.osti.gov/bridge

[67] Y. Cheng, Y. Luo, J. Wang, K. Dai, W. Wang, and A. El Damatty, 'Fragility and vulnerability development of offshore wind turbines under aero-hydro loadings', *Eng. Struct.*, vol. 293, Oct. 2023, doi: 10.1016/j.engstruct.2023.116625.

[68] B. J. Jonkman, 'TurbSim User's Guide', 2012. [Online]. Available: www.nrel.gov/publications.

[69] P. J. Moriarty and A. C. Hansen, 'AeroDyn Theory Manual', 2005. [Online]. Available: http://www.osti.gov/bridge

[70] R. Shirzadeh, 'Dynamic Modeling and Analysis of a Monopile Offshore Wind Turbine Focused on Damping and New Monitoring Strategies', 2015.

[71] Glauert H, *Aerodynamic Theory, chapter Windmills and fans*. Springer Berlin Heidelberg, 1935. doi: 10.1007/978-3-642-91487-4.

[72] J. M. Jonkman, G. J. Hayman, B. J. Jonkman, and R. R. Damiani, 'AeroDyn v15 User's Guide and Theory Manual'. [Online]. Available: www.nrel.gov/publications.

[73] K. Hasselmann *et al.*, 'Measurements of wind-wave growth and swell decay during the Joint North Sea Wave Project (Jonswap).', *Ergaenzungsheft zur Deutschen Hydrographischen Zeitschrift, Reihe A*, 1973.

[74] J. R. Morison, J. W. Johnson, and S. A. Schaaf, 'The Force Exerted by Surface Waves on Piles', *Journal of Petroleum Technology*, vol. 2, no. 05, pp. 149–154, May 1950, doi: 10.2118/950149-G.

[75] J. M. Jonkman, A. N. Robertson, and G. J. Hayman, 'HydroDyn User's Guide and Theory Manual', 2015. [Online]. Available: www.nrel.gov/publications.

[76] S. K. Chakrabarti, 'HANDBOOK OF OFFSHORE ENGINEERING Volume I 2005 ELSEVIER', 2005. [Online]. Available: www.bookaid.org

[77] R. Nagavinothini and S. Chandrasekaran, 'Dynamic analyses of offshore triceratops in ultra-deep waters under wind, wave, and current', *Structures*, vol. 20, pp. 279–289, Aug. 2019, doi: 10.1016/j.istruc.2019.04.009.

[78] A. Robertson *et al.*, 'Definition of the Semisubmersible Floating System for Phase II of OC4', 2014. [Online]. Available: www.nrel.gov/publications.

[79] B. J. Jonkman, 'NREL is operated for DOE by the Alliance for Sustainable Energy, LLC Contract No. DE-AC36-08-GO28308 TurbSim User's Guide: Version 1.50', 2009. [Online]. Available: http://www.osti.gov/bridge

[80] H. Li, W. Peng, C.-G. Huang, and C. Guedes Soares, 'Failure rate assessment for onshore and floating offshore wind turbines', *J. Mar. Sci. Eng.*, vol. 10, no. 12, p. 1965, 2022.

[81] Y. Sun, H. Li, L. Sun, and C. G. Soares, 'Failure analysis of floating offshore wind turbines with correlated failures', *Reliab. Eng. Syst. Saf.*, vol. 238, p. 109485, 2023.

[82] DNV, ‘DNV-OS-J101: Design of Offshore Wind Turbine Structures. Offshore Standard’, 2014.

[83] DNV, ‘DNV-ST-0119: Floating wind turbine structures’, 2021.

[84] R. De Risi, S. Bhattacharya, and K. Goda, ‘Seismic performance assessment of monopile-supported offshore wind turbines using unscaled natural earthquake records’, *Soil Dynamics and Earthquake Engineering*, vol. 109, pp. 154–172, 2018.

[85] C. Sheng and H. P. Hong, ‘Reliability and fragility assessment of offshore floating wind turbine subjected to tropical cyclone hazard’, *Structural Safety*, vol. 93, p. 102138, 2021.

[86] Y. Cheng, Y. Luo, J. Wang, K. Dai, W. Wang, and A. El Damatty, ‘Fragility and vulnerability development of offshore wind turbines under aero-hydro loadings’, *Eng. Struct.*, vol. 293, p. 116625, 2023.

[87] D. Wilkie and C. Galasso, ‘A probabilistic framework for offshore wind turbine loss assessment’, *Renew. Energy*, vol. 147, pp. 1772–1783, Mar. 2020, doi: 10.1016/j.renene.2019.09.043.

[88] D. Wilkie and C. Galasso, ‘Site-specific ultimate limit state fragility of offshore wind turbines on monopile substructures’, *Eng. Struct.*, vol. 204, Feb. 2020, doi: 10.1016/j.engstruct.2019.109903.

[89] S. T. Hallowell *et al.*, ‘Hurricane risk assessment of offshore wind turbines’, *Renew. Energy*, vol. 125, pp. 234–249, Sep. 2018, doi: 10.1016/j.renene.2018.02.090.

[90] S. Okpokparoro and S. Sriramula, ‘Uncertainty modeling in reliability analysis of floating wind turbine support structures’, *Renew. Energy*, vol. 165, pp. 88–108, Mar. 2021, doi: 10.1016/j.renene.2020.10.068.

Author’s publications

1. Zimbalatti S., Parisi F. (2025). *Seismic fragility curves for onshore wind turbines including effects of earthquake-induced landslides*. European Safety and Reliability Conference, ESREL2025, Stavanger, Norway.

2. Zimbalatti S., Parisi F. (2025). *Curve di fragilità per turbine eoliche onshore soggette a frane sismo-indotte.* VI convegno di Ingegneria forense, VII convegno su CRolli, Affidabilità Strutturale e Consolidamento, IFCRASC’25, Naples, Italy.